VOLUME 83 NO. ST3
MAY 1957

JOURNAL of the

Structural Division

PROCEEDINGS OF THE

AMERICAN SOCIETY OF CIVIL ENGINEERS

BASIC REQUIREMENTS FOR MANUSCRIPTS

This Journal represents an effort by the Society to deliver information to the reader with the greatest possible speed. To this end the material herein has none of the usual editing required in more formal publications.

Original papers and discussions of current papers should be submitted to the Manager of Technical Publications, ASCE. The final date on which a discussion should reach the Society is given as a footnote with each paper. Those who are planning to submit material will expedite the review and publication procedures by complying with the following basic requirements:

1. Titles should have a length not exceeding 50 characters and spaces.

2. A 50-word summary should accompany the paper.

3. The manuscript (a ribbon copy and two copies) should be double-spaced on one side of 8½-in. by 11-in. paper. Papers that were originally prepared for oral presentation must be rewritten into the third person before being submitted.

4. The author's full name, Society membership grade, and footnote reference stating present employment should appear on the first page of the paper.

5. Mathematics are reproduced directly from the copy that is submitted. Because of this, it is necessary that capital letters be drawn, in black ink, 3/16-in. high (with all other symbols and characters in the proportions dictated by standard drafting practice) and that no line of mathematics be longer than 6½-in. Ribbon copies of typed equations may be used but they will be proportionately smaller in the printed version.

6. Tables should be typed (ribbon copies) on one side of 8½-in. by 11-in. paper within a 6½-in. by 10½-in. invisible frame. Small tables should be grouped within this frame. Specific reference and explanation should be made in the text for each table.

7. Illustrations should be drawn in black ink on one side of 8½-in. by 11-in. paper within an invisible frame that measures 6½-in. by 10½-in.; the caption should also be included within the frame. Because illustrations will be reduced to 69% of the original size, the capital letters should be 3/16-in. high. Photographs should be submitted as glossy prints in a size that is less than 6½-in. by 10½-in. Explanations and descriptions should be made within the text for each illustration.

8. Papers should average about 12,000 words in length and should be no longer than 18,000 words. As an approximation, each full page of typed text, table, or illustration is the equivalent of 300 words.

Further information concerning the preparation of technical papers is contained in the "Technical Publications Handbook" which can be obtained from the Society.

This Journal is published bi-monthly by the American Society of Civil Engineers. Publication office is at 2500 South State Street, Ann Arbor, Michigan. Editorial and General Offices are at 33 West 39 Street, New York 18, New York. $4.00 of a member's dues are applied as a subscription to this Journal. Second-class mail privileges are authorized at Ann Arbor, Michigan.

HY,PO,SA,ST.

Journal of the
STRUCTURAL DIVISION
Proceedings of the American Society of Civil Engineers

CONTENTS

May, 1957

Papers

Paper 1231 ST 3

Journal of the
STRUCTURAL DIVISION
Proceedings of the American Society of Civil Engineers

COLUMN DESIGN SIMPLIFIED

Richard H. J. Pian,[1] A.M. ASCE
(Proc. Paper 1231)

SYNOPSIS

A simple general approach for the analysis of columns within elastic range is developed. The application to practical design problems is simplified to a great extent by the introduction of a four-quadrant graph. This graph may be used for column design with different degrees of imperfections, different end conditions, and with materials having different yielding stresses.

INTRODUCTION

In the rational approach of column design, it is the usual procedure to assume, from the beginning, certain unavoidable inaccuracies in a column and then to derive a formula that contains not only the dimensions of the column and the quantities defining the mechanical properties of the materials but also the assumed inaccuracies. The well-known secant formula for columns with eccentric loading is derived from this approach. It was recommended as a working formula by the ASCE Special committee on Steel Column Research in 1933[2] and, since that time, has found increasing acceptance in standard design specifications, such as the AREA specifications. The main objection to the use of the secant formula in practice is the length of time needed for its solution.[3]

There is a real need for a simple general approach on a rational basis for the analysis of columns within the elastic range. In the present study it is shown that practical column design problems may be solved by means of a four-quadrant graph.

Note: Discussion open until October 1, 1957. Paper 1231 is part of the copyrighted Journal of the Structural Division of the American Society of Civil Engineers, Vol. 83, No. ST 3, May, 1957.

1. Associate Prof. of Civ. Eng., Michigan State Univ., East Lansing, Mich.
2. "Final Report of the Special Committee on Steel Column Research," ASCE Trans., Vol. 98, p. 1449, 1933.
3. "Steel Columns—A Survey and Appraisal of Past Work," by A. A. Jakkula and H. K. Stephenson, Texas Engineering Experiment Station Bulletin No. 91, p. 6, 1947.

Determination of Bending Moments

The resultant column bending moment due to primary and secondary action is expressed by Westergaard[4] thus:

$$M' = M + \sum \frac{\alpha}{n^2-\alpha} M$$

$$= M + M_1 \frac{\alpha}{1-\alpha} + M_2 \frac{\alpha}{4-\alpha} + M_3 \frac{\alpha}{9-\alpha} + \cdots \quad (1)$$

where $\alpha = \frac{P}{P_{cr}}$ and

$$M = \Sigma M_n = M_1 + M_2 + M_3 + \cdots + M_n \quad (2)$$

is the primary bending moment. For columns with initial imperfections the primary moment **M** is defined as the moment caused by initial imperfections alone and the resultant bending moment **M'** takes into consideration additional deflection due to axial load.

The primary moment **M** which is expressed as a trigonometric series can be determined from the theory of Fourier series. Formula (1) is a convergent series. If one takes only the first two terms of the series and let M_{01} be the modified value of M_1 (in order to take care of the effect of omitting the remaining terms), a very good approximation for **M'** can be written as:

$$M' = M \frac{1+i\alpha}{1-\alpha} \quad (3)$$

where $i = \frac{M_{01}}{M} - 1$ and $\alpha = \frac{P}{P_{cr}}$. The value of i for columns with different imperfections will be found in the following paragraphs.

The principal imperfections which make the behavior of actual columns so different from the assumptions of Euler's theory are: (1) initial curvature of the member and (2) unavoidable eccentricity in the application of the axial load.

(1) Compression member with initial curvature. (Fig. 1)

The primary bending moment, **M**, due to the initial curvature alone, can be expressed:

$$M = M_1 + M_2 + M_3 + \cdots + M_n \quad (2)$$

The initial shape of the member can be represented in the form of a sine series:

$$y_o = a_1 \sin \frac{\pi x}{L} + a_2 \sin \frac{2\pi x}{L} + a_3 \sin \frac{3\pi x}{L} + \cdots + a_n \frac{n\pi x}{L} \quad (4)$$

4. "Buckling of Elastic Structures" by H. W. Westergaard, ASCE Trans., Vol. 85, p. 590, 1922.

where x is the distance measured from one end; and M which is equal to Py_0, can be written:

$$M = \Sigma M_n = \Sigma P a_n \frac{n\pi x}{L} \tag{5}$$

By substituting these expressions for M_n in Formula (1), the following can be written:

$$M' = P\left(a_1 \sin\frac{\pi x}{L} + a_2 \sin\frac{2\pi x}{L} + \cdots\cdots\cdots\right.$$
$$+ P a_1 \sin\frac{\pi x}{L}\,\frac{\alpha}{1-\alpha} + P a_2 \sin\frac{2\pi x}{L}\,\frac{\alpha}{4-\alpha}$$
$$\left. + P a_2 \sin\frac{3\pi x}{L}\,\frac{\alpha}{9-\alpha} + \cdots\right) \tag{6}$$

To find the maximum at center, substitute $x = \frac{L}{2}$ in the above formula:

$$M' = P\left(a_1 + \frac{a_1\alpha}{1-\alpha}\right) - P\left(a_3 \frac{a_3\alpha}{1-\alpha}\right) + \cdots \tag{7}$$

where $\alpha = \frac{P}{P_{cr}}$. Since α is always less than one and approaches unity when P approaches P_{cr}, the first term in the expression usually has predominant importance.

Letting $a_1 = a$,

$$M' = Pa\,\frac{1}{1-\alpha} \tag{8}$$

This same result can be obtained by using differential equations.[5] It is found that:

$$\delta = a\,\frac{1}{1-\alpha} \tag{9}$$

That is, the final deflection at center of the deflection curve is the initial deflection a multiplied by $1/1 - \alpha$. Substituting $M' = P\delta$, Formula (8) can be obtained.

Formula (8) is a special form of the general formula (3) derived earlier. By substituting $i = 0$ (or $M_{01} = M$), Formulae (8) and (3) are identical.

(2) Compression member with eccentricity, e. (Fig. 2)

The primary bending moment, M, due to the eccentricity, e, alone ($M = Pe$), can be written:

$$M = \Sigma M_n = M_1 + M_2 + M_3 + \cdots + M_n \tag{2}$$

5. "Theory of Elastic Stability," by S. Timoshenko, p. 32, 1936.

If x is the distance measured from one end, the equation for M_n may be written:

$$M_n = b_n \sin \frac{n\pi x}{L} \tag{10}$$

where b_n is a constant to be determined. M is given by a rectangular moment diagram (Fig. 2-b), that is:

$$M = Pe \tag{11}$$

The series, ΣM_n, is a trigonometric series. It is known, from the theory of Fourier series, that any diagram can be represented by an infinite trigonometric series. It is possible, then, to find a set of constants, b_n, which make $M = \Sigma M_n$. From the theory of Fourier series:

$$b_n = \frac{2}{L} \int_0^L M \sin \frac{n\pi x}{L} \, dx \tag{12}$$

Substituting the value for $M = Pe$:

$$b_n = \frac{2Pe}{L} \int_0^L \sin \frac{n\pi x}{L} \, dx$$

$$= \frac{2Pe}{n\pi} \left(-\cos n\pi + 1 \right)$$

for n even, $M_n = 0$

for n odd, $M_n = \frac{4Pe}{n\pi} \sin \frac{n\pi x}{L}$ (13)

Hence, the series for M may be written:

$$M = \Sigma M_n = \frac{4Pe}{\pi} \left(\sin \frac{\pi x}{L} + \frac{1}{3} \frac{3\pi x}{L} + \cdots\cdots \right) \tag{14}$$

The expression for M_n appears in this series with the constant factor Pe. By substituting these expressions for M_n in Formula (1), the following formula is found for the resultant moment, M', produced at any point:

$$M' = M + \frac{4Pe}{\pi} \left(\frac{\alpha}{1-\alpha} \sin \frac{\pi x}{L} + \frac{1}{3} \frac{\alpha}{9-\alpha} \sin \frac{3\pi x}{L} + \cdots\cdots \right.$$

$$\left. + \frac{1}{n} \frac{\alpha}{n^2-\alpha} \sin \frac{n\pi x}{L} \right) \tag{15}$$

At the center, when $x = L/2$, $\sin \frac{n\pi x}{L} = \pm 1$. The substitution of these values

in the above equation leads to:

$$M' = Pe + \frac{4Pe}{\pi}\left(\frac{\alpha}{1-\alpha} - \frac{1}{3}\frac{\alpha}{9-\alpha} + \cdots\cdots\right)$$
$$= Pe\left(1 + \frac{4}{\pi}\frac{\alpha}{1-\alpha} - \frac{4}{3\pi}\frac{\alpha}{9-\alpha} + \frac{4}{5\pi}\frac{\alpha}{25-\alpha} - \cdots\right) \quad (16)$$

where $\alpha = P/P_{cr}$. A very close approximation for M' is obtained by considering the first two terms only:

$$M' = Pe\left(1 + \frac{1.26\alpha}{1-\alpha}\right)$$
$$= Pe\,\frac{1+0.26\alpha}{1-\alpha} \quad (17)$$

It is noted that Formula (17) is, again, a special form of the general formula (3) derived earlier. It is easily seen that by substitution i = 0.26 (or M_{01} = 1.26M), Formulas (17) and (3) are identical.

Practical Design Formulas and Curves

1. First consider the case of a compression member with an initial curvature only. The maximum resultant bending moment at the center of the member, as found earlier, is

$$M' = Pa\,\frac{1}{1-\alpha} \quad (8)$$

The maximum fiber stress of the member is

$$\sigma_{max} = \frac{P}{A} + \frac{M'c}{I} \quad (18)$$

Substituting the value of M' into Equation (18) gives

$$\sigma_{max} = \frac{P}{A} + \frac{Pac}{I}\,\frac{1}{1-\alpha}$$
$$= \frac{P}{A}\left(1 + \frac{ac}{r^2}\,\frac{1}{1-\alpha}\right) \quad (19)$$

Another illuminating way of writing this equation is the following:

$$\sigma_{max} = \sigma_1 + \sigma_2 \quad (20)$$

where $\sigma_1 = \frac{P}{A}$ is the direct stress, due to the compressive force P, and $\sigma_2 = \frac{M^1 c}{I}$, is the bending stress due to bending of P caused by deflection.

$$\sigma_2' = \frac{M'c}{I} = \frac{Pac}{I} \frac{1}{1-\alpha} = \sigma_2' \frac{1}{1-\alpha} \tag{21}$$

where $\sigma_2{}^1 = \frac{Pac}{I}$ is that bending stress which would be caused if, under load, the member retained its initial shape (maximum deviation a). Thus the expression for the maximum stress

$$\sigma_{max} = \sigma_1' + \sigma_2' \frac{1}{1-\alpha} \tag{22}$$

suggests a simple way of determining the extreme fibre stress in an initially distorted column. It is only necessary to find, in addition to the usual direct stress, the bending stress due to P which would be caused in the section farthest displaced from the straight line connecting the end points if the additional deflections under load are disregarded. The bending stress multiplied by the so-called magnification factor $\frac{1}{1-\alpha}$ gives the correct bending stress under any load.

The carrying capacity of the compression member is determined by finding that load P which would cause the σ_{max} to become equal to the yielding stress of the material. Making $\sigma_{max} = \sigma_{yp}$, Equation (22) may be written:

$$\sigma_{yp} = \sigma_1' + \sigma_2' \frac{1}{1-\alpha} \tag{23}$$

$$= \sigma_1' + \kappa \sigma_1' \frac{1}{1-\alpha} \tag{24}$$

where $k = \frac{\sigma_2{}^1}{\sigma_1}$ represents the ratio of the bending stress to the direct compressive stress. In this case, k can be found as follows:

$$\kappa \sigma_1' = \sigma_2' = \frac{Pac}{I} = \frac{P}{A} \frac{ac}{r^2}$$
$$\kappa = \frac{ac}{r^2} \tag{25}$$

Curves may be plotted from Equation (24) for any given value of σ_{yp} and various values of k. These curves, which show the average compressive stress σ_1, as a function of the slenderness-ratio L/r, at which yielding first begins, have been developed by Young.[6]

For every steel of a known yield point, a separate set of curves is necessary. A simpler and more general method is developed in the following manner:

6. "Rational Design of Steel Columns," by D. H. Young, ASCE Trans., vol. 101, p. 431, 1936.

$$\sigma_{yp} = \sigma_1 + K\sigma_1 \frac{1}{1 - \frac{\sigma_1}{\sigma_{cr}}} \tag{24}$$

$$(\sigma_{yp} - \sigma_1)\left(1 - \frac{\sigma_1}{\sigma_{cr}}\right) - K\sigma_1 = 0$$

$$\sigma_{yp} - \sigma_1 - \frac{\sigma_{yp}}{\sigma_{cr}}\sigma_1 + \frac{1}{\sigma_{cr}}\sigma_1^2 - K\sigma_1 = 0$$

$$\sigma_1^2 - (\sigma_{cr} + \sigma_{yp} + K\sigma_{cr})\sigma_1 + \sigma_{yp}\sigma_{cr} = 0$$

Solving for σ_1,

$$\sigma_1 = \frac{1}{2}\left[\sigma_{cr}(1+K) + \sigma_{yp} - \sqrt{\{(1+K)\sigma_{cr} + \sigma_{yp}\}^2 - 4\sigma_{yp}\sigma_{cr}}\right]$$

Dividing by σ_{yp},

$$\frac{\sigma_1}{\sigma_{yp}} = \frac{1}{2}\left[1 + (1+K)\frac{\sigma_{cr}}{\sigma_{yp}} \sqrt{\left\{1 + (1+K)\frac{\sigma_{cr}}{\sigma_{yp}}\right\}^2 - 4\frac{\sigma_{cr}}{\sigma_{yp}}}\right] \tag{26}$$

Equation (26) is non-dimensional and a set of curves may be plotted from it for various values of k. These curves can be used for any σ_{yp}. The following calculated values are used in the plotting of the curves as shown on the chart.

A number of other curves are included in the four-quadrant chart (Fig. 3). The third quadrant curves, which must first be used for computation, give the relation between L/r and $1/\sigma_{cr}$. The straight lines in the fourth and second quadrants are drawn for different values of σ_{yp}. The curves in the first quadrant are those plotted from values obtained by evaluating Equation (26).

Table 1.

$x = \frac{\sigma_{yp}}{\sigma_{cr}}$	$y = \frac{\sigma_1}{\sigma_{yp}}$			
	k = 0.1	k = 0.25	k = 0.5	k = 1.0
0.1	0.90	0.79	0.65	0.485
0.2	0.89	0.77	0.63	0.475
0.5	0.857	0.72	0.585	0.44
1.0	0.73	0.61	0.50	0.38
1.5	0.575	0.495	0.42	0.335
2.0	0.46	0.41	0.36	0.293
3.0	0.32	0.296	0.27	0.235
4.0	0.24	0.23	0.213	0.19
5.0	0.197	0.188	0.178	0.164
6.0	0.163	0.16	0.15	0.14

2. The solution of the problem presented by a compression member with a given amount of eccentricity, e, follows. The maximum bending moment at the center of the member, as found earlier, is

$$M' = Pe\,\frac{1+0.26\alpha}{1-\alpha} \tag{17}$$

The maximum fibre stress of the member is

$$\begin{aligned}\sigma_{max} &= \frac{P}{A} + \frac{M'c}{I} = \sigma_1 + \sigma_2 \\ &= \sigma_1 + \sigma_2'\,\frac{1+0.26\alpha}{1-\alpha}\end{aligned} \tag{27}$$

Making σ max = σ yp, equation (27) may be written

$$\sigma_{yp} = \sigma_1 + \sigma_2'\,\frac{1+0.26\alpha}{1-\alpha} \tag{28}$$

$$\sigma_{yp} = \sigma_1 + K\sigma_1\,\frac{1+0.26\alpha}{1-\alpha} \tag{29}$$

where $k = \frac{\sigma_2{}^1}{\sigma_1}$ can be written as follows:

$$K = \frac{Pe\,\frac{c}{I}}{\frac{P}{A}} = \frac{ec}{r^2} \tag{30}$$

Equation (29) is actually another form of the well known secant formula. Equation (29) is derived from the Secant formula in the following manner:

$$\sigma_{yp} = \frac{P}{A}\left[1 + \frac{ec}{r^2}\,\sec\frac{L}{2r}\sqrt{\frac{P}{AE}}\right] \tag{31}$$

But

$$\begin{aligned}\sec\frac{L}{2r}\sqrt{\frac{P}{AE}} &= \sec\frac{L}{2r}\sqrt{\frac{P}{P_{cr}}\,\frac{\pi^2 EI}{L^2}\,\frac{1}{AE}} \\ &= \sec\frac{L}{2r}\,\frac{\pi r}{L}\sqrt{\frac{P}{P_{cr}}} = \sec\frac{\pi}{2}\sqrt{\alpha}\end{aligned}$$

$$\therefore\quad \sigma_{yp} = \frac{P}{A}\left[1 + \frac{ec}{r^2}\,\sec\frac{\pi}{2}\sqrt{\alpha}\right] \tag{32}$$

A very close approximation for the secant (0^0 to $\pi/2$) is

$$\sec x = \frac{1 + \frac{4x^2}{\pi^2}\,0.26}{1 - \frac{4x^2}{\pi^2}} \tag{33}$$

$$\sec\frac{\pi}{2}\sqrt{\alpha} = \frac{1+0.26\alpha}{1-\alpha} \tag{34}$$

$$\sigma_{yp} = \frac{P}{A}\left[1 + \frac{ec}{r^2}\,\frac{1+0.26\lambda}{1-\lambda}\right] = \sigma_1 + \kappa\,\sigma_1\,\frac{1+0.26\lambda}{1-\lambda} \tag{29}$$

A simple useful non-dimensional formula, similar to the one for the case of a compression member with an initial curvature, can be derived in the following form:

$$\frac{\sigma_1}{\sigma_{yp}} = \frac{1}{2(1-0.26\kappa)}\left[1+(1+\kappa)\,\frac{\sigma_{cr}}{\sigma_{yp}} - \sqrt{\left\{1+(1+\kappa)\,\frac{\sigma_{cr}}{\sigma_{yp}}\right\}^2 - 4(1-0.26\kappa)\,\frac{\sigma_{cr}}{\sigma_{yp}}}\right] \tag{35}$$

A similar set of curves can be plotted from Eq. (35) for various values of k. The following calculated values are used to draw these curves.

Table 2

$x = \frac{\sigma_{yp}}{\sigma_{cr}}$	$y = \frac{\sigma_1}{\sigma_{yp}}$			
	k = 0.1	k = 0.25	k = 0.5	k = 1.0
0.1	0.892	0.79	0.65	0.48
0.2	0.885	0.765	0.63	0.47
0.5	0.846	0.706	0.575	0.435
1.0	0.71	0.59	0.484	0.368
1.5	0.564	0.477	0.406	0.32
2.0	0.45	0.4	0.35	0.28
3.0	0.317	0.29	0.262	0.229
4.0	0.238	0.226	0.21	0.184
5.0	0.196	0.185	0.149	0.137

For comparison, this set of curves is drawn on the same chart.

It is seen that the curves for initial eccentricity and for initial deflection are practically coincident. This may be demonstrated numerically. Taking

the value k = 0.25, the following comparison is made:

Table 3

$X = \frac{\sigma_{yp}}{\sigma_{cr}}$	$y = \frac{\sigma_1}{\sigma_{yp}}$		
	initial curvature	eccentricity	difference in %
0.1	0.79	0.79	-
0.2	0.77	0.765	0.7
0.5	0.72	0.706	2.0
1.0	0.61	0.59	3.2
1.5	0.495	0.477	3.6
2	0.41	0.4	2.4
3	0.296	0.29	2.0
4	0.23	0.226	1.7
5	0.188	0.185	1.6
6	0.16	0.158	1.25

Therefore, for practical purposes, either of the two sets of curves may be used for computation. For the case of a compression member with both initial curvature and eccentricity, k can be found from the expression

$$K = \frac{(e+a)c}{r^2} \tag{36}$$

Using the same curves, with k found from the above expression, the carrying capacity of the compression member is determined by finding the stress σ_1 from the same chart (Fig. 3).

Magnitude of Imperfections

Many investigators have tried to estimate the magnitude of imperfections in columns based on available experimental data. These estimates differ greatly. An initial deflection of a = L/750 and an eccentricity of loading of e = L/1000 were proposed by Salmon.[7] If the effect of non-homogeneity of material and of unavoidable variation in cross section are also considered, an equivalent initial deflection of a = L/400 should be sufficient to compensate for all probable imperfections in a column. A value of $ec/r^2 = 0.25$ is recommended by the Steel Column Research Committee of the ASCE[8] as a rational allowance for imperfection.

7. "Column," by E. H. Salmon, London, 1921.
8. "Final Report of the Special Committee on Steel Column Research," ASCE Trans., vol. 98, p. 1449, 1933.

End Conditions

In order to take account of the conditions of end support the critical buckling load (P_{cr}) may be written in the form of $P_{cr} = \pi^2 EI/(qL)^2$. The term qL, which may be defined as the effective length of the column, is the length between the points of contraflexure. The values of q for different end conditions are as follows:

(a) Both ends pinned (free to rotate) . . . . . q = 1

(b) Both ends fixed . . . . . q = 1/2

(c) One end fixed and one end free to turn (but not free to move in position . . . . . $q = 1/\sqrt{2}$

(d) One end fixed and one end free from all restraints . . . . q = 2

The selection of the effective length for most columns in practice is a matter of judgment of the engineers. According to the AREA and AASHO specifications the effective length of riveted end steel columns is taken as three-fourths the actual length of the member (q = 3/4). The Steel Column Research Committee of the ASCE mentioned earlier has made a similar recommendation.

Factor of Safety

In most steel structures the allowable design stresses are established with a safety factor with respect to the yielding point of the material. The design is carried out in such a way that the actual stresses do not exceed the working stresses at design load. In airplane design the anticipated maximum loads are multiplied by a factor of safety to obtain that limit load at which the structure is supposed to fail. The two approaches are interchangeable as long as the structure is such that deformations and stresses are linear functions of the load. Structures, such as slender columns, are not of this type, however. As a consequence any column design problem carried out for the design load will give no information on the amount of overload the structure is capable of resisting. It is recommended, therefore, the design procedures similar to those in airplane engineering are to be followed.

Accepted factors of safety for steel structures are from 1.5 to 1.8 for buildings and bridges.

Design Procedure

The following procedure is recommended for the design of compression members (Fig. 3):

1. Estimate the approximate area required and select a column section. Compute the minimum radius of gyration of this section.

2. Enter L/r of the section selected, go vertically downward to the curve corresponding to the end condition, then turn horizontally to the value of $1/\sigma cr$. (Quadrant III).

3. Continue to go horizontally to the given value of σyp and turn vertically upward again to the given value of $\sigma yp/\sigma cr$. (Quadrant IV).

4. From there, go upward to the given value of k and turn horizontally to the value of $1/\sigma_{yp}$. (Quadrant I).

5. Again go horizontally to the given value of σ_{yp} and turn vertically downward to the required value of σ_1. (Quadrant II).

6. Compute the required area A by dividing the product of load and factor of safety n by σ_1 juse determined.

7. If the actual area of the section does not exceed the required area by more than 2 or 3 per cent, the section represents a good choice.

8. If the actual area of the section exceeds the required area by more than 5 per cent, the section is oversafe and uneconomical, and its area can usually be reduced.

9. If the actual area is smaller than the required area, its area should be increased by selecting a new section.

Design Example

The proposed column design is illustrated by a numerical example.

A four in. pipe column 15 feet long with pinned ends is loaded with an axial compression of P. It is required to determine the design load P_w (the factor of safety being assumed as 1.65), if a value of $k = (a + e)\, c/r^2 = 0.25$ is selected. $\sigma_{yp} = 33{,}000$ p.s.i.

The solution follows:

L	=	180 in.
A	=	3.17 sq. in.
I	=	7.23 in. 4
c	=	2.25 in.
r	=	1.51 in.
L/r	=	180/1.51 = 119

Quadrant 3. For L/r = 119, one has $1/\sigma_{cr} = 4.7 \times 10^{-5}$

Quadrant 4. For $1/\sigma_{cr} = 4.7 \times 10^{-5}$ & $\sigma_{yp} = 33{,}000$, one has $\sigma_{yp}/\sigma_{cr} = 1.58$

Quadrant 1. For $\sigma_{yp}/\sigma_{cr} = 1.58$ & k = 0.25, one has $\sigma_1/\sigma_{yp} = 0.48$

Quadrant 2. For $\sigma_1/\sigma_{yp} = 0.48$ & $\sigma_{yp} = 33{,}000$, one has $\sigma_1 = 15{,}500$

$P = \sigma_1 A = 15{,}500 \times 3.17 = 49{,}100$ lb.
But the factor of safety is 1.65,
$P_w = 49{,}100/1.65 = 29{,}800$ lb.

CONCLUSION

A simple general approach for the analysis of columns within elastic range has been developed. The application to practical design problems is simplified to a great extent by the introduction of a four-quadrant graph. A typical design example is given to illustrate the simplicity of the proposed column design procedure. This same general approach may be applied likewise to many other problems, such as the case of columns subjected to different types of transverse loads.

ACKNOWLEDGMENTS

The author wishes to acknowledge the many helpful suggestions given in the preparation of this paper by his colleagues at Michigan State University. He is also indebted to George Winter, M. ASCE, for many valuable discussions several years ago on Cornell University campus related to this paper.

REFERENCES

S. Timoshenko, "Theory of Elastic Stability," McGraw-Hill Book Company, Inc., 1936.

H. W. Westergaard, "Buckling of Elastic Structures," Trans. American Society of Civil Engineering, vol. 85, 1922.

D. H. Young, "Rational Design of Steel Columns," Trans. American Society of Civil Engineering, vol. 101, 1936.

A. A. Jakkula & H. K. Stephenson, "Steel Columns—A Survey and Appraisal of Past Work," Texas Engineering Experiment Station Bulletin No. 91, 1947.

E. H. Salmon, "Column," London, 1921.

"Final Report of the Special Committee on Steel Column Research," ASCE Trans., vol. 98, 1933.

NOTATION

M	-	Bending moment
M'	-	Resultant bending moment
P	-	Axial load
P_{cr}	-	Critical axial load
α	-	P/P_{cr}
a	-	Initial deflection
x, y	-	Rectangular coordinates
L	-	Length of column
e	-	Eccentricity
σ	-	Normal stress, axial or bending
A	-	cross-sectional area
c	-	Distance from neutral axis to outside fibers
I	-	moment of inertia
r	-	Radius of gyration
σ_{yp}	-	Yielding stress
σ_{cr}	-	P_{cr}/A, Critical axial stress
E	-	Young's modulus of elasticity

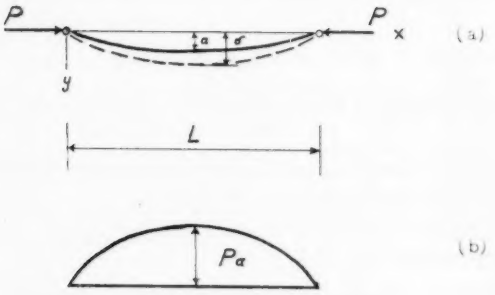

Fig. 1 Compression Member with Initial Curvature

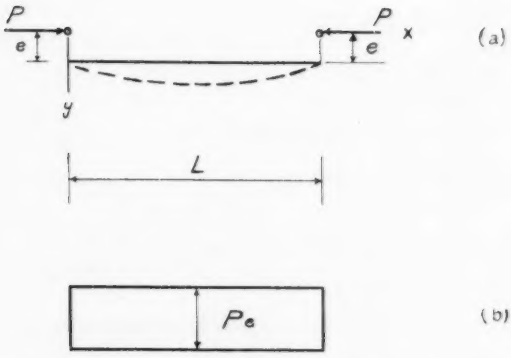

Fig. 2 Compression Member with Eccentricity

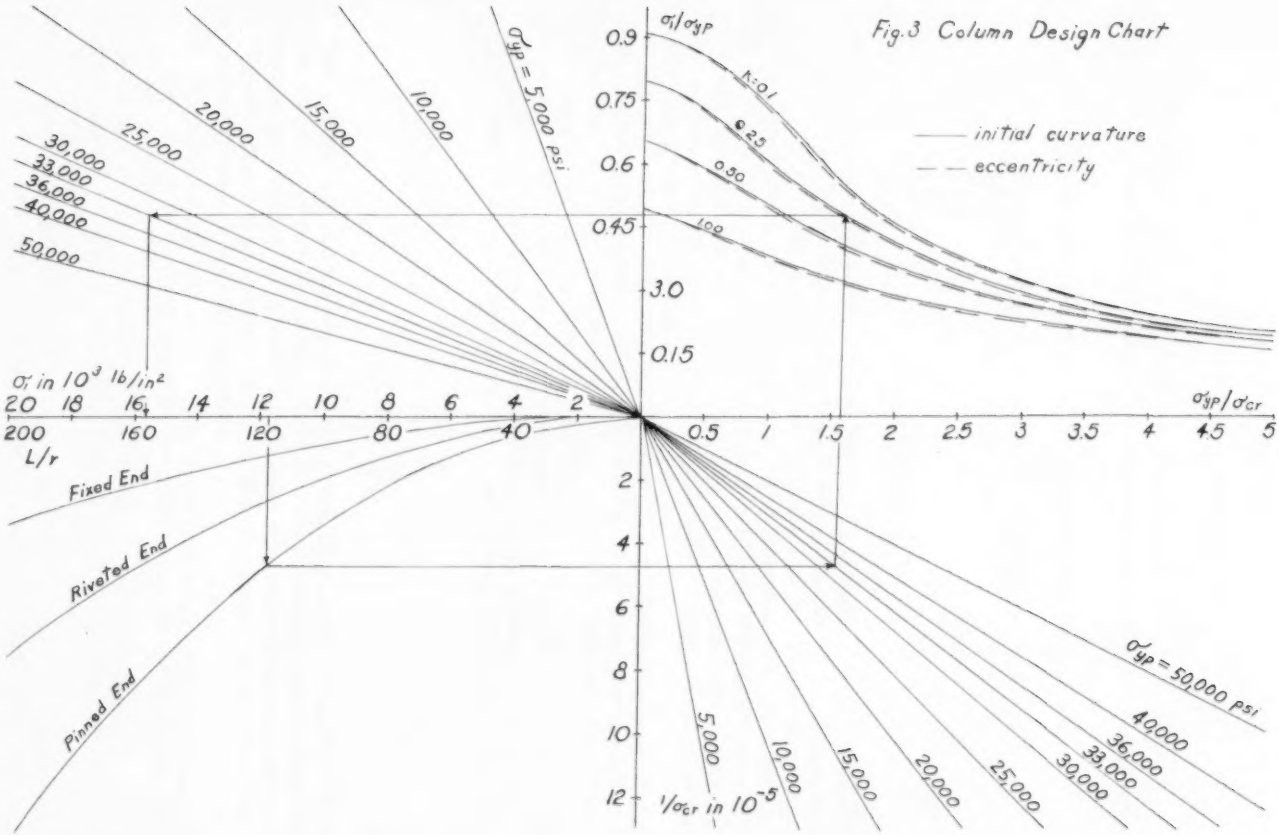
Fig.3 Column Design Chart
σi/σyp
0.9
0.75
0.6
0.45
3.0
0.15
k=0.1
0.25
0.30
1.00
initial curvature
eccentricity
σyp = 50,000 psi
40,000
36,000
33,000
30,000
25,000
20,000
15,000
10,000
5,000
σi in 10³ lb/in²
20 18 16 14 12 10 8 6 4 2
200 160 120 80 40
L/r
Fixed End
Riveted End
Pinned End
σyp/σcr
0.5 1 1.5 2 2.5 3 3.5 4 4.5 5
2
4
6
8
10
12
1/σcr in 10⁻⁵

Paper 1232 ST 3

Journal of the
STRUCTURAL DIVISION
Proceedings of the American Society of Civil Engineers

INELASTIC BEHAVIOR OF IMPULSIVELY LOADED BEAMS

M. J. Greaves[1] and F. T. Mavis,[2] Members ASCE
(Proc. Paper 1232)

SYNOPSIS

This paper presents useful methods for solving design problems involving a simple beam where (a) the applied load is impulsive and (b) the distortions are inelastic. A useful analogy between deflections in the simple beam and moments in an analogous beam is pointed out wherein the analogous beam, with its length corresponding to time, is loaded with the unbalanced impulse applied to the simple beam. This analogy permits a designer who is familiar with the usual concepts of static design to cope with this more difficult problem involving yield and motion.

A non-dimensional characteristic number is proposed which varies directly as the product of the mass of a beam and the "braking" energy of inelastic bending distortion, and inversely as the square of the driving impulse. This number is the link between seemingly different forms of impact and impulsive loads and provides a new means of classifying all such loads on a single basis. This number also facilitates the determination of the dynamic yield resistance of a beam from test data where this resistance is often confounded with inertial resistance.

The Problem

The emphasis in engineering design is generally placed on solutions wherein the materials behave elastically. This is natural because most engineering materials behave elastically when the stresses are within the customary working limits. There are, however, certain situations where it is necessary or desirable to consider inelastic behavior.

Note: Discussion open until October 1, 1957. Paper 1232 is part of the copyrighted Journal of the Structural Division of the American Society of Civil Engineers, Vol. 83, No. ST 3, May, 1957.

1. Development Engr., Arthur G. McKee and Co., Cleveland, Ohio.
2. Prof. and Head, Dept., of Div. Eng., Carnegie Inst. of Technology, Pittsburgh, Pa.

Note: Excerpts from a thesis by Melvin J. Greaves submitted in partial fulfillment of the requirements for the degree of Doctor of Philosophy, Carnegie Institute of Technology.

The problem is further complicated when the applied loads are functions of time. Unfortunately, solutions of problems involving the elastic behavior of impulsively loaded beams(1) and the inelastic behavior of statically loaded beams(2) can not in general be combined by direct superposition. The authors present on the following pages some methods which should prove useful in this area.

Dynamic Analogy

Consider a mass, $\frac{W}{g}$, acted upon by two opposed co-linear forces, $F_{(t)}$ and $R(t)$, directed at the center of gravity of the mass and compatible with the following definitions. $F_{(t)}$ and $R_{(t)}$ are functions of time and not equal for part of the time. At times t_1 and t_2, $F_{(t_1)}$ and $F_{(t_2)}$ are equal to F_y. The value of the integral $\int_{t_1}^{t_3} (F_{(t)} - F_y)\, dt$ is zero. When t is less than t_1 or greater than t_3, $R_{(t)}$ is equal to $F_{(t)}$; when t is between t_1 and t_3, $R_{(t)}$ is equal to F_y.

This problem is encountered when a driving force $F_{(t)}$ moves a heavy object in opposition to dry friction, uniform yield forces, or other steady (limited) resistance, $R_{(t)}$. The resistance can also be due to one or more plastic hinges in a beam where the load $F_{(t)}$ is applied transversely and $\frac{W'}{g}$ is the effective mass of the beam. For a beam of uniform cross section, $\frac{W'}{g}$ can be taken as one-third of the mass of the beam. Fig. 1 shows a well developed plastic hinge produced by an impulsive load.

The motion of the object can be analyzed by means of Newton's laws and simple calculus. The equations are analogous to those relating load, shear and moment for a prismatic beam where: (a) the time coordinate of the motion problem corresponds to distance along the axis of the beam and (b) the quantity (unbalanced force/effective mass) corresponds to the load on the beam. Table 1 illustrates the relations that exist between analogous quantities.

Impulse Characteristic Number

From Table 1

$$x_3 = \frac{1}{W'/g}\, I_a\, k\Delta t$$

$$F_y\, x_3 = \frac{1}{W'/g}\, I_a\, k\, (F_y \Delta t)$$

where

- E_b = braking work, $x_3 F_y$
- I_a = accelerating impulse
- I_b = braking impulse, $F_y \Delta t$
- W/g = mass
- W'/g = effective mass

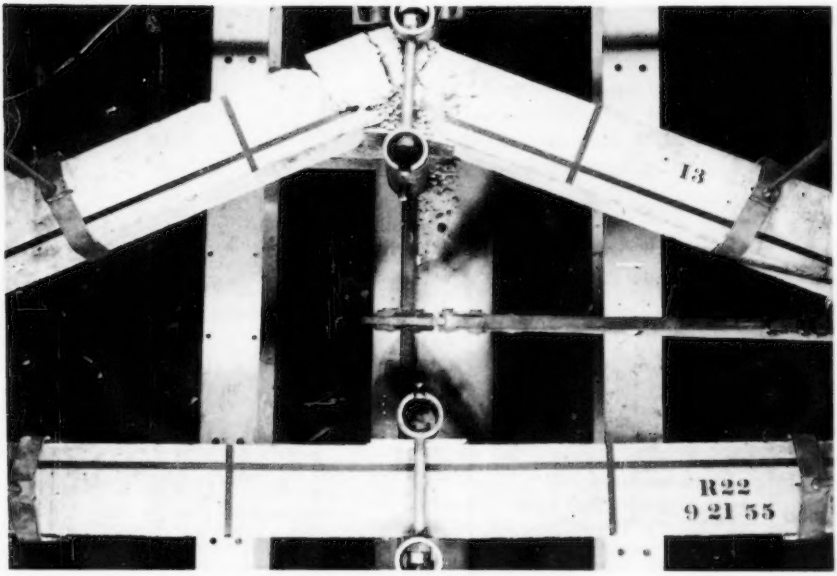

Fig. 1. Typical "plastic hinge" after an 8.5 kip test.

$$E_b = \frac{1}{W'/g}(I_a)\,k\,(I_b)$$

$$\frac{W'}{g}E_b = (kab)\,I^2$$

and

$$\begin{cases} a = I_a/I \\ b = I_b/I \\ c = W/W' \\ I = \text{applied impulse } \int F_{(t)}\,dt \end{cases}$$

The impulse characteristic number is defined as:

$$N_I = kabc = \frac{WE_b}{gI^2}$$

Only that part of the applied impulse which corresponds to the interval of time between t_1 and t_3 is effective. The factor "b" takes this into account. Furthermore, only the net or accelerating impulse sets the mass in motion. The factor "a" takes this into account. Finally, the shape of the impulse is taken into account by the factor "k".

The above methods can be adapted to a step-function impulse, $2\,I_a = 2\,F\delta\,t$, acting on a simple beam. Taking one-half of the beam as a free-body:

TABLE 1

Analogous Beam		Motion		
Load	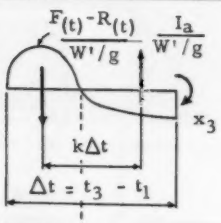	Acceleration $\frac{F}{W'/g}$	$\frac{dv}{dt}$	$\frac{d^2x}{dt^2}$
Shear	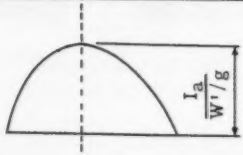	$\int \frac{F}{W'/g}\,dt$	Velocity v	$\frac{dx}{dt}$
Moment	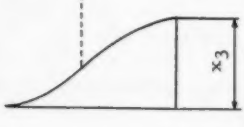	$\iint \frac{F}{W'/g}\,dtdt$	$\int v\,dt$	Displacement x

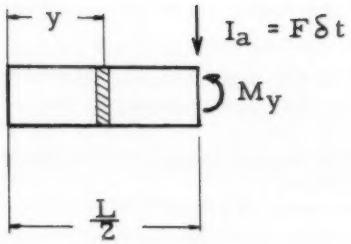

M_y is the dynamic yield moment of the beam, assumed to be constant and small compared to F x L/2. "w" is the weight per unit length, assumed to be constant and W is the total weight of one-half of the beam.

The polar moment of inertia $J = \int_0^{L/2} \frac{w}{g} y^2 \, dy = \frac{1}{3}\frac{W}{g}(\frac{L}{2})^2$

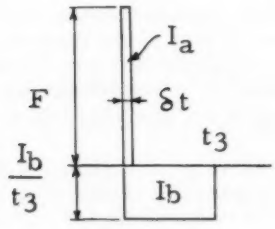

I_a is the driving impulse which in this case is also approximately equal to the applied impulse, I.

I_b is the braking impulse due to the dynamic yield moment which is effective only while the beam is actually yielding.

The angular impulse as a function of time is:

$$(\tfrac{L}{2})\, I_{(t)} = (\tfrac{L}{2})\, I_a\, (1 - \tfrac{t}{t_3})$$

The corresponding change in the angular momentum is $J\frac{d\theta}{dt}$. Since the motion of the beam starts from rest, this angular impulse is equal to the angular momentum.

$$(\tfrac{L}{2})\, I_a\, (1 - \tfrac{t}{t_3}) = J\, \tfrac{d\theta}{dt}$$

Multiplying by $\frac{I_b}{t_3}\, dt$ and integrating

$$\frac{I_a I_b}{t_3}\,\frac{L}{2}\int_0^{t_3} (1 - \tfrac{t}{t_3})\, dt = \frac{I_b}{t_3} J \int_0^{\theta_3} d\theta$$

$$\frac{I_a I_b}{t_3}(\tfrac{1}{2}t_3) = \frac{J}{L/2}(\frac{I_b}{t_3}\theta_3) = \frac{1}{3}(\frac{W}{g})\frac{L}{2}(\frac{I_b}{t_3})\theta_3$$

$$\frac{1}{2} I_a I_b = \frac{1}{3}\,\frac{W}{g} \text{ (braking work)}$$

Since $I \approx I_a = I_b$ the impulse characteristic number is

$$N_I = \frac{W}{g}\,\frac{E_b}{I^2} = kabc = 1.5$$

where E_b = braking work or energy absorbed in inelastic yielding
k = 0.5 since both accelerating and braking impulses are rectangular
$a \approx 1$ since the dynamic yield resistance is assumed to be small compared to the force of the impulse
b = 1 since all of the applied impulse is effective
c = 3 since the two halves of the beam rotate as rigid bodies about their reaction points.

Dynamic Yield Resistance

The concepts and methods behind the impulse characteristic number can be employed to determine the dynamic yield resistance of any beam when sufficient data are available. The instantaneous resistance that a beam can offer to a transverse impulsive force will be called its dynamic beam strength. The dynamic beam strength is equal to the sum of the dynamic yield resistance and the inertial resistance of the beam.

The dynamic yield resistance of a beam involves bending stresses only. Since the dynamic yield stress of a material is generally greater than its static yield stress, the dynamic yield resistance of a beam is correspondingly greater than its static yield resistance.

The inertial resistance involves weights and accelerations only, and it is equal to

$$\sum \frac{\Delta W \bar{a}}{g}$$ where ΔW = weight of an element of the beam
$\bar{a}$ = acceleration of that element
g = acceleration of gravity

For example, the authors conducted a series of tests in which the load applied to the beam can be represented approximately by relations of the form

$$F_{(t)} = F_o \exp - \frac{t}{\lambda e} \qquad (1)$$

For one series of tests this relation is:

$$F_{(t)} = 8500 \exp - \frac{t}{0.0135\,e} \text{ lb.}$$

Fig. 6 shows this function plotted along with measured loads from one test of this series.

The "driving" impulse due to this load is equal to:

$$8500 \int_{t_1 = 0}^{t_3} (\exp - \frac{t}{0.0135\,e})\,dt \qquad (2)$$

The "resisting" impulse due to the yield resistance of the beam is:

$$\int_{t_1 = 0}^{t_3} F_y\,dt \qquad (3)$$

Assuming an average dynamic yield resistance, F_y, equal to 4150 lbs which is 15 per cent more than the ultimate strength of the control beams t_3 is 0.061 sec from equations (2) and (3).

In other words, if elastic deflections are neglected (the maximum elastic deflection is about five per cent of the maximum inelastic deflection), the beam which is at rest at time $t = 0$ is again at rest at time $t = 0.061$ sec.

Considering each half of the beam as a rigid free body:
The polar moment of inertia is

$$J = 2\int_0^{L/2} \frac{w}{g} \dot{y}^2 dy = \frac{2}{3}\frac{w}{g}\left(\frac{L}{2}\right)^3 = \frac{w}{3g}\frac{L}{2}\left(\frac{L}{2}\right)^2$$

$$J = \frac{W}{3g}\left(\frac{L}{2}\right)^2$$

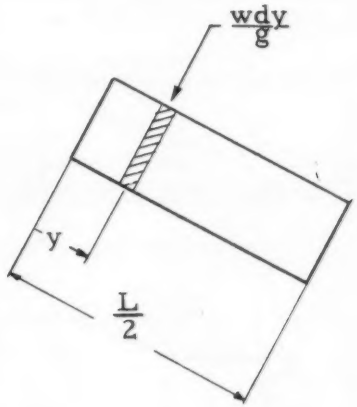

The angular momentum is $J\frac{d\theta}{dt}$.

The angular impulse as a function of time:

$$\frac{L}{2}\int_0^t \left[8500 \exp - \frac{t}{0.0135e} - 4150\right] dt =$$

$$\frac{L}{2}\left[8500 \times 0.0135e \left(1 - \exp - \frac{t}{0.0135e}\right) - 4150t\right]$$

Equating the angular impulse to the change in the angular momentum and substituting $\frac{dx}{dt}$ for $\frac{L}{2}\frac{d\theta}{dt}$

$$\frac{L}{2}\left[312 \left(1 - \exp - \frac{t}{0.0135e}\right) - 4150t\right] = \frac{L}{2}\frac{W}{3g}\frac{dx}{dt}$$

$$312\int dt - 312\int\left(\exp - \frac{t}{0.0135e}\right) dt - 4150\int t dt = \frac{W}{3g}\int dx$$

$$312t - 312 \times 0.0135e \left(1 - \exp - \frac{t}{0.0135e}\right) - \frac{4150t^2}{2} = \frac{W}{3g}x$$

$$312t - 11.45 \left(1 - \exp - \frac{t}{0.0135e}\right) - 2075t^2 = \frac{x}{8.05}$$

For $t = 0.061$ sec the final calculated deflection $x_3 = 16$ in. which agrees with the observed value.

These calculations, based on an assumed yield resistance of 4150 lb, predict the correct maximum deflection of 16 in. Hence 4150 lb is the average dynamic yield resistance for the over-all dynamic test.

Similar calculations, based on the same yield resistance, predict equally accurate deflections for other series of tests wherein different loads were applied to similar beams.

The average dynamic yield resistance of a typical beam tested by Mavis and Richards[3] can be computed from observed quantities. The weight of this beam was 150 lb. No algebraic equations are available to characterize the loading function. However, the necessary data can be determined graphically from Fig. 2, which shows load as a function of time and load as a function of deflection.

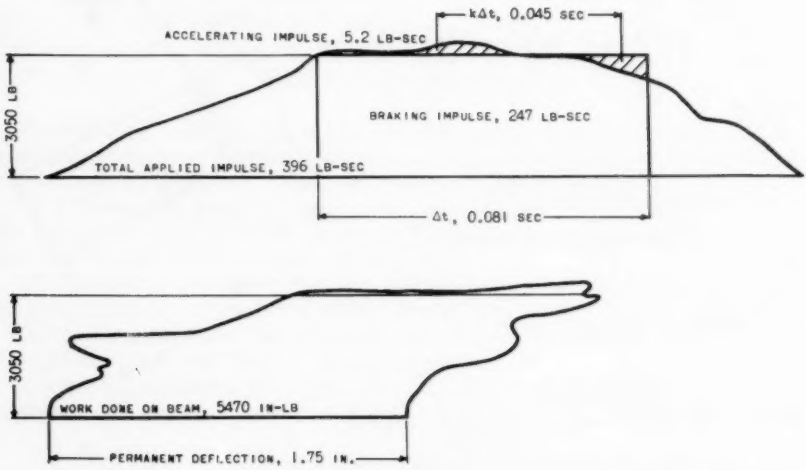

Fig. 2. Dynamic balance diagram for a typical "near blast" test.

The impulse characteristic number from these data is

$$N_I = \frac{W E_b}{g I^2} = \frac{150 \times 5470}{386 \times 396^2} = 0.014$$

The measured load and deflection curves from which the value for "E_b" and "I" were taken are shown in Fig. 2. The yield resistance, F_y, was found by trial to be 3050 lb to make the quantity

$$N_I = kabc = 0.56 \times 0.013 \times 0.62 \times 3 = 0.014$$

This is the correct value and confirms the value of 3050 lb as the average dynamic yield resistance of the beam. Similar control beams had an ultimate strength of 2900 lb.

Equivalent Impact

The impulse characteristic number has an additional connotation for the special case where the impulse is produced by an inelastic collision. For example, let a hammer of weight W_1, and velocity v_a strike a beam of weight, W_2.

$$\text{The impulse } I = \frac{W_1 v_a}{g} \qquad I^2 = 2\frac{W_1}{g}\left(\frac{W_1 v_a^2}{2g}\right)$$

$$N_I = \frac{W_2 E_b}{g I^2} = \frac{W_2 E_b}{2 W_1 \frac{W_1 v_a^2}{2g}} = \frac{1}{2}\left(\frac{W_2}{W_1}\right)\left(\frac{\text{Energy absorbed by inelastic flexure}}{\text{Kinetic energy of blow}}\right)$$

In this form the impulse characteristic number is the product of a weight ratio and an energy ratio. To find the energy ratio for a simply supported beam,

Assume: (1) The effective mass of the beam at the time of the initial impact is $\frac{17W_2}{35g}$.

(2) The hammer and beam remain in contact after initial impact.

(3) The energy remaining after initial impact is absorbed by the beam in inelastic flexure.

By the law of conservation of momentum the common velocity which will be established at the first moment of impact is:

$$v_b = \frac{W_1}{W_1 + \frac{17}{35} W_2} v_a$$

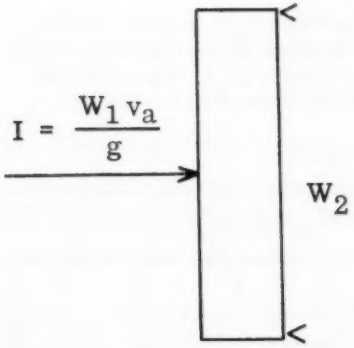

The kinetic energy before impact is:

$$\frac{W_1 v_a^2}{2g}$$

The kinetic energy after impact, which must be absorbed by inelastic flexure subsequently, is

$$\frac{(W_1 + \frac{17}{35} W_2)\, v_b^2}{2g}$$

The energy ratio is:

$$\frac{\left[\begin{matrix}\text{Energy absorbed}\\ \text{by inelastic flexure}\end{matrix}\right]}{\left[\begin{matrix}\text{Kinetic energy}\\ \text{of hammer}\end{matrix}\right]} \quad \frac{\frac{W_1 + \frac{17}{35}W_2}{2g}\left[\frac{W_1}{W_1 + \frac{17}{35}W_2}\right]^2 v_a^2}{\frac{W_1 v_a^2}{2g}} = \frac{W_1}{W_1 + \frac{17}{35}W_2}$$

The impulse characteristic number is:

$$N_I = \frac{1}{2}\frac{W_2}{W_1}\frac{W_1}{W_1 + \frac{17}{35}W_2} = \frac{1}{2}\frac{W_2}{W_1 + \frac{17}{35}W_2}$$

The impulse characteristic number permits many forms of destructive impulse tests to be compared on a single basis. For example, the tests of Mavis and Richards,(3) Simms,(4) and Mylrea(5) can be numerically ordered along with the authors' tests as shown in Table 2.

Table 3 illustrates how a second comparison can also be made in which the ratio of weight of an equivalent hammer to weight of beam is computed which will correspond to the impulse characteristic number of the given test.

Fig. 3 shows the computed impulse characteristic number as a function of the weight ratio. The relative order of the above series of tests are indicated on this curve.

The significance of the impulse characteristic number is now evident. It is a measure of the quality of an impulse which makes some impulses more destructive than others, although the $\int F dt$ is the same. In the tests conducted by Mavis and Richards, 396 lb-sec were required to produce 1.75 in. permanent deflection in a beam having a static load capacity of 2900 lb, whereas in the tests conducted by Mavis and Greaves, beams of about the same weight required only 311 lb-sec for complete destruction even though the static load capacity was 3600 lb. In the first case the impulse characteristic number was 0.014. The corresponding equivalent hammer would be a 5300 lb weight moving horizontally with a velocity of 29 in. per sec. In the second case the impulse characteristic number was 0.15. The corresponding equivalent hammer would be a 410 lb weight moving horizontally with a velocity of 290 in. per sec.

The equivalent to a conventional short time test would be a very heavy weight moving at a low velocity. The impulse characteristic number would be very small. At the other extreme, a small projectile hitting a massive target would correspond to a very large impulse characteristic number.

Relative Impact Resistance

Destructive impulse loads on a beam are initially resisted by the inertia (weight) of the member. Subsequently the kinetic energy associated with this

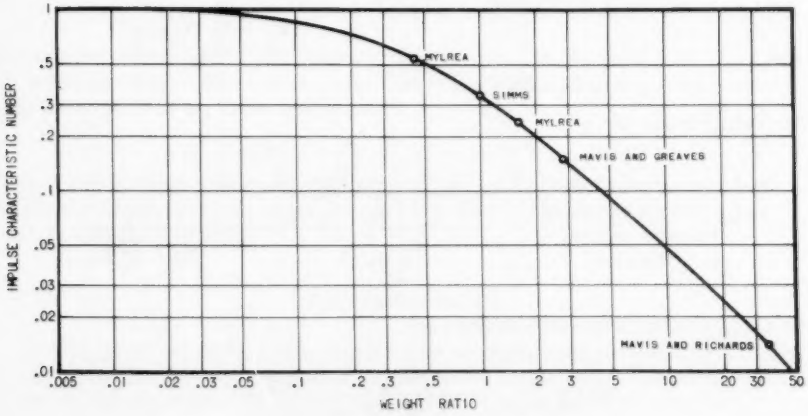

Fig. 3. Impulse characteristic number for various weight ratios.

TABLE 2

(1) Mylrea Series I Tests $W_1 = 560$ lb $W_2 = 1280$ lb

$$N_I = \frac{1}{2} \times \frac{1280}{560 + \frac{17}{35} \times 1280} = \text{- - - - - - - - - - - -} \quad 0.54$$

(2) Simms $W_1 = W_2$

$$N_I = \frac{1}{2} \times \frac{1}{1 + \frac{17}{35}} = \text{- - - - - - - - - - - -} \quad 0.34$$

(3) Mylrea Series II Tests $W_1 = 2040$ lb $W_2 = 1280$ lb

$$N_I = \frac{1}{2} \times \frac{1280}{2040 + \frac{17}{35} \times 1280} = \text{- - - - - - - - - - - -} \quad 0.24$$

(4) Mavis and Greaves Series 50 Tests

$I = 311$ lb-sec
$W = 145$ lb
$E_b = 38,000$ in-lb

$$N_I = \frac{WE_b}{gI^2} = \frac{145 \times 38000}{386 \times 311^2} = \text{- - - - - - - - - - - -} \quad 0.15$$

(5) Mavis and Richards

$I = 396$ lb-sec
$W = 150$ lb
$E_b = 5470$ in-lb

$$N_I = \frac{WE_b}{gI^2} = \frac{150 \times 5470}{386 \times 396^2} = \text{- - - - - - - - - - - -} \quad 0.014$$

TABLE 3

(1)	Mylrea Series I Tests	$W_1 = 560$ lb	$W_2 = 1280$ lb	
		$\frac{W_1}{W_2} = \frac{560}{1280}$	$\frac{W_1}{W_2} =$ - - - -	.44
(2)	Simms	$W_1 = W_2$	$\frac{W_1}{W_2} =$ - - - -	1.0
(3)	Mylrea Series II Tests	$W_1 = 2040$ lb	$W_2 = 1280$	
		$\frac{W_1}{W_2} = \frac{2040}{1280}$	$\frac{W_1}{W_2} =$ - - - -	1.6
(4)	Mavis and Greaves	$\frac{1}{2} \times \frac{W_2}{W_1 + \frac{17}{35} W_2} = 0.15$		
		$W_2 = 0.30 W_1 + 0.15 W_2$		
		$\frac{W_1}{W_2} = \frac{1 - 0.15}{0.30}$ or $\frac{W_1}{W_2} =$ - - - -		2.8
(5)	Mavis and Richards	$\frac{1}{2} \times \frac{W_2}{W_1 + \frac{17}{35} W_2} = 0.014$		
		$W_2 = 0.028 W_1 + 0.01 W_2$		
		$\frac{W_1}{W_2} = \frac{1 - 0.01}{0.028}$ or $\frac{W_1}{W_2} =$ - - - -		35

motion must be absorbed to bring the member to rest. Similarly the excess load impulse, that impulse of load in excess of the flexural resistance of the beam, appears as momentum which must be absorbed before the loaded system comes back to rest. When the flexural resistance is high and the excess load impulse is low, a relatively large portion of the load impulse itself is ineffective in causing damage. This is especially true when the load impulse is applied over a time interval longer than the natural period of vibration of the beam.

The impulse characteristic number facilitates an orderly arrangement of the factors which influence a beam's capacity to resist an impulsive load.

By definition $N_I = \frac{WE_b}{gI^2} = kabc$

Solving for the square of the applied impulse, $I^2 = (\frac{1}{kc})(\frac{W}{g})\, E_b\, (\frac{1}{ab})$ where I is the impulse applied to a beam of weight W and E_b is the amount of energy absorbed by the beam. The effect of an increase in yield resistance F_y is a decrease in "a" and "b" and a corresponding increase in the quantity $\frac{1}{ab}$. The factor $\frac{1}{kc}$ is generally a constant for any particular problem and its value usually falls between the limits of 1/2 and 2/3.

The impulse, I, a given beam can resist is therefore seen to depend upon the weight, energy absorbing capacity and strength of the beam. Specifically,

(1) If two beams of different weights are otherwise identical the heavier beam can resist the larger impulse.
(2) If two beams with different capacities of absorbing energy are otherwise identical, the beam with the larger energy absorption capacity can resist the larger impulse.
(3) If two beams have different strengths but are otherwise identical, the stronger beam can resist the larger impulse.

The authors have experimentally verified these observations many times.

The Philadelphia grain elevator explosion(6) shown in Figs. 4 and 5 illustrates the role of mass and strength as well as energy absorption capacity in resisting blast loads. (a) The reinforced concrete and structural steel both had high strength and energy absorption capacity. The reinforced concrete remained intact, but the structural steel failed because it lacked sufficient mass. (b) The reinforced concrete and brick walls both had a large mass. The brick work disintegrated because it lacked sufficient strength. (c) Plate glass windows and panels of corrugated steel siding in near-by buildings had comparable mass and strength. The siding deformed but did not fail whereas the glass was shattered because it lacked sufficient energy absorption capacity.

Experimental Results

During the course of the investigation reported in this paper the authors tested each hypothesis and theoretical conclusion by a full scale laboratory test. Beams were tested in the specially constructed testing machine shown in Fig. 1. The loads were produced by a spring loading mechanism and were applied instantly by fracturing a temporary link.

Fig. 4. Damage to structural steel by grain elevator explosion. (Courtesy Dr. C. F. Peck, Jr., Carnegie Institute of Technology, Pittsburgh, Pennsylvania.)

Typical load-time and reaction-time records for these tests are shown in Figs. 6 and 7. The solid lines represent the formulas shown in the upper right. The measured loads and the reactions are represented by the dotted lines. They were measured by means of electrical resistance strain gages and recorded on film by means of a high speed camera. The initial spring load for this test was 8.5 kips.

The high speed camera was also used to measure deflections and rotations of the end tangents. Fig. 8 shows the angular deflection and angular velocity of the end tangents as a function of time for one test where the initial spring load was 6.5 kips.

The beams for which the above experimental data apply were 4.2 in. wide, 5.9 in. deep and 78 in. long, centrally loaded on a 72 in. span. They were made of reinforced concrete and weighed 24 lb per foot. Static load-deflection curve I-2 and dynamic load-deflection curve I-5 shown in Fig. 9 are typical. The dynamic load-deflection curve is from a test in which the initial spring load was 7.5 kips.

CONCLUSIONS

The equations of motion for beams under destructive impulse loads are analogous to those relating load, shear and moment in an analogous beam

Fig. 5. Damage to reinforced concrete by grain elevator explosion. (Courtesy Dr. C. F. Peck, Jr., Carnegie Institute of Technology, Pittsburgh, Pennsylvania.)

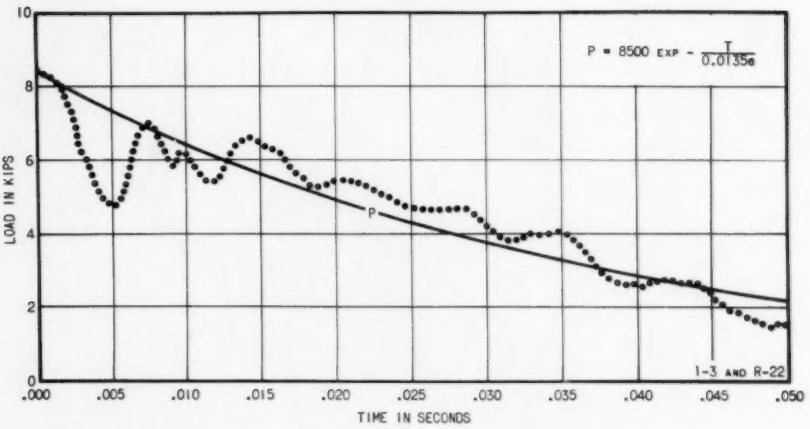

Fig. 6. Typical load-time curve for an 8.5 kip test.

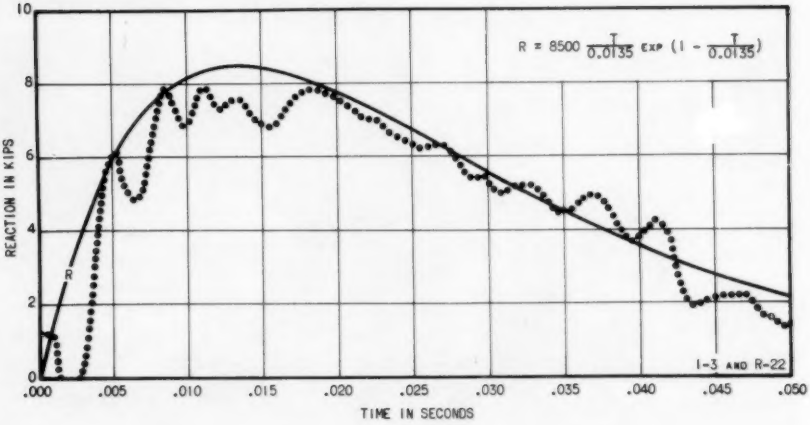

Fig. 7. Typical reaction-time curve for an 8.5 kip test.

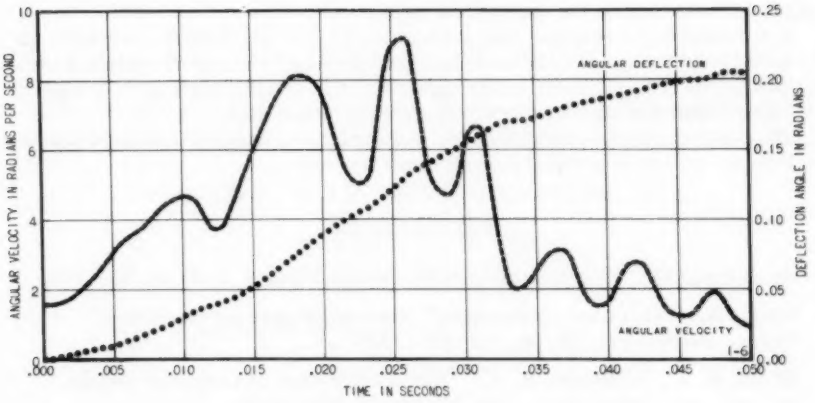

Fig. 8. Typical angular deflection-time and angular velocity-time curves for a 6.5 kip test.

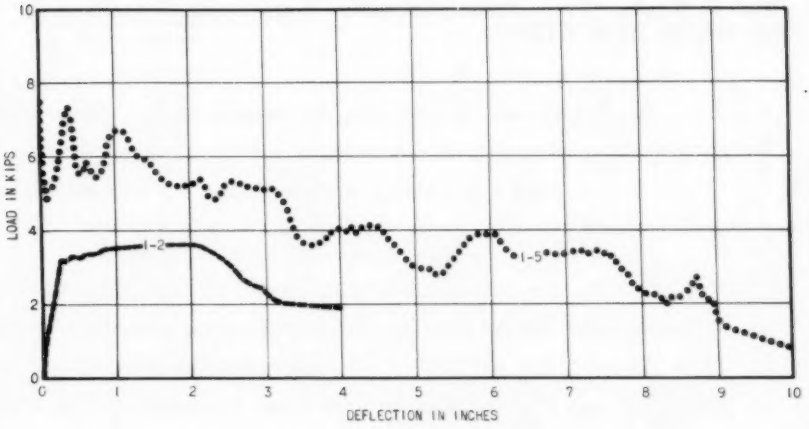

Fig. 9. Typical load-deflection curves for a destructive static and dynamic test.

where (a) the time coordinate of the motion problem corresponds to distance along the axis of the beam, and (b) the quantity (unbalanced force/effective mass) corresponds to the load on the beam.

A dimensionless impulse characteristic number which varies directly as the product of the mass of a beam and the "braking" energy of inelastic bending distortion and inversely as the square of the driving impulse is a significant parameter for inelastic beam design and research.

The performance of a beam under a destructive impulse-load depends on its weight, energy absorbing capacity and strength.

BIBLIOGRAPHY

1. Boussinesq, J., "Application des Potentiels," Paris, 1885 pp. 435-577.

2. Nadai, A., "Theories of Strength," Journal of Applied Mechanics Trans., ASME, Vol. 55, pp. 111-129 (1933).

3. Mavis, F. T., Richards, F. A., "Impulse Testing of Concrete Beams," Journal, Am. Concr. Inst., Vol. 27, pp. 93-102 (1955).

4. Simms, L. G., "Actual and Estimated Impact Resistance of Some Reinforced Concrete Units Failing in Bending," Journal, Inst. Civ. Eng., Vol. 23, pp. 163-179 (1945).

5. Mylrea, T. D., "Effects of Impact on Reinforced Concrete Beams," Proceedings, Highway Research Board, National Research Council, Vol. 18, pp. 130-139 (1938) and Journal, Am. Concr. Inst., Vol. 11, pp. 581-596 (1940).

6. Peck, C. F., Jr., "Philadelphia Explosion," Engineering News-Record, Vol. 156, No. 20, p. 8 (1956).

Paper 1233 ST 3

Journal of the
STRUCTURAL DIVISION
Proceedings of the American Society of Civil Engineers

ANALYSIS OF MULTI-STORY BUILDING FRAMES

T. F. Hickerson,[1] M. ASCE
(Proc. Paper 1233)

INTRODUCTION

The analysis of multi-story building frames presented here is based on the well known slope-deflection theorem. Applying statical equilibrium at each joint and in every story of the frame gives as many equations as unknowns, but the task of solving these equations is prohibitive. Hence approximate methods converging rapidly toward accuracy are desirable.

Notation

S = Story shear.

h = story height.

M = $S \times h$ = story moment; M_1 referring to first story, etc.

K = Stiffness factor = moment of inertia divided by length of member.

ΣK_J = Sum of K's of all members meeting at a joint.

ΣK_C = Sum of K's of all columns in a story, ΣK_L and ΣK_U sometimes representing ΣK_C in two adjacent stories.

R = $\frac{1}{12} M/\Sigma K_C$; R_1 referring to first story, etc.

Δ = Sidesway (assumed constant for each column in a story).

E = Modulus of elasticity.

$\times$ = $E \times \frac{\Delta}{h}$ = sidesway ratio; x_1 (1st story) = $E \times \frac{\Delta_1}{h_1}$; $x_2 = E \times \frac{\Delta_2}{h_2}$, etc.

θ = $E \times$(true joint rotation), positive when clockwise; θ_1, θ_2, etc., applying to joints 1, 2, etc., while $\bar{\theta}_1$, $\bar{\theta}_2$, etc., represent preliminary rotations in floors 1, 2, etc.

Note: Discussion open until October 1, 1957. Paper 1233 is part of the copyrighted Journal of the Structural Division of the American Society of Civil Engineers, Vol. 83, No. ST 3, May, 1957.

1. Formerly Prof. of Civ. Eng., Univ. of North Carolina, Chapel Hill, N. C.

n = Number of columns in a story (applying only to cases when all the columns are alike.)

The Joint Equation

It will be assumed that the end tangents of all members meeting at a joint rotate through the same angle.

Applying $\Sigma M = 0$ at any joint [(say joint 1 (J = 1) in Columns A, Fig. 1)], we have, by the slope-deflection theorem:

$$2K_1(2\theta_1 + \theta_o - 3x_1) + 2K_2(2\theta_1 + \theta_2 - 3x_2) + 2K_{G1}(2\theta_1 + \theta_1') = 0 \qquad (1)$$

Dividing by 2, and solving, we get

$$\theta_1 = \frac{3(K_1x_1 + K_2x_2) - K_1\theta_o - K_2\theta_2 - K_{G1}\theta_1'}{2\Sigma K_J}, \qquad (2)$$

where $\Sigma K_J = K_1 + K_2 + K_{G1}$ at joint 1.

For convenience of computation, Eq. (2) is written:

$$\theta_1 = 3\left[\left(\frac{K_1}{2\Sigma K_J}\right)x_1 + \left(\frac{K_2}{2\Sigma K_J}\right)x_2\right] - \left(\frac{K_1}{2\Sigma K_J}\right)\theta_o - \left(\frac{K_2}{2\Sigma K_J}\right)\theta_2 - \left(\frac{K_{G1}}{2\Sigma K_J}\right)\theta_1', \qquad (3)$$

in which the quantities within the parentheses represent both rotation and carry-over factors, as shown by arrows (see Figs. B). These factors (totaling 0.5 at each joint) depend entirely upon the rigidity of the framework-and they can be calculated prior to the analysis.

If, as an approximation, the rotations at the far ends of the members are assumed equal to that at the near end (J), that is, if $\theta_o = \theta_J$, $\theta_2 = \theta_J$, etc., Eq. (2) becomes (with J = 1):

$$\theta_1 \text{ (1st approx.)} = \frac{K_1x_1 + K_2x_2}{\Sigma K_J}, \qquad (4)$$

which is written:

$$\theta_1 \text{ (1st approx.)} = \left(\frac{K_1}{\Sigma K_J}\right)x_1 + \left(\frac{K_2}{\Sigma K_J}\right)x_2. \qquad (5)$$

Similarly, we have

$$\theta_2 \text{ (1st approx.)} = \left(\frac{K_2}{\Sigma K_J}\right)x_2 + \left(\frac{K_3}{\Sigma K_J}\right)x_3, \text{ etc.,} \qquad (6)$$

where $\Sigma K_J = K_2 + K_3 + K_{G2}$ at joint 2.

If the bases of the columns are fixed ($\theta_o = 0$, $\theta_o' = 0$, etc.); Eq. (4) becomes:

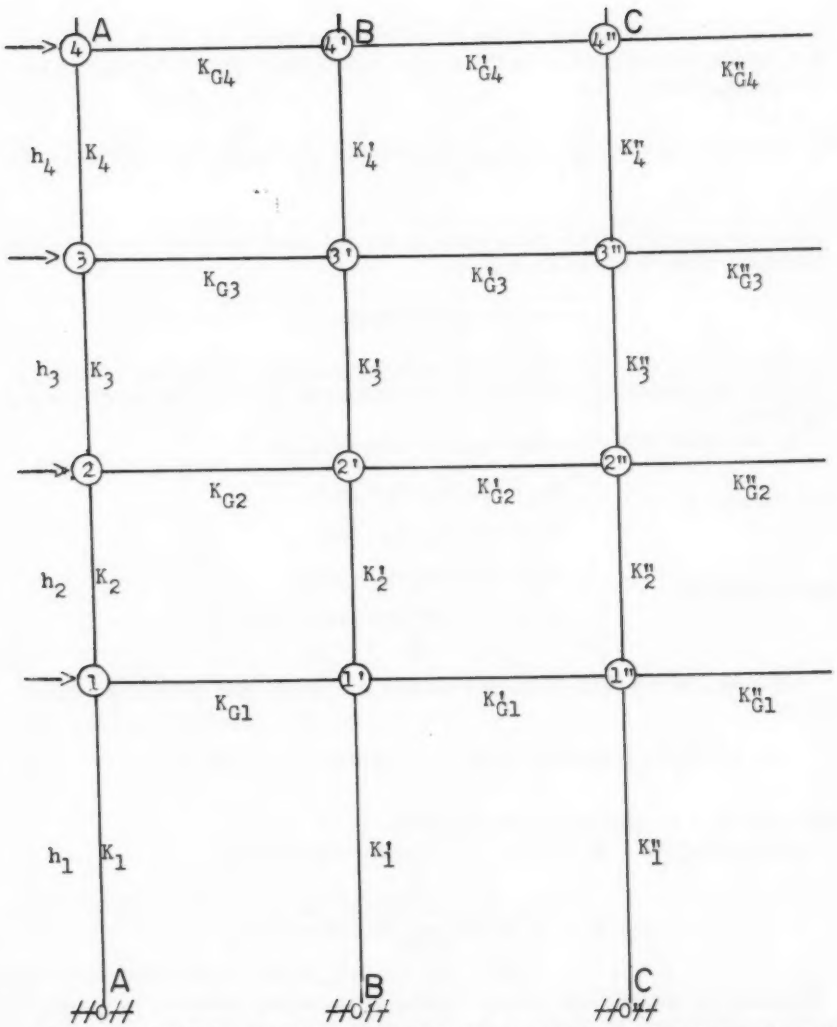

Fig. 1- BUILDING FRAME[Left half of symmetrical 6-Column Frame]

$$\theta_1 \text{ (1st approx.)} = \frac{K_1x_1+K_2x_2}{\Sigma K_J - \frac{1}{3}K_1} = [(\frac{K_1}{\Sigma K_J})x_1+(\frac{K_2}{\Sigma K_J})x_2]\times\frac{\Sigma K_J}{\Sigma K_J - \frac{1}{3}K_1}. \quad (7)$$

For the second approx. of the θ's in the first floor, Eq. (3) is to be used. But for the second approx. of the θ's in upper floors, Eq. (3) is slightly rearranged. Thus:

$$\theta_2 \text{ (2nd approx.)} = \frac{3}{2}[(\frac{K_2}{\Sigma K_J})x_2+(\frac{K_3}{\Sigma K_J})x_3]-(\frac{K_2}{2\Sigma K_J})\theta_1-(\frac{K_3}{2\Sigma K_J})\theta_3-(\frac{K_{G2}}{2\Sigma K_J})\theta_2', \quad (8)$$

where the quantity within the bracket is Eq. (6) itself (already calculated and written in Figs. B of the Examples.)

The Story Equation

Let θ_U, θ'_U, etc. equal rotations at the upper joints of any story, while θ_L, θ'_L, etc., equal the rotations at corresponding joints in the lower floor of the story.

By the slope deflection theorem, we have (Fig. 2):

For Column A:
$$M_{UL} = 2K(2\theta_U+\theta_L-3x);$$
$$M_{LU} = 2K(2\theta_L+\theta_U-3x).$$

For Column B:
$$M'_{UL} = 2K'(2\theta'_U+\theta'_L-3x);$$
$$M'_{LU} = 2K'(2\theta'_L+\theta'_U-3x); \text{ etc.}$$

Applying $\Sigma M = 0$ (Fig. 2) to the columns in a story, and collecting terms, we have

$$6K(\theta_U+\theta_L)+6K'(\theta'_U+\theta'_L)+ \ldots . -12(K+K'+\ldots)+M = 0, \quad (9)$$

where **M** = S × h = (Shear) × (Story height).

Letting $\Sigma K_C = K + K' + K'' + \ldots$, and solving, we get

$$x = R + \frac{K(\theta_U+\theta_L)+K'(\theta'_U+\theta'_L)+ \ldots .}{2\Sigma K_C}. \quad (10)$$

Knowing the loading and column rigidities, the values of R can be written opposite each story, as shown in the Examples.

For columns symmetrical about a vertical center line of the frame, the θ's on the leeward side equal those in corresponding positions on the windward side, hence Eq. (10) becomes:

$$x = R + \frac{K(\theta_U+\theta_L)+K'(\theta'_U+\theta'_L)+ \ldots .}{\Sigma K_C}, \quad (11)$$

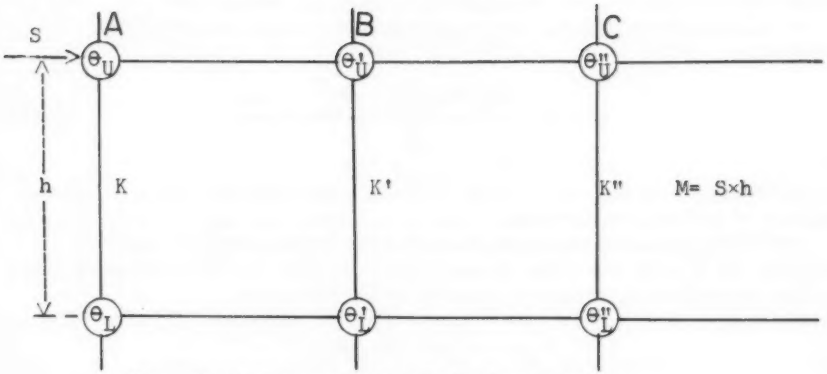

Fig. 2- Any Story of a Building Frame

(a) 5-Column Symmetrical Frame: $\Sigma K_G = 2K_{G2} + 2K'_{G2}$

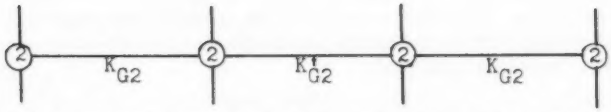

(b) 4-Column Symmetrical Frame: $\Sigma K_G = 2K_{G2} + K'_{G2}$

(c) 3-Column Symmetrical Frame: $\Sigma K_G = 2K_{G2}$

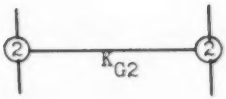

(d) 2-Column Symmetrical Frame: $\Sigma K_G = K_{G2}$

Fig. 3-Symmetrical Frames (2nd Floor)

where the θ's include only one-half the total of the story.

If the columns in a story have equal rigidity (K = K', etc.), Eq. (10) becomes:

$$x = R + \frac{(\theta_U+\theta_L)+(\theta_U'+\theta_L')+ \cdots}{n}, \tag{12}$$

in which the θ's of the left (or right) half only are included; and n = the total number of columns in the story.

Eqs. (3) and (10-12) are exact formulas for joint and story rotations. Knowing the θ's for the joints in every floor, and the x's for each story, the column moments are readily calculated by the formulas:

$$\begin{aligned} M_{NF} &= -2K(3x-2\theta_N-\theta_F), \\ M_{FN} &= -2K(3x-\theta_N-2\theta_F), \end{aligned} \tag{13}$$

in which θ_N and θ_F refer to the "near" and "far" ends of the column.

If the external wind moments are clockwise, the θ's and x's are properly positive, but the column moments are left-handed or negative, as shown by Eq. (13), since they are, by definition, resisting (or reactive moments).

Since the girders in any floor are considered to move horizontally, that is, with no sidesway, we have (by Fig. 1),

$$M(\text{Girder}) = 2K_G(2\theta + \theta'), \text{ etc.} \tag{14}$$

Note: To avoid a preponderance of negative signs, all the column moments in the accompanying examples are taken to be positive, although the external wind moments are clockwise. This procedure is, in effect, equivalent to reversing the signs before Eqs. (13) and (14).

Preliminary Approximate Formulas for $\bar{\theta}$ and x

Assuming $\theta_U' + \theta_L' = \theta_U + \theta_L$, etc., Eq. (10) becomes

$$x = R + \frac{\theta_U+\theta_L}{2}. \tag{15}$$

Applying Eq. (15) to any two adjacent stories, as Stories 1 and 2, we have

$$x_1 = R_1 + \frac{\bar{\theta}_o+\bar{\theta}_1}{2}, \tag{16}$$

$$x_2 = R_2 + \frac{\bar{\theta}_1+\bar{\theta}_2}{2}, \tag{17}$$

where $\bar{\theta}_o$, $\bar{\theta}_1$, $\bar{\theta}_2$, etc., equal preliminary joint rotations at the three consecutive floors.

Approximating still further, and in line with the preliminary assumptions of Goldberg,[1] we shall let $\bar{\theta}_o = \bar{\theta}_1 = \bar{\theta}_2 = \theta$; that is, all the joint rotations in

1. John E. Goldberg, Trans. ASCE, 1934, page 962.

any floor are considered to be, for the moment, the same as those in the adjacent upper and lower floors. Accordingly, Eqs. (16) and (17) become:

$$x_1 = \frac{M_1}{12\Sigma K_L} + \theta, \tag{18}$$

$$x_2 = \frac{M_2}{12\Sigma K_U} + \theta, \tag{19}$$

where R_1 and R_2 have been replaced by their equivalents.

Applying in turn $\Sigma M = 0$ to the joints in any floor, say the first floor (Fig. 1), we have:

Joint 1: $2K_1(3\theta-3x_1)+2K_2(3\theta-3x_2)+2K_{G1}(3\theta)= 0;$ (20)

Joint 1': $2K'_1(3\theta-3x_1)+2K_{G1}(3\theta)+2K'_2(3\theta-3x_2)+2K'_{G1}(3\theta)= 0;$ (21)

Joint 1'': $2K''_1(3\theta-3x_1)+2K'_{G1}(3\theta)+2K''_2(3\theta-3x_2)+2K''_{G1}(3\theta)= 0.$ (22)

Adding, dividing by 6, and factoring, we get

$$[\Sigma K_L+\Sigma K_U+2K_{G1}+2K'_{G1}+K''_{G1}+ \ldots]\times\theta = x_1(\Sigma K_L)+x_2(\Sigma K_U). \tag{23}$$

Substituting Eqs. (18) and (19) in Eq. (23), and reducing, we get

$$\theta = \frac{1}{2\Sigma K_G}\left[\frac{M_1}{12} + \frac{M_2}{12}\right], \tag{24}$$

where (for the 6-column symmetrical frame, Fig. 1), $\Sigma K_G = 2(K_{G1} + K_{G1}) + K''_{G1}$.

Fig. (3-(a)-(d)) shows values of ΣK_G for other symmetrical frames.

Eq. (24) can be extended to represent in turn the preliminary rotations at all the upper floors.

If the first story columns are fixed at the bases, Eq. (24) is slightly modified. Thus, with $\theta_o = 0$, $\theta'_o = 0$, etc., Eq. (18) becomes

$$x_1 = \frac{M_1}{12\Sigma K_L} + \frac{\theta}{2}, \tag{25}$$

while Eq. (19) remains unchanged. Hence Eq. (23) is replaced by

$$[2\Sigma K_L+3\Sigma K_U+6K_{G1}+6K'_{G1}+3K''_{G1}]\times\theta = 3x_1\Sigma K_L+3x_2\Sigma K_U. \tag{26}$$

Substituting Eqs. (19) and (25) in Eq. (26), and reducing, we get

$$\theta = \frac{1}{1/6\ \Sigma K_L+2\Sigma K_G}\left[\frac{M_1}{12} + \frac{M_2}{12}\right], \tag{27}$$

applying only to the first floor (where θ becomes $\bar{\theta}_1$.)

Routine Preliminary Calculations

Knowing the K-value of every member, calculate $2\Sigma K_J$ for each joint, ΣK_C for each story, and $2\Sigma K_G$ for the girders in each floor. Knowing the horizontal wind shear in each story, calculate M, and write the values of $\frac{1}{12}M$, ΣK_C, and R in each story (as in Figs. A of the Examples).

At every joint, write the numerical values of $\frac{K}{2\Sigma K_J}$ on each member, as shown by arrows in Figs. B of the Examples. Then double these quantities, that is, write on each member the values of $\frac{K}{\Sigma K_J}$ as shown in Figs. A of the Examples. Exception: The joints 1, 1', of the first floor are to have an additional factor $\frac{\Sigma K_J}{\Sigma K_J - \frac{1}{3}K_1}$, $\frac{\Sigma K_J}{\Sigma K_J - \frac{1}{3}K'}$, etc.

Initial Analysis Procedure [Applied to sym. 6-column Frame (Fig. 1)]

Calculate the values of $\bar{\theta}$ for each floor. Thus: (a) $\bar{\theta}_1$ (1st floor) = $\frac{1}{2\Sigma K_G + \frac{1}{6}\Sigma K_L}[\frac{M_1}{12} + \frac{M_2}{12}]$; $\bar{\theta}_2$ (2nd floor) = $\frac{1}{2\Sigma K_G}[\frac{M_2}{12} + \frac{M_3}{12}]$; etc.

(b) Calculate the x's for each story and record the numerical results as in Figs. A of the Examples. Thus: By the Formulas;

$$x_1 = R_1 + \frac{0+\bar{\theta}_1}{2} \; ; \quad x_2 = R_2 + \frac{\bar{\theta}_1+\bar{\theta}_2}{2} \; ; \text{ etc.}$$

1st Convergence

(a) Calculate the θ's at each joint, as indicated in Figs. A, these being, in effect, adaptations of Eqs. (5) or (7). Transfer the totals to Figs. B.
(b) Calculate the x's in each story by using Eqs. (10), (11), or (12), depending on the type of frame. Record the results in Fig. B.

2nd Convergence

(a) Calculate the θ's at each joint by adaptations of Eq. (8). Record these results in Figs. B, replacing previous values. Make use of the revised θ's at the far ends of members as the work proceeds.
(b) Calculate the revised x's in each story by a repetition of the foregoing procedure (b). Record the results in Figs. B.

Conclusions

A continued "3rd convergence"—which would result from an adaptation of Eq. (3) for the θ's and Eq. (10) for the x's-appears unnecessary to give sufficient accuracy.

To expedite the computation of moments, evaluate the quantity $3x - (\theta_U + \theta_L)$, etc., for each column in a story, then deduct in turn θ_U, θ_L, etc., and multiply by 2K, 2K', etc.

It is believed that the method presented herewith-and the accompanying examples—will prove it to be simple, rapid, workable, and surprisingly accurate after the second convergence. Attention is called to the considerable proportion of routine preliminary calculations (with slide rule, desk calculator, or automatic computing equipment) that may be done by an assistant unversed in structural theory.

EXAMPLES

Example 1

Given a 2-column unsymmetrical frame (Figs. A and B). The K-values are listed in the table which follows. Required: The end moments.

Joint	Member	K	K/2ΣK	K/ΣK	Joint	Member	K	K/2ΣK	K/ΣK
2	2-1	1	.1667	.333	2'	2'-1'	2	.2500	.500
	2-2'	2	.3333	.667		2'-2	2	.2500	.500
	2ΣK =	6	.5000	1.000		2ΣK =	8	.5000	1.000
1	1-2	1	.1000	.200	1'	1'-2'	2	.1250	.250
	1-0	2	.2000	.400		1'-0'	4	.2500	.500
	1-1'	2	.2000	.400		1'-1	2	.1250	.250
	2ΣK =	10	.5000	1.000		2ΣK =	16	.5000	1.000

Preliminary Values of θ and x:

$$\bar{\theta}_1 = \frac{37.5 + 8.333}{1 + 4} = 9.167; \quad \bar{\theta}_2 = \frac{8.333}{4} = 2.083.$$

$$x_1 = 6.25 + \frac{0 + 9.167}{2} = 10.8333; \quad x_2 = 2.778 + \frac{9.167 + 2.083}{2} = 8.403.$$

1st Convergence (See Fig. A):

$$\theta_1 = .462x_1 + .231x_2 = 6.94; \quad \theta'_1 = .600x_1 + .300x_2 = 9.02; \quad \theta_2 = 2.80; \quad \theta'_2 = 4.20.$$

$$x_1 = 6.25 + \frac{2(0 + 6.94) + 4(0 + 9.02)}{2(6)} = 10.413; \quad x_2 = 2.778 + \frac{1(9.74) + 2(13.22)}{2(3)} = 8.808.$$

2nd Convergence (See Fig. B):

$$\theta_1 = 3[.200(10.413) + .100(8.808)] - 0 - .100(2.80) - .20(9.02) = 6.806.$$

$$\theta'_1 = 3[.250(10.413) + .125(8.808)] - 0 - .125(6.806) - .125(4.20) = 9.736.$$

$$\theta_2 = \frac{3}{2}[2.80] - .1667(6.806) - .3333(4.20) = 1.666.$$

$$\theta'_2 = \frac{3}{2}[4.20] - .250(9.736) - .250(1.666) = 3.450.$$

$$x_1 = 6.25 + \frac{52.556}{2(6)} = 10.630; \quad x_2 = 2.778 + \frac{34.844}{2(3)} = 8.585.$$

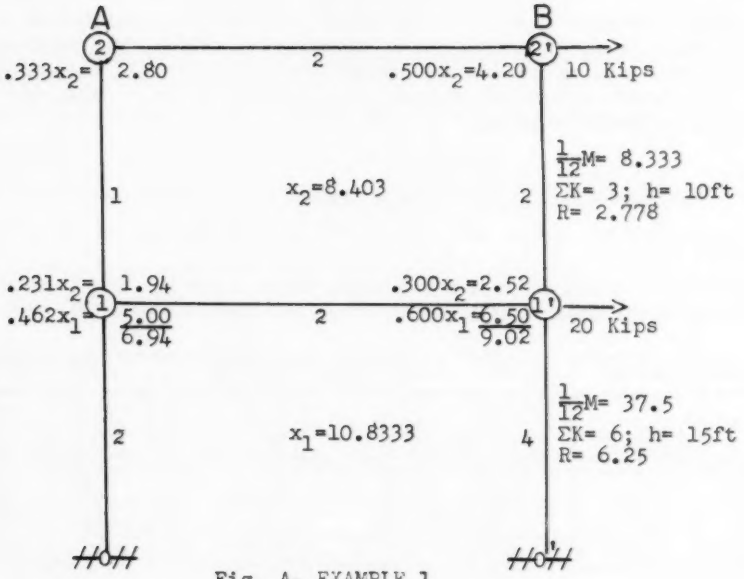

Fig. A- EXAMPLE 1

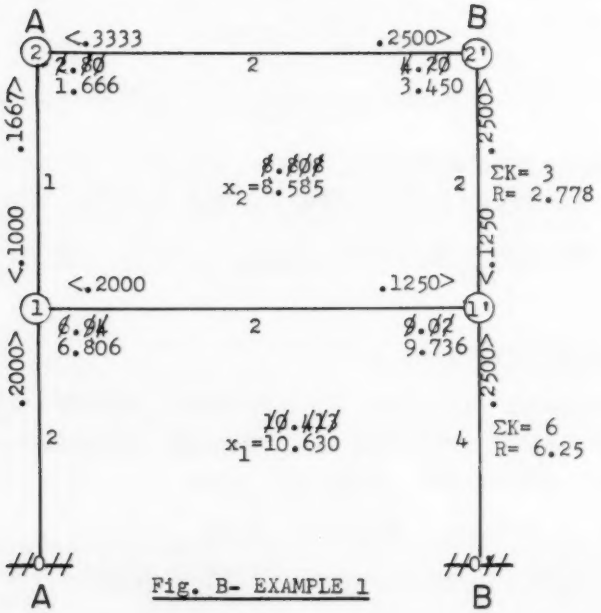

Fig. B- EXAMPLE 1

Final Moments

(Note: The quantities in brackets are exact values from the solution of 6 equations):

$M_{10} = 4(3(10.630) - 2(6.806)) = 73.11\,[73.99]$; $M'_{10} = 8(12.418) = 99.34\,[97.04]$.

$M_{01} = 4(3(10.630) - 6.806) = 100.34\,[101.49]$; $M'_{01} = 8(22.154) = 177.23\,[177.50]$.

$M_{21} = 2(3(8.585) - 2(1.666) - 6.806) = 31.23\,[30.87]$; $M'_{21} = 4(9.119) = 36.48\,[36.91]$.

$M_{12} = 2(3(8.585) - 1.666 - 2(6.806)) = 20.95\,[21.25]$; $M'_{12} = 4(2.833) = 11.33\,[10.98]$.

As an independent check (closely true), $M_{11}' = -4\,[2(6.806) + 9.736] = -93.39$; $M_{12} + M_{10} = 20.95 + 73.11 = 94.06$.

Example 2

Given a 5-story symmetrical frame (Figs. A and B). The K-values are listed in the table which follows. Required: The end moments. For comparison with these moments, the exact values obtained by a solution of 12 simultaneous equations will be given in brackets.

Joint	Member	K	K/2ΣK	K/ΣK	Joint	Member	K	K/2ΣK	K/ΣK
					5B	5-4	1	.2500	.500
						5-5	1	.2500	.500
						2ΣK =	4	.5000	1.000
					4B	4-5	1	.1000	.200
						4-3	2	.2000	.400
						4-4	2	.2000	.400
						2ΣK =	10	.5000	1.000
					3B	3-4	2	.1250	.250
						3-2	3	.1875	.375
						3-3	3	.1875	.375
						2ΣK =	16	.5000	1.000
2A	2-1	4	.2500	.500	2B	2-1	4	.1333	.267
						2-3	3	.1000	.200
	2-2B	4	.2500	.500		2-2A	4	.1333	.267
						2-2B	4	.1333	.267
	2ΣK =	16	.5000	1.000		2ΣK =	30	.5000	1.000
1A	1-2	4	.1429	.286	1B	1-2	4	.1053	.211
	1-0	5	.1786	.357		1-0	5	.1316	.263
	1-1B	5	.1786	.357		1-1A	5	.1316	.263
						1-1B	5	.1316	.263
	2ΣK =	28	.5000	1.000		2ΣK =	38	.5000	1.000

Preliminary Values of θ and x:

$$\bar{\theta}_1 = \frac{200 + 106.25}{3.333 + 30} = 9.187;\ \bar{\theta}_2 = \frac{106.25 + 50}{24} = 6.510;\ \bar{\theta}_3 = \frac{50 + 43.75}{6} = 15.625;$$

$$\bar{\theta}_4 = \frac{43.75 + 8.333}{4} = 13.021;\ \bar{\theta}_5 = \frac{8.333}{2} = 4.167.$$

$$x_1 = 10 + \frac{0 + 9.187}{2} = 14.593;\ x_2 = 6.641 + \frac{9.187 + 6.510}{2} = 14.49;\ x_3 = 8.333 + \frac{6.510 + 15.625}{2} = 19.400;\ x_4 = 10.937 + \frac{15.625 + 13.021}{2} = 25.260;\ x_5 = 12.761.$$

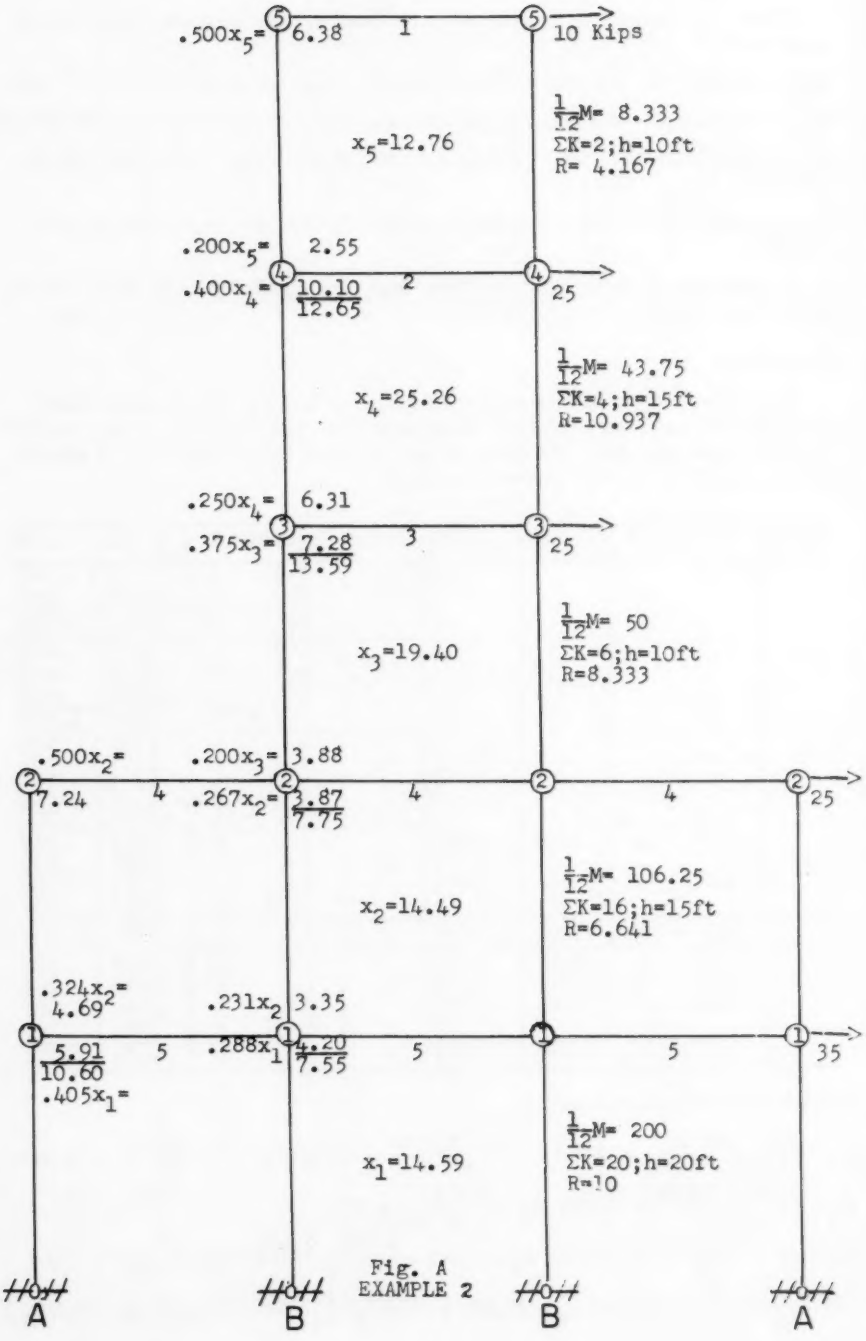

Fig. A
EXAMPLE 2

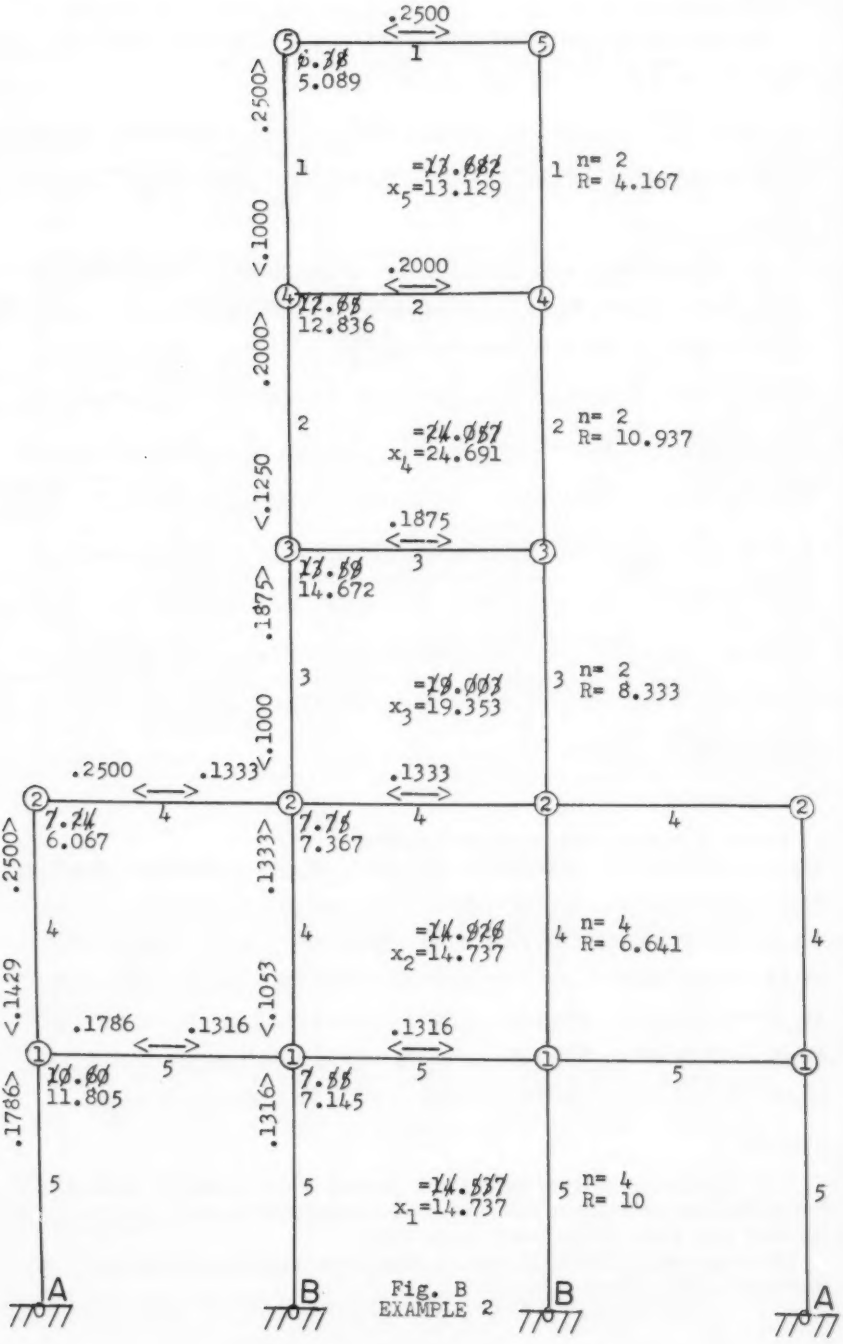

Fig. B
EXAMPLE 2

1st Convergence

(See Fig. A): $\theta_1A = 10.60$; $\theta_1B = 7.55$; $\theta_2A = 7.24$; $\theta_2B = 7.75$; $\theta_3B = 13.59$; $\theta_4B = 12.65$; $\theta_5B = 6.38$.

$x_1 = 10 + \frac{18.15}{4} = 14.537$; $x_2 = 6.641 + \frac{17.84 + 15.30}{4} = 14.926$; $x_3 = 8.333 + \frac{21.34}{2} = 19.003$; $x_4 = 10.937 + \frac{26.24}{2} = 24.057$; $x_5 = 4.167 + \frac{19.03}{2} = 13.682$.

2nd Convergence

(See Fig. B): $\theta_1A = 3[.1786(14.537) + .1429(14.926)] - 0 - .1429(7.24) - .1786(7.55) = 11.805$; $\theta_1B = 3[.1316(14.537) + .1053(14.926)] - 0 - .1053(7.75) - .1316(11.805) - 0.1316\theta_1B$; then $\theta_1B = \frac{8.0848}{1.1316} = 7.145$.

$\theta_2B = \frac{3}{2}[7.75] - .100(13.59) - .1333(7.145) - .1333(7.24) - 0.1333\theta_2B$; then $\theta_2B = \frac{8.349}{1.1333} = 7.367$. $\theta_2A = \frac{3}{2}[7.24] - .250(11.805) - .250(7.367) = 6.067$.

$\theta_3B = \frac{3}{2}[13.59] - .125(12.65) - .1875(7.367) - 0.1875\theta_3B$; then $\theta_3B = \frac{17.4225}{1.1875} = 14.672$. $\theta_4B = \frac{3}{2}[12.65] - .100(6.38) - .200(14.672) - 0.200\theta_4B$; then $\theta_4B = \frac{15.403}{1.2} = 12.836$. $\theta_5B = \frac{3}{2}[6.38] - .25(12.836) - 0.25\theta_5B$; then $\theta_5B = \frac{6.361}{1.25} = 5.089$. $x_1 = 10 + \frac{11.805 + 7.145}{4} = 14.737$; $x_2 = 6.641 + \frac{17.872 + 14.512}{4} = 14.737$; $x_3 = 8.333 + \frac{22.039}{2} = 19.353$; $x_4 = 10.937 + \frac{27.508}{2} = 24.691$; $x_5 = 4.167 + \frac{17.925}{2} = 13.129$.

Final Moments:

(Note: The exact values are in brackets)

$M_{10}A = 10(3(14.737) - 2(11.805)) = 206$ [202]; $M_{10}B = 10(29.921) = 299.2$ [301].

$M_{01}A = 10(3(14.737) - 11.805) = 324.1$ [324]; $M_{01}B = 10(37.066) = 370.7$ [373].

$M_{21}A = 8(3(14.737 - 2(6.067) - 11.805) = 162.2$ [161]; $M_{21}B = 178.7$ [181].

$M_{12}A = 8(3(14.737) - 6.067 - 2(11.805)) = 116.3$ [114]; $M_{12}B = 180.4$ [183].

$M_{32}B = 6(3(19.353) - 2(14.672) - 7.367) = 128.1$ [130]; $M_{23}B = 171.9$ [170].

$M_{43}B = 4(3(24.691) - 2(12.836) - 14.672) = 134.9$ [134]; $M_{34}B = 127.6$ [128].

$M_{54}B = 2(3(13.129) - 2(5.089) - 12.836) = 32.7$ [32]; $M_{45}B = 17.3$ [18].

Example 3.

It is required to analyze the 5 lower stories of the American Insurance Union Building—a problem that was solved completely by Ross and Morris in the May 1928 Proc. of the ASCE, page 1395.

The K-values (in the table which follows) are in inch units and the moments = inch pounds ÷ 10,000.

The analysis given here includes the irregular part of the building. The exact values obtained from the solution of numerous equations are given in brackets. On account of symmetry, only the left half of the frame is considered.

Joint	Mbr	K	K/2ΣK	Joint	Mbr	K	K/2ΣK	Joint	Mbr	K	K/2ΣK
	6-7	40.6	.1819		6-7	46.1	.1442		6-7	63.7	.1561
6A	6-5	42.2	.1891	6B	6-5	47.9	.1498	6C	6-5	66.2	.1622
	6-B	28.8	.1290		6-A	28.8	.0901		6-B	37.1	.0909
					6-C	37.1	.1160		6-C	37.1	.0909
	2ΣK =	223.2	.5000		2ΣK =	319.8	.5000		2ΣK =	408.2	.5000
	5-6	42.2	.1939		5-6	47.9	.1528		5-6	66.2	.1657
5A	5-4	37.8	.1737	5B	5-4	42.9	.1369	5C	5-4	59.3	.1485
	5-B	28.8	.1324		5-A	28.8	.0919		5-B	37.1	.0929
					5-C	37.1	.1184		5-C	37.1	.0929
	2ΣK =	217.6	.5000		2ΣK =	313.4	.5000		2ΣK =	399.4	.5000
	4-5	37.8	.0799		4-5	42.9	.0478		4-5	59.3	.0546
4A	4-3	62.8	.1328	4B	4-3	77.7	.0867	4C	4-3	131.5	.1210
	4-B	135.8	.2872		4-A	135.8	.1515		4-B	191.9	.1766
					4-C	191.9	.2140		4-C	160.7	.1479
	2ΣK=	472.8	.5000		2ΣK =	896.6	.5000		2ΣK=	1086.8	.5000
	3-4	62.8	.1650		3-4	77.7	.1331		3-4	131.5	.1850
3A	3-2	73.9	.1942	3B	3-2	91.4	.1566	3C	3-2	154.8	.2178
	3-B	53.6	.1408		3-A	53.6	.0918		3-B	69.1	.0972
					3-C	69.1	.1184				
	2ΣK=	380.6	.5000		2ΣK =	583.6	.4999		2ΣK=	710.8	.5000
	2-3	73.9	.2064		2-3	91.4	.1645		2-3	154.8	.2333
2A	2-1	51.5	.1439	2B	2-1	63.7	.1146	2C	2-1	107.9	.1626
	2-B	53.6	.1497		2-A	53.6	.0965		2-B	69.1	.1041
					2-C	69.1	.1244				
	2ΣK=	358.0	.5000		2ΣK =	555.6	.5000		2ΣK=	663.6	.5000
	1-2	51.5	.1118		1-2	63.7	.0739		1-2	107.9	.0826
1A	1-0	43.0	.0934	1B	1-0	39.7	.0460	1C	1-0	59.9	.0458
	1-B	135.8	.2948		1-A	135.8	.1575		1-B	191.9	.1468
					1-C	191.9	.2226		1-C	293.8	.2248
	2ΣK=	460.6	.5000		2ΣK =	862.2	.5000		2ΣK=	1307.0	.5000

Preliminary Values of θ and x:

$\bar{\theta}_1 = \frac{393.4 + 327.8}{23.77 + 949.2} = 0.7412$; $\bar{\theta}_2 = \frac{327.8 + 221.7}{245.4} = 2.239$; $\bar{\theta}_3 = \frac{221.7 + 253.4}{245.4} = 1.936$; $\bar{\theta}_4 = \frac{253.4 + 190.8}{816.1} = 0.5443$; $\bar{\theta}_5 = \frac{190.8 + 166.6}{168.9} = 2.116$; $\bar{\theta}_6 = \frac{166.6 + 169.0}{168.9} = 1.987$.

$x_1 = 2.759 + \frac{0 + 0.74.12}{2} = 3.135$; $x_2 = 1.469 + \frac{0.7412 + 2.239}{2} = 2.959$; $x_3 = 0.6926 + \frac{2.239 + 1.936}{2} = 2.780$; $x_4 = 0.9316 + \frac{1.936 + 0.5443}{2} = 2.172$; $x_5 = 1.363 + 1.330 = 2.693$.

1st Convergence

(See Fig. A): $\theta_1A = 1.328$; $\theta_1B = 0.748$; $\theta_1C = 0.801$; $\theta_2A = 2.000$; $\theta_2B = 1.593$; $\theta_2C = 2.260$; $\theta_3A = 1.796$; $\theta_3B = 1.448$; $\theta_3C = 2.016$;

$\theta_4A = 1.009$; $\theta_4B = 0.635$; $\theta_4C = 0.820$; $\theta_5A = 2.143$; $\theta_5B = 1.691$; $\theta_5C = 1.831$.

$x_1 = 2.759 + \frac{43(1.328) + 39.7(0.748) + 59.9(0.801)}{285.2} = 3.232$; $x_2 = 1.469 + \frac{51.5(3.328) + 63.7(2.341) + 107.9(3.061)}{446.2} = 2.928$; $x_3 = 0.6926 + \frac{1220.396}{640.2} = 2.599$; $x_4 = 0.9316 + \frac{710.937}{544} = 2.239$; $x_5 = 1.363 + \frac{376.135}{280} = 2.706$.

2nd Convergence

(See Fig. B): $\theta_1A = 3[.0934(3.232) + .1118(2.928)] - 0 - .118(2.000) - .2948(.748) = 1.444$; $\theta_1B = 3[.0460(3.232) + .0739(2.928)] - 0 - .0739(1.593) - .1575(1.444) - .2226(.801) = 0.572$; $\theta_1C = 3[.0458(3.232) + .0826(2.928)] - 0 - .0826(2.260) - .1468(.572) - 0.2248\theta_1C$; then $\theta_1C = \frac{.8990}{1.2248} = 0.734$; $\theta_2A = \frac{3}{2}[2.000] - .1439(1.444) - .2064(1.796) - .1497(1.593) = 2.183$; $\theta_2B = \frac{3}{2}[1.593] - .1147(.572) - .1645(1.448) - .0965(2.183) - .1244(2.26) = 1.594$; $\theta_2C = \frac{3}{2}[2.260] - .1626(.734) - .2333(2.016) - .1041(1.594) = 2.636$; $\theta_3A = \frac{3}{2}[1.796] - .1942(2.183) - .1650(1.009) - .1408(1.448) = 1.900$; $\theta_3B = \frac{3}{2}[1.448] - .1566(1.594) - .1331(.635) - .0918(1.900) - .1184(2.016) = 1.425$; $\theta_3C = \frac{3}{2}[2.016] - .2178(2.636) - .1850(.820) - .0972(1.425) = 2.160$; $\theta_4A = \frac{3}{2}[1.009] - .1328(1.900) - .0799(2.143) - .2872(.635) = 0.908$; $\theta_4B = \frac{3}{2}[.635] - .0867(1.425) - .0478(1.691) - .1515(.908) - .2140(.820) = 0.4355$; $\theta_4C = \frac{3}{2}[.820] - .1210(2.160) - .0546(1.831) - .1766(.4355) - 0.1479\theta_4C$; then $\theta_4C = \frac{0.7917}{1.1479} = .690$.

$x_1 = 2.759 + \frac{43(1.444) + 39.7(.572) + 59.9(.734)}{285.2} = 3.2105$; $x_2 = 1.469 + \frac{688.388}{446.2} = 3.012$; $x_3 = 0.6926 + \frac{1320.09}{640.2} = 2.755$; $x_4 = 0.9316 + \frac{695.67}{544} = 2.2104$.

Final Moments

(See Fig. B): Note: Values by Ross and Morris in brackets:
$M_{10}A = 86(3(3.2105) - 2(1.444)) = 579.9\,[583]$; $M_{10}B = 704.1\,[713]$; $M_{10}C = 978\,[1000]$; $M_{01}A = 86(3(3.2105) - 1.444) = 704.1\,[713]$; $M_{01}B = 719.3\,[730]$; $M_{01}C = 1066\,[1086]$; $M_{21}A = 103(3(3.012) - 2(2.183) - 1.444) = 332.3\,[332]$; $M_{21}B = 672.2\,[678]$; $M_{21}C = 654\,[670]$; $M_{12}A = 103(3(3.012) - 2.183 - 2(1.444)) = 408.4\,[400]$; $M_{12}B = 802.4\,[802]$; $M_{12}C = 1064\,[1078]$; $M_{32}A = 147.8(3(2.755) - 2(1.9) - 2.183) = 337.3\,[333]$; $M_{32}B = 698.5\,[702]$; $M_{32}C =$

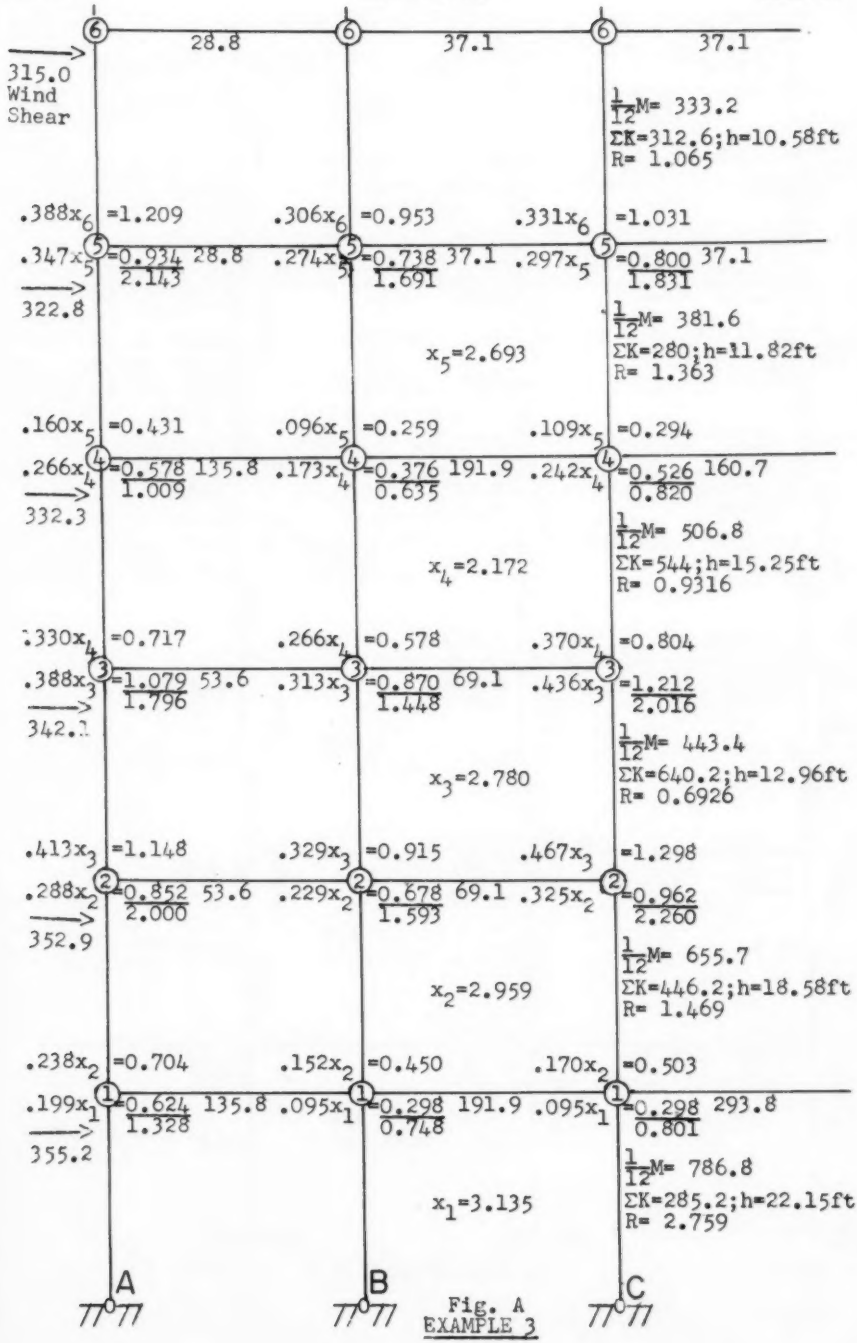

Fig. A
EXAMPLE 3

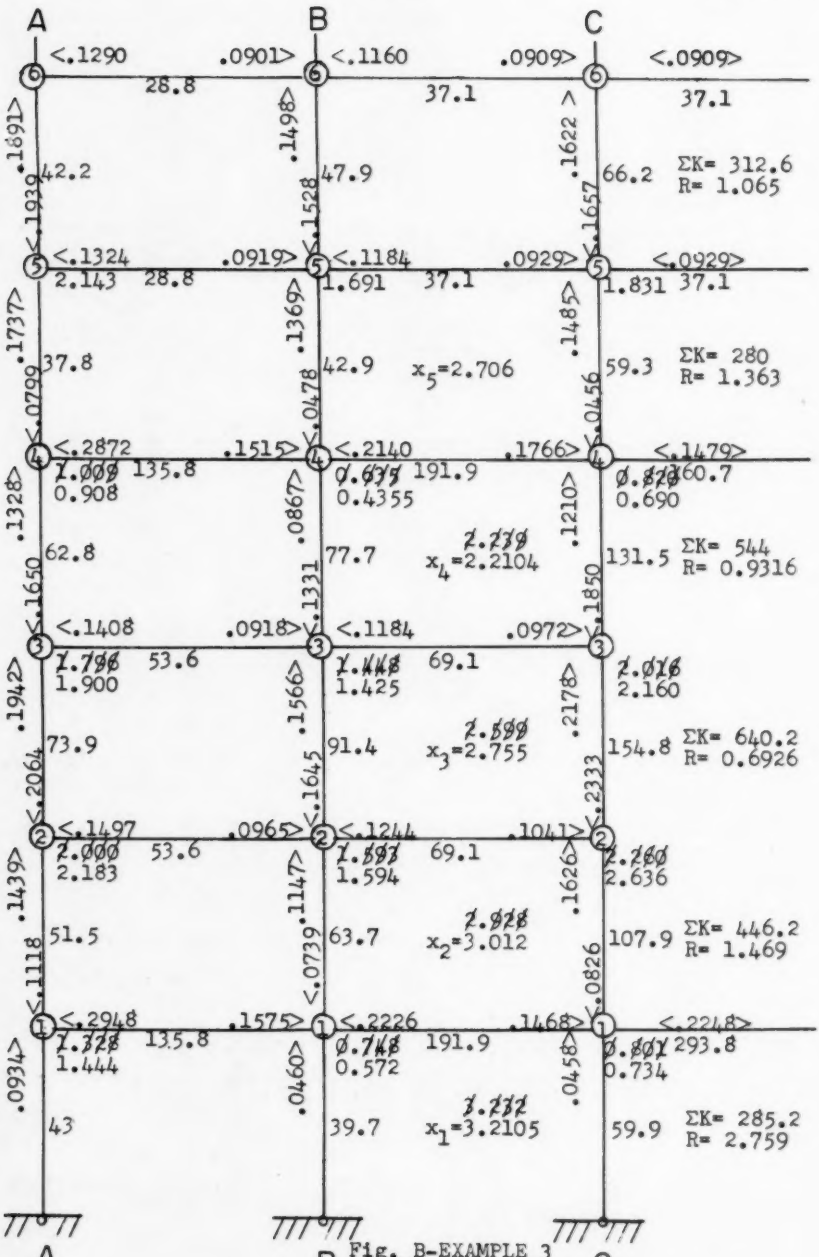

Fig. B-EXAMPLE 3

405.3 [391]; $M_{23}A$ = 147.8(3(2.755) - 1.9 - 2(2.183)) = 295.5 [301]; $M_{23}B$ = 667.6 [681]; $M_{23}C$ = 258 [269]; $M_{43}A$ = 125.6(3(2.2104) - 2(.908) - 1.9) = 366.1 [362]; $M_{43}B$ = 674 [678]; $M_{43}C$ = 813 [825]; $M_{34}A$ = 125.6(3(2.2104) - .908 - 2(1.9)) = 241.6 [239]; $M_{34}B$ = 520 [526]; $M_{34}C$ = 426.4 [427].

For the column moments, it will be seen that $\Sigma M = 0$ is satisfied in each story. This requirement is expected to follow automatically from the application of Eq. (10) in the calculation of the x's.

Also, after the 2nd convergence, a reasonable check is attained at the joints. Thus, at joint 1C: $M_1CB + M_1CC$ = -384.8[2(0.734) + 0.572]- 587.6[3(0.734)] = -2079; $M_{12}C + M_{10}C$ = 2042. This is a little better than a 2 per cent check.

At joint 2C: M_2CB = -138.2 [2(2.636) + 1.594] = - 948.9; $M_{23}C + M_{21}C$ = 912. This is about a 4 per cent check.

At joint 3C: M_3CB = -138.2[2(2.160) + 1.425] = -794; $M_{34}C + M_{32}C$ = 832. This is better than a 5 per cent check.

At joint 1A: M_1AB = - 271.6 [2(1.444) + 0.572] = -940; $M_{12}A + M_{10}A$ = 988. This is about a 5 per cent check.

At joint 2A: M_2AB = -107.2 [2(2.183) + 1.900] = - 671; $M_{23}A + M_{21}A$ = 628. This is about a 6 per cent check.

At joint 3A: M_3AB = -107.2 [2(1.900) + 1.425] = -560; $M_{34}A + M_{32}A$ = 579. This is a 3.5 per cent check.

Paper 1234 ST 3

Journal of the
STRUCTURAL DIVISION
Proceedings of the American Society of Civil Engineers

BEAM DEFLECTION IN BRIDGES DESIGNED FOR CONTINUITY

Guillermo Villena,[a] J.M. ASCE
(Proc. Paper 1234)

ABSTRACT

This paper presents a formula for deflection at any point, for continuous beam bridges where the beams are of constant moment of inertia and constant modulus of elasticity. Application may also be made for variable moment of inertia. The formula applies to any number of continuous spans.

In the design of bridges to be used over creeks or as highway overpasses, where rolled steel beams are used, it is always necessary to determine the maximum deflection due to dead loads. This maximum deflection, and deflections at few other points, assist in determining the amount of camber to be given to each of the beams that form the floor system. Cross bracings are placed mainly for lateral support and each of the floor beams will deflect in ratio of the amount of load assigned to carry.

The case presented here deals with beams of constant I and constant E.

The necessity of expansion joints limits, in many cases, the number of continuous spans in a bridge. This formula applies to any number of continuous spans.

Nomenclature:

M_S = Simple beam moment in span = $\frac{wL^2}{8}$

M_L = Final moment @ left support (by any method)

M_R = Final moment @ right support (by any method)

L = Length of span

X = Distance, within the span, at any point from left support = $C.L$

C = Ratio of distance X to L (X/L)

Note: Discussion open until October 1, 1957. Paper 1234 is part of the copyrighted Journal of the Structural Division of the American Society of Civil Engineers, Vol. 83, No. ST 3, May, 1957.

a. Project Engr., Alfred LeFeber & Associates, Cons. Engrs., Cincinnati, Ohio.

w = Uniform load per linear foot of beam

EI = Constant within a beam

Δ_C^S = Deflection @ center of simple beam = $\frac{5}{384}\ \frac{wL^4}{EI}$

Δ_X^S = Deflection @ any point of simple beam = $\frac{wX}{24\ EI}(L^3-2LX^2+X^3)$

$= \frac{wL^2}{8} \times \frac{L^2}{3\ EI}(C-2C^3+C^4)$

Δ_X^F = Deflection due to end restraint

Δ_X = Total deflection at any point in the beam

Since the deflection curve for the simple beam uniformly loaded is symmetrical about the center of the span, with its maximum value at the center, it will be easy to determine Δ_X^S as a function of Δ_C^S is Δ_C^S is made as the unity (see table).

In any span of the bridge designed with continuity, the deflection Δ_X at any point in the beam is the algebraic sum of the deflections as simple beam (Δ_X^S) which acts downward and is considered positive, and the deflection due to end restraint (Δ_X^F) which acts upwards and is considered negative

$$\text{Thus: } \Delta_X = \Delta_X^S - \Delta_X^F \qquad (1)$$

To calculate the deflection at any point in the beam it will be necessary to take the statical moment of the area bounded by the M/EI diagram from left support to the point in reference, about the point in reference. Since EI is constant its value will cancel out as can be seen later; therefore it is made the unity.

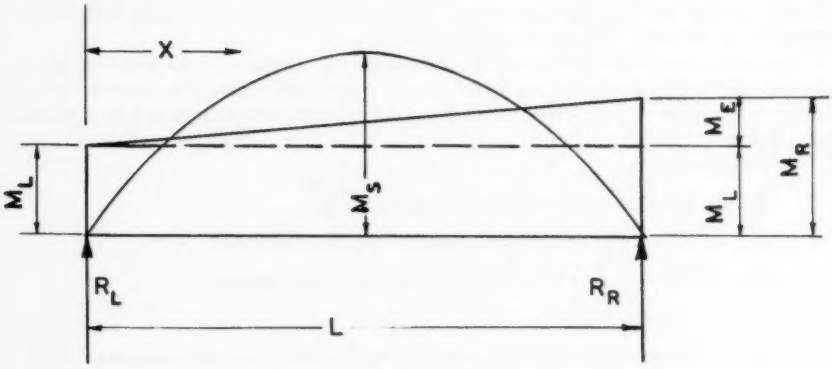

Fig. 1.

$$M_E = M_R - M_L \qquad (2)$$

Figure (1) shows a general case in a span when separated from the rest of them and loaded with the $\frac{M}{EI}$ diagram.

The value Δ_X^S can be obtained from:

$$\Delta_X^S = \frac{M_S L^2}{3}(C-2C^3+C^4)$$

$$\Delta_X^S = \frac{M_S L^2}{3}\, C(1-C)(1+C-C^2) \qquad (3)$$

The value Δ_X^F will be computed as stated above by taking moment about the given point.

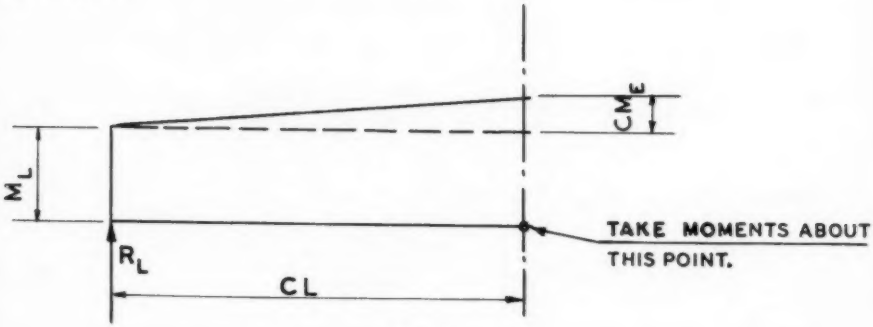

Fig. 2.

Reaction:

$$R_L = \frac{M_L . L}{2} + \frac{M_E L}{6} \qquad (4)$$

Load:

$$\text{Load} = C . L M_L + \frac{C^2 . M_E . L}{2} \qquad (5)$$

Moment:

$$\text{Moment} = \Delta_X^F = R_L . CL - \text{Load times arm distance}$$

$$\Delta_X^F = \frac{C . M_L . L^2}{2} + \frac{C . M_E . L^2}{6} - \left[\frac{C^2 . M_L . L^2}{2} + \frac{C^3 M_E L^2}{6}\right]$$

Substituting equation (2) and adding:

$$\Delta_X^F = \frac{M_L . L^2}{6}(2C-3C^2+C^3) + \frac{M_R L^2}{6}(C-C^3)$$

Transforming:

$$\Delta^F_X = \frac{M_L \cdot L^2}{6}\left[C(1-C)(2-C)\right] + \frac{M_R L^2}{6}\left[C(1-C)(1+C)\right] \qquad (6)$$

Dividing equation (6) by equation (3) and reducing:

$$\frac{\Delta^F_X}{\Delta^S_X} = \frac{M_L}{2M_S} \times \frac{(2-C)}{(1+C-C^2)} + \frac{M_R}{2M_S} \times \frac{(1+C)}{(1+C-C^2)}$$

Then:

$$\Delta^F_X = \left[\frac{M_L}{2M_S} \times \frac{(2-C)}{(1+C-C^2)} + \frac{M_R}{2M_S} \times \frac{(1+C)}{(1+C-C^2)}\right] \times \Delta^S_X \qquad (7)$$

Since $$\Delta_X = \Delta^S_X - \Delta^F_X \qquad (1)$$

$$\Delta_X = \Delta^S_X \left[1 - \frac{M_L(2-C) + M_R(1+C)}{2M_S(1+C-C^2)}\right] \qquad (8)$$

In equation (9) the value Δ^S_X can be obtained from table where it is given as a function of Δ^S_C.

Equation (8) also can be written as:

$$\Delta_X = \Delta^S_X \left[1 - \frac{D.M_L + E.M_R}{F.M_S}\right] \qquad (9)$$

Where values Δ^S_X, D, E and F can be obtained from table for any point in the beam.

Example: A four span bridge as shown in Fig. 3 and Fig. 4 was designed according to specifications and the following values were obtained:

Beam size = 36WF194 ($I = 12103.4$ in^4)

$w = 1194$#/ft. $= 99.50$ #/in.

$M_A = 0$

(D.L.) $M_B = 498$ ft.-kips

(D.L.) $M_C = 515$ ft.-kips

(D.L.) $M_D = 498$ ft.-kips

$M_E = 0$

Suppose we want to find Δ_X @ 20' from B

$$\Delta_X = \Delta^S_X \left[1 - \frac{DM_L + EM_R}{F.M_S}\right] \qquad (9)$$

$C = 20/80 = 0.25$

$M_L = M_B = 498$ ft. - kips

$M_R = M_C = 515$ ft. - kips

$M_S = M_2 = .125 \times 1.194 \times 6400 = 955$ ft. - kips

$$\Delta^S_C = \frac{5 \times 99.5 \times (80 \times 12)^4}{384 \times 29 \times 10^6 \times 12103.4} = 3.1349''$$

From table:

$\Delta^S_X = .7125 \times 3.1349 = 2.23''$

$D = 1.75$

$E = 1.25$

$F = 2.3750$

Then:

$$\Delta_X = 2.23\left[1 - \frac{1.75 \times 498 + 1.25 \times 515}{2.375 \times 955}\right] = 2.23 \times .332 = \underline{.74''}$$

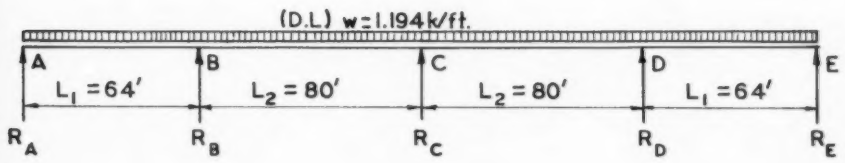

Fig. 3.

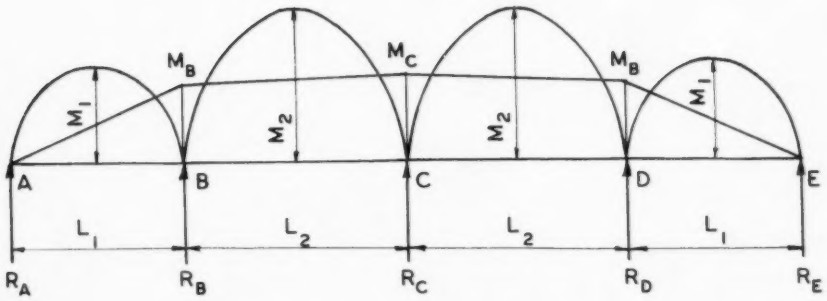

MOMENT DIAGRAM

Fig. 4.

For complete camber diagram see Fig. 5 when C = .12, .25, .37, .50, .62, .75, .87.

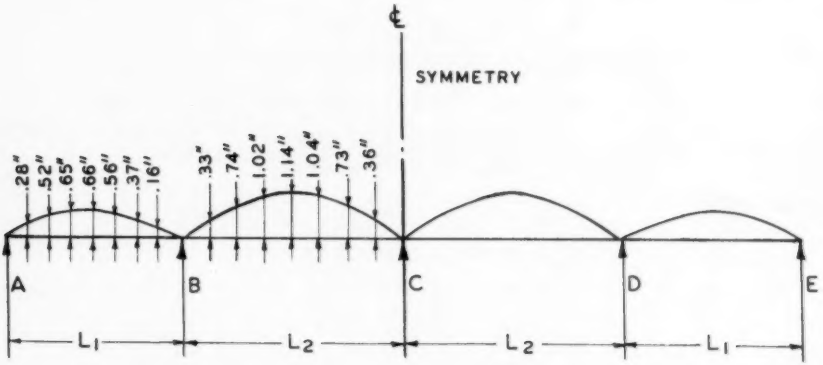

CAMBER DIAGRAM

Fig. 5. Camber Diagram.

TABLE

C	C^2	D	E	F	Δ^S_X
.00	.0000	2.00	1.00	2.00	0
.01	.0001	1.99	1.01	2.0198	.031994 x Δ^S_C
.02	.0004	1.98	1.02	2.0392	.063949 "
.03	.0009	1.97	1.03	2.0582	.095830 "
.04	.0016	1.96	1.04	2.0768	.127599 "
.05	.0025	1.95	1.05	2.0950	.159220 "
.06	.0036	1.94	1.06	2.1128	.190659 "
.07	.0049	1.93	1.07	2.1302	.221882 "
.08	.0064	1.92	1.08	2.1472	.252854 "
.09	.0081	1.91	1.09	2.1638	.283544 "
.10	.0100	1.90	1.10	2.18	.313920 "
.11	.0121	1.89	1.11	2.1958	.343950 "
.12	.0144	1.88	1.12	2.2112	.373604 "
.13	.0169	1.87	1.13	2.2262	.402853 "
.14	.0196	1.86	1.14	2.2403	.431668 "
.15	.0225	1.85	1.15	2.2550	.460020 "
.16	.0256	1.84	1.16	2.2688	.487883 "
.17	.0289	1.83	1.17	2.2822	.515229 "
.18	.0324	1.82	1.18	2.2952	.542034 "
.19	.0361	1.81	1.19	2.3078	.568273 "
.20	.0400	1.80	1.20	2.32	.593920 "
.21	.0441	1.79	1.21	2.3318	.618953 "
.22	.0484	1.78	1.22	2.3432	.643349 "
.23	.0529	1.77	1.23	2.3542	.667086 "
.24	.0576	1.76	1.24	2.3648	.690143 "
.25	.0625	1.75	1.25	2.3750	.712500 "
.26	.0676	1.74	1.26	2.3848	.734137 "
.27	.0729	1.73	1.27	2.3942	.755035 "
.28	.0784	1.72	1.28	2.4032	.775176 "
.29	.0841	1.71	1.29	2.4118	.794543 "
.30	.0900	1.70	1.30	2.42	.813120 "
.31	.0961	1.69	1.31	2.4278	.830890 "
.32	.1024	1.68	1.32	2.4252	.847839 "
.33	.1089	1.67	1.33	2.4422	.863953 "
.34	.1156	1.66	1.34	2.4488	.879217 "
.35	.1225	1.65	1.35	2.4550	.893620 "
.36	.1296	1.64	1.36	2.4608	.907149 "
.37	.1369	1.63	1.37	2.4662	.919794 "
.38	.1444	1.62	1.38	2.4712	.931544 "
.39	.1521	1.61	1.39	2.4758	.942389 "
.40	.1600	1.60	1.40	2.48	.952320 "
.41	1681	1.59	1.41	2.4838	.961330 "
.42	.1764	1.58	1.42	2.4872	.969411 "
.43	.1849	1.57	1.43	2.4902	.976557 "
.44	1936	1.56	1.44	2.4928	.982761 "
.45	.2025	1.55	1.45	2.4950	.988020 "
.46	.2116	1.54	1.46	2.4968	.992328 "
.47	.2209	1.53	1.47	2.4982	.995683 "
.48	.2304	1.52	1.48	2.4992	.998081 "
.49	.2401	1.51	1.49	2.4998	.999520 "
.50	.2500	1.50	1.50	2.50	1.000000 "

TABLE

C	C^2	D	E	F	Δ^S_X
.51	.2601	1.49	1.51	2.4998	.999520 x Δ^S_C
.52	.2704	1.48	1.52	2.4992	.998081 "
.53	.2809	1.47	1.53	2.4982	.995683 "
.54	.2916	1.46	1.54	2.4968	.992328 "
.55	.3025	1.45	1.55	2.4950	.988020 "
.56	.3136	1.44	1.56	2.4928	.982761 "
.57	.3249	1.43	1.57	2.4902	.976557 "
.58	.3364	1.42	1.58	2.4872	.969411 "
.59	.3481	1.41	1.59	2.4838	.961330 "
.60	.3600	1.40	1.60	2.48	.952320 "
.61	.3721	1.39	1.61	2.4758	.942389 "
.62	.3844	1.38	1.62	2.4712	.931544 "
.63	.3969	1.37	1.63	2.4662	.919794 "
.64	.4096	1.36	1.64	2.4608	.907149 "
.65	.4225	1.35	1.65	2.4550	.893620 "
.66	.4356	1.34	1.66	2.4488	.879217 "
.67	.4489	1.33	1.67	2.4422	.863953 "
.68	.4624	1.32	1.68	2.4352	.847839 "
.69	.4761	1.31	1.69	2.4278	.830890 "
.70	.4900	1.30	1.70	2.42	.813120 "
.71	.5041	1.29	1.71	2.4118	.794543 "
.72	.5184	1.28	1.72	2.4032	.775176 "
.73	.5329	1.27	1.73	2.3942	.755035 "
.74	.5476	1.26	1.74	2.3848	.734137 "
.75	.5625	1.25	1.75	2.3750	.712500 "
.76	.5776	1.24	1.76	2.3648	.690143 "
.77	.5929	1.23	1.77	2.3542	.667086 "
.78	.6084	1.22	1.78	2.3432	.643349 "
.79	.6241	1.21	1.79	2.3318	.618953 "
.80	.6400	1.20	1.80	2.3200	.593920 "
.81	.6561	1.19	1.81	2.3078	.568273 "
.82	.6724	1.18	1.82	2.2952	.542034 "
.83	.6889	1.17	1.83	2.2822	.515229 "
.84	.7056	1.16	1.84	2.2688	.487883 "
.85	.7225	1.15	1.85	2.2550	.460020 "
.86	.7396	1.14	1.86	2.2408	.431668 "
.87	.7569	1.13	1.87	2.2262	.402853 "
.88	.7744	1.12	1.88	2.2112	.373604 "
.89	.7921	1.11	1.89	2.1958	.343950 "
.90	.8100	1.10	1.90	2.1800	.313920 "
.91	.8281	1.09	1.91	2.1638	.283544 "
.92	.8464	1.08	1.92	2.1472	.252854 "
.93	.8649	1.07	1.93	2.1302	.221882 "
.94	.8836	1.06	1.94	2.1128	.190659 "
.95	.9025	1.05	1.95	2.0950	.159220 "
.96	.9216	1.04	1.96	2.0768	127599 "
.97	.9409	1.03	1.97	2.0582	.095830 "
.98	.9604	1.02	1.98	2.0392	.063949 "
.99	.9801	1.01	1.99	2.0198	.031994 "
1.00	1.0000	1.00	2.00	2.0000	0

Paper 1254 ST 3

Journal of the
STRUCTURAL DIVISION
Proceedings of the American Society of Civil Engineers

THE BEHAVIOR OF ONE-STORY REINFORCED CONCRETE SHEAR WALLS

Jack R. Benjamin,[1] A.M. ASCE, and Harry A. Williams,[2] M. ASCE
(Proc. Paper 1254)

SYNOPSIS

This paper gives the results of an investigation of one-story plain and reinforced concrete shear walls subject to shear forces applied in the plane of the wall. Panel proportions and reinforcing, and column proportions and reinforcing were investigated.

Some approximate relationships are suggested as a means of predicting the load-deflection curves for these walls.

INTRODUCTION

This paper is based upon an investigation of the strength and behavior of shear walls which was conducted at Stanford University during the period 1951 to 1956. The project was conducted under Contract W-591 with Sandia Corporation, Albuquerque, New Mexico during 1951 and under Contract DA 49-129-Eng-193 with the Office of the Chief of Engineers, Department of the Army, Washington, D. C. during the period 1952 through 1956.

The purpose of the investigation was to develop data on the resistance of shear walls which could be used in the design of structures to resist atomic blast loads. The advantages of shear walls as primary lateral load resisting elements for blast resistant structures was recognized in 1948 during the initial development of methods for design of such structures by the Office of the Chief of Engineers. Full scale tests of shear wall structures were conducted in 1951 at Operation Greenhouse in the Pacific Proving Ground for atomic weapons. Laboratory tests on shear walls were initiated in 1949 by the Chief of Engineers at the Massachusetts Institute of Technology.[3] These studies were subsequently continued at Stanford University by contractual arrangements with the Sandia Corporation and the Office of the Chief of Engineers of the Army.

Note: Discussion open until October 1, 1957. Paper 1254 is part of the copyrighted Journal of the Structural Division of the American Society of Civil Engineers, Vol. 83, No. ST 3, May, 1957.

1. Associate Prof. of Structural Eng., Stanford Univ., Stanford, Calif.
2. Prof. of Civ. Eng., Stanford Univ., Stanford, Calif.

3. "Behavior of Structural Elements Under Impulsive Loads." Part I, April 1950; Part II, Nov. 1950. Reports submitted to New England Division, Corps of Engineers, Department of the Army. Supervised by John B. Wilbur.

Although shear walls have been used in earthquake resistant design for many years, little was known concerning their ultimate strength or behavior in the cracked range. Some studies [4,5] of shear walls for earthquake resistance have been made by Japanese investigators.

This paper is concerned with the behavior of one-story reinforced concrete shear walls without openings of the type shown in Fig. 1. The wall is loaded through a distributing member at the top of the wall. This may be a beam or a floor diaphragm. Both tension and compression columns are provided and the wall is supported on an essentially rigid foundation. The tension and compression columns may have the same thickness as the panel but are provided with special steel in any case. Face walls may act as the bounding columns.

The important variables are:

1) Loading
2) Materials
3) Panel design
   a) Thickness and proportions
   b) Reinforcing
4) Tension column design
5) Compression column design
6) Method of construction

Shear walls can be subjected to three different loadings. The shear load from lateral forces acting in the plane of the wall constitutes the primary condition covered in this paper. The wall can also be used as a bearing wall and it can be subjected to loads perpendicular to its face. Under dynamic loading conditions from blast or earthquake, the combinations of loadings become complex because of the time relationships that can exist between the three types of loads.

The shear wall itself is subject to many variables. The materials of construction can vary considerably, both concrete and steel. Variations in panel proportions, length, height, thickness, and reinforcing influence the wall behavior. Similarly, variations in tension and compression column design are important. Finally, the details of construction, pour joints, doweling, keying, curing, etc., must be considered.

The general problem is best studied from the standpoint of a typical load-deflection curve and the influence of the variables on this curve. The typical wall is shown by the type C specimen in Fig. 1 and the typical load-deflection curve in Fig. 2. The problem is considered solved if the following are known:

1) Load at break in load-deflection curve, V_c
2) Deflection at break in load-deflection curve, δ_c
3) Ultimate load, V_u
4) Deflection, δ_u, at ultimate load
5) Post ultimate general behavior
6) Mode of failure, failure characteristics, and extent of damage at particular load points.

Reinforced concrete is a statistical material. Considerable variation in experimental results always occurs. The method of prediction of shear wall behavior must fit the observed mode of failure and generally agree with the observed load-deflection curve.

---

4. "Study of Vibration Resistant Walls," by T. Taniquchi, Transactions of the Architectural Institute of Japan, n. 41, Aug. 1953, p. 62.
5. "Stress Analysis of Walls with Rectangular Holes," by K. Otsuki. Transactions of the Architectural Institute of Japan, n. 41, Aug. 1953, p. 72.

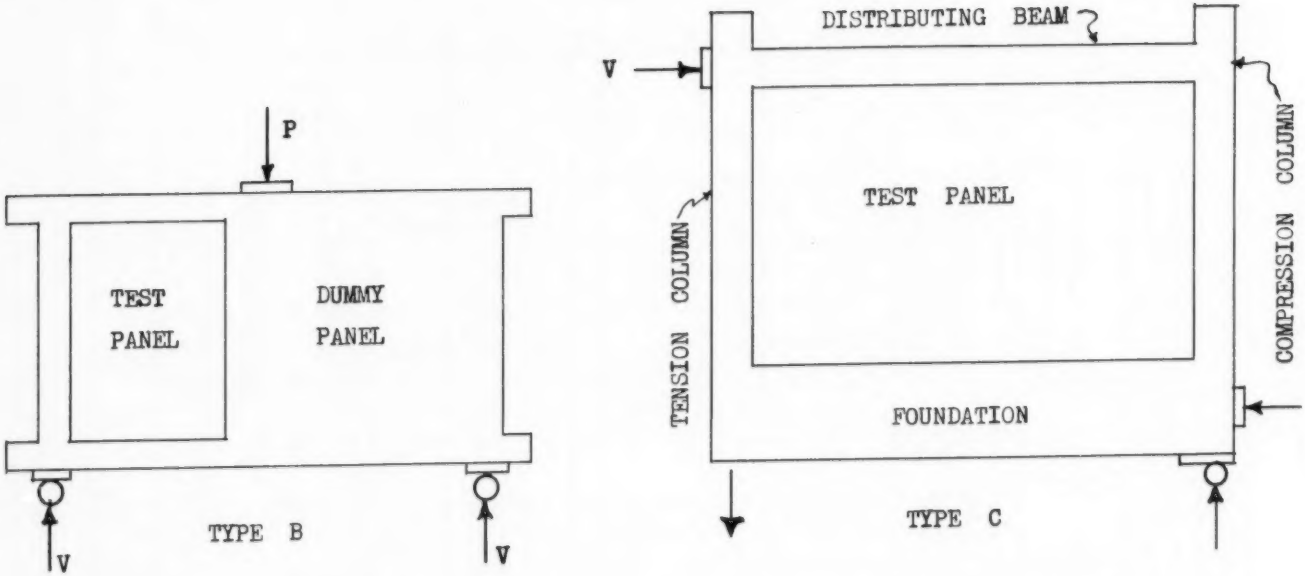

FIG. 1 SPECIMENS B AND C AND METHODS OF LOADING

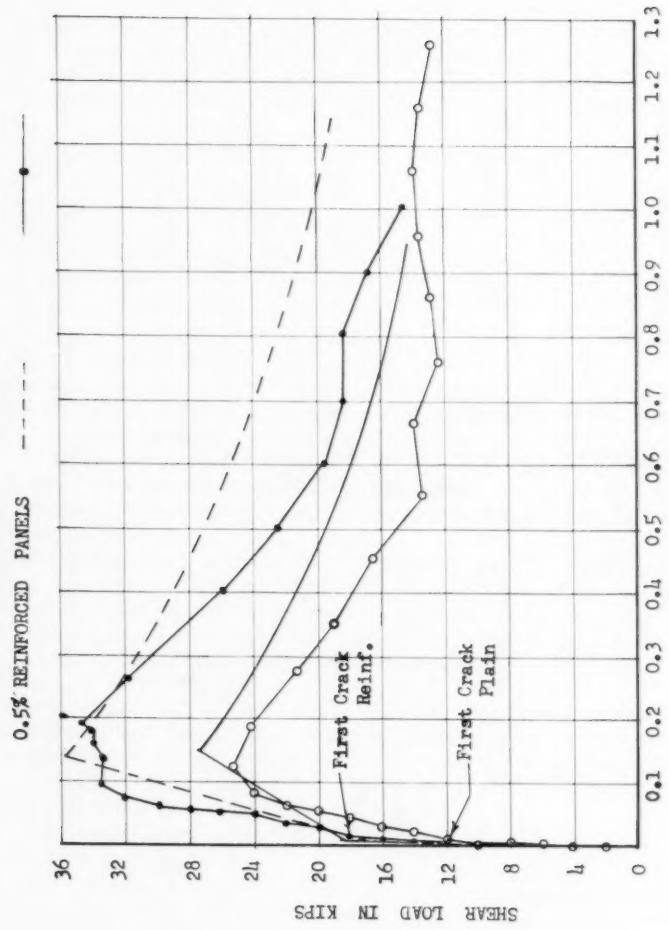

FIG. 2. - EXPERIMENTAL & THEORETICAL CURVES FOR PLAIN & REINF. PANELS.

Mathematical Investigations

Extensive mathematical and experimental studies were made during the program. The mathematical studies were based on a simplification of the lattice analogy.[6,7] They were invaluable in acquiring a basic understanding of shear wall behavior. However, the complex procedures did not produce more accurate results than ordinary strength of materials in the prediction of general shear wall behavior because reinforced concrete is so highly variable in behavior.

The load-deflection curve is essentially linear up to some point close to the formation of the first crack although it is not elastic in behavior. The cracked behavior can be approximated by lattice analogy solutions if crack locations are assumed. SR-4 rosettes were mounted on the wall panels and SR-4 A-7 gages on the column steel of several model walls. The results were not conclusive in either proving or disproving mathematical studies. The difficulty is that the panel concrete cracks at a very low stress and once the panel is cracked the rosette gages have little value. The strains to be measured before cracking are very small. Three or four points on a load-strain curve are obtained before the wall cracks and the probable error in any one reading is of the same order of magnitude as the difference in strains between the load points. Gages mounted on the column steel were of value only after extensive cracking had taken place providing the bond failed in the vicinity of the gage without rupturing the leads. Intensive mathematical studies, therefore, were instructive but not inconclusive.

Scale Effect

The first problem facing any study using models is to determine if a scale effect is involved. Areas scale differently from moments of inertia. Will a quarter scale model yield results consistent with the prototype? A series of reinforced concrete walls ranging from one-eighth to three-eighth scale were tested. Full scale was assumed as an 8 ft. high by 12 ft. long wall with an 8" thick panel. All walls were proportioned on a purely geometric basis. The testing machine capacity limited the largest specimen to three-eighth scale.

No scale effect was observed from these tests. If present, it was hidden by the general scatter of results. The model details are given in Fig. 3 and load-deflection curves transformed to full scale values in Figs. 4 and 5. The one-eighth scale models were cracked before testing began due to shrinkage stresses in the thin panels.

Experimental Procedures

Model walls were of two general types. They are shown in Fig. 1. The small models were usually of type B and were tested in a 200,000 lb. Reihle testing machine. A photograph of a model under test is given in Fig. 6.

---

6. "Solutions of Problems of Elasticity by the Framework Method," by A. Hrennikoff. Journal of Applied Mechanics, Dec. 1941.
7. "A Lattice Analogy for the Solution of Stress Problems," by Douglas McHenry. Journal of the Institution of Civil Engineers, Dec. 1943.

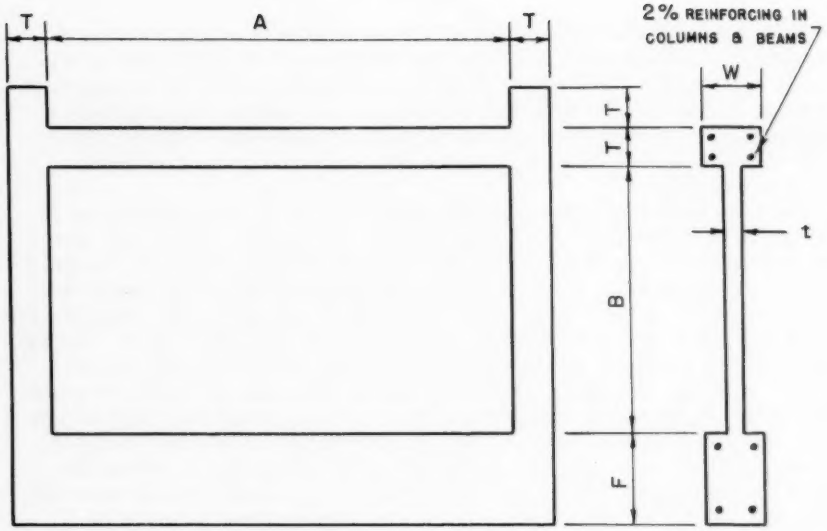

TYPE C MODELS

λ	A (IN.)	B (IN.)	T (IN.)	W (IN.)	t (IN.)	F (IN.)
1	232	134	20	30	8	48
3/8	87	50¼	7½	11¼	3	18
¼	58	33½	5	7½	2	12
⅛	29	16¾	2½	3¾	1	6

FIG. 3. SKETCH AND DIMENSIONS OF SCALE EFFECT MODELS. 0.5% REINFORCING USED IN SPECIMENS WITH REINFORCED PANELS.

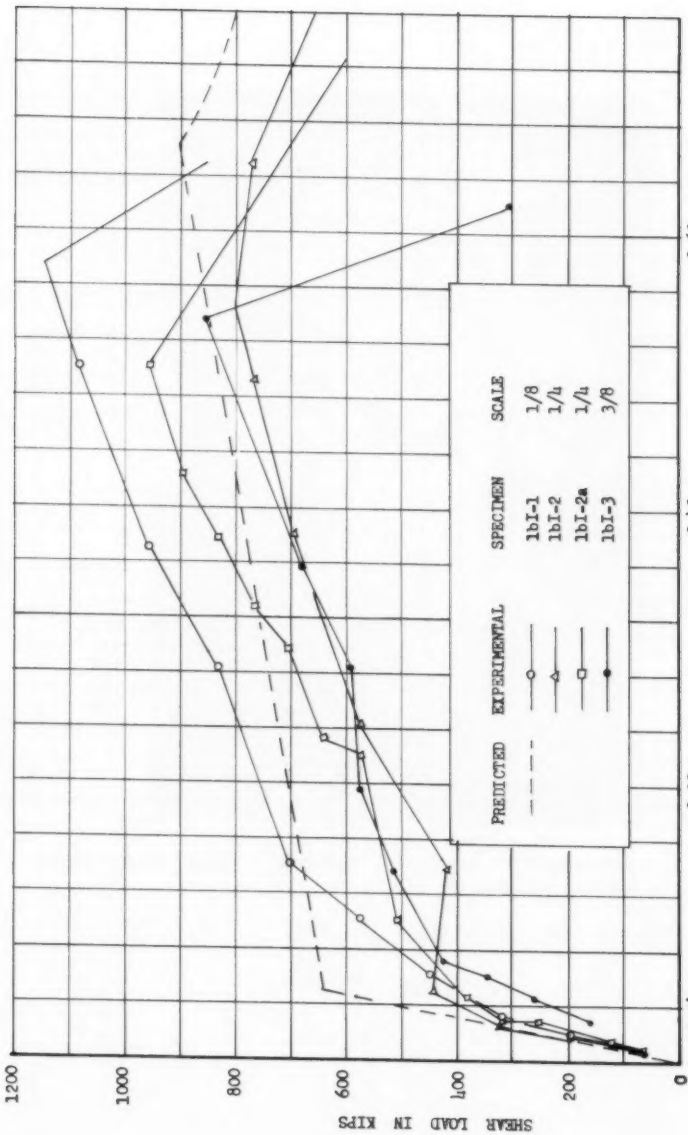

FIG. 4. LOAD-DEFLECTION CURVES FOR PROTOTYPE - SCALE EFFECT MODELS WITH PLAIN PANELS.

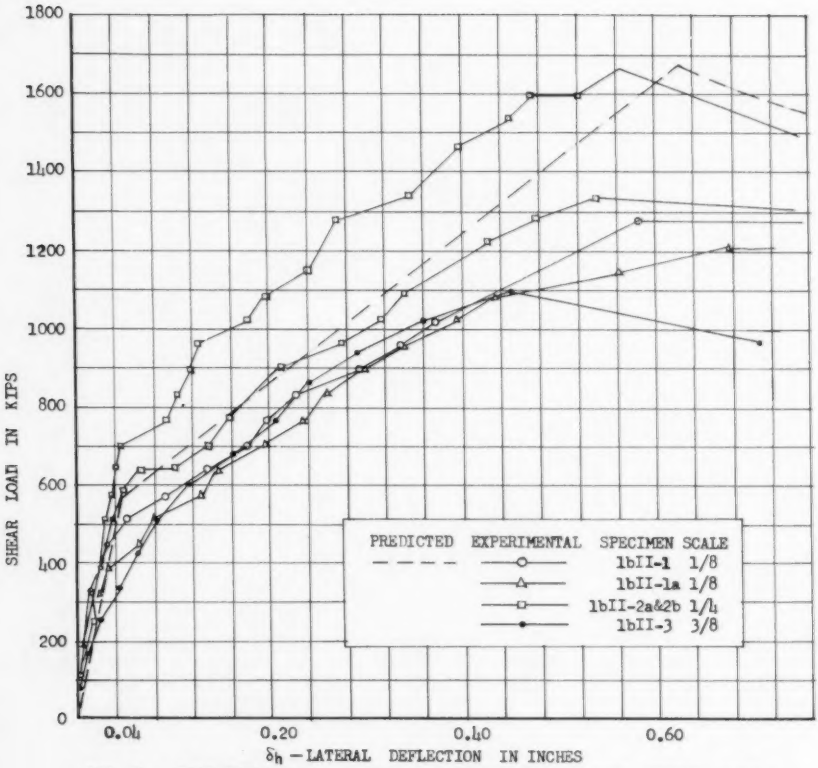

FIG. 5. - LOAD-DEFLECTION CURVES FOR PROTOTYPE - SCALE EFFECT MODELS WITH 0.5% REINFORCED PANELS.

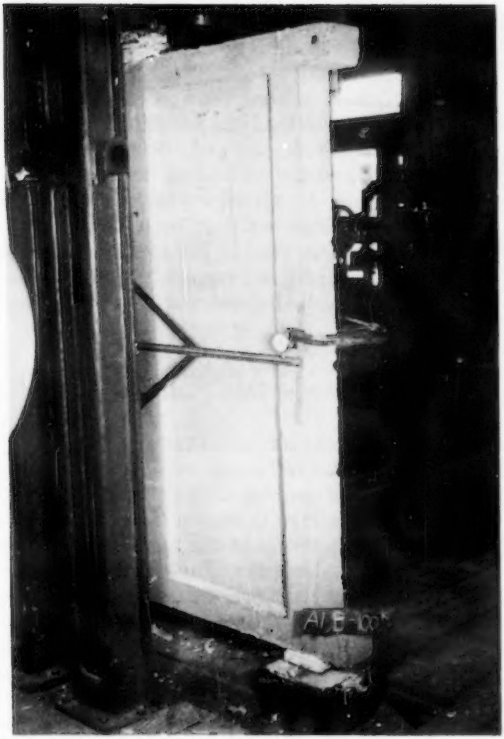

FIG. 6 - TYPE B SPECIMEN IN REIHLE TESTING MACHINE

Large models and assemblies were tested in the specially constructed shear jig shown in Fig. 7.

Type I Portland cement was usually used in the concrete mix with a small amount of additive to improve workability. High-early cement was used occasionally as dictated by the testing program. Walls were generally tested after about two weeks when the concrete strength approximated 3000 psi. Actual strengths as tested varied from 2300 to 3800 psi. The reinforcing steel was of structural or intermediate grade. All bars 3/8" diameter and over were standard deformed reinforcing bar; those less than 3/8" diameter were smooth.

The test procedure consisted of applying a predetermined load and then reading all gages. In general, the load did not decrease during the reading period before the concrete cracked. Once cracking began, the load did drop off during the reading period and the amount of drop off was a direct function of the amount of disintegration. No attempt was made to maintain the load on the Type B specimens in the Reihle machine because the magnitude of drop off was generally less than ten per cent of the applied load. Tests in the shear jig often involved a much larger drop off. The load was essentially maintained during the reading period if more than a ten percent load reduction was involved.

Modes of Wall Failure

The walls had several different modes of failure. As near as could be determined, the steel had negligible influence until the concrete cracked. Reinforcing steel then controlled the opening of the crack and its propagation.

The first possible mode of failure is characterized as a tension column failure. If insufficient steel is present at the junction of the tension column and the foundation to take up the load when the concrete cracks, this crack opens and rapidly runs along the junction of the panel and the foundation to the compression column as shown for specimens C-3 and 3A2-4 of Figs. 8 and 10. If first cracking in the tension column does not stress the tensile column steel to the yield point, this crack may occur but it does not open up and is difficult to see by visual inspection.

The second possible mode of failure involves the panel cracking diagonally in the tensile stress region. If the panel is unreinforced, or lightly reinforced, this cracking follows the patterns shown in Fig. 8 and depends on the amount of column steel. With unreinforced panels this first panel crack rapidly spreads to the foundation and tension column. A further increase in shear load then produces cracks along the foundation to the compression column and along the tension column to the beam. The first break in the load-deflection curve occurs approximately at this load (Fig. 9). The shear load will then increase further with more and more panel cracking until the compression column cracks at the foundation and finally shears off. Ultimate load occurs at this point.

The shearing resistance of the wall drops rapidly after the compression column shears off. Studies show that this compression column failure is a function of steel area, concrete strength, and panel proportions. The concrete area is unimportant as long as the bars are adequately covered. The failure mechanism apparently involves a cracking of the concrete at such an angle that friction is unimportant. Actual failure then occurs when the

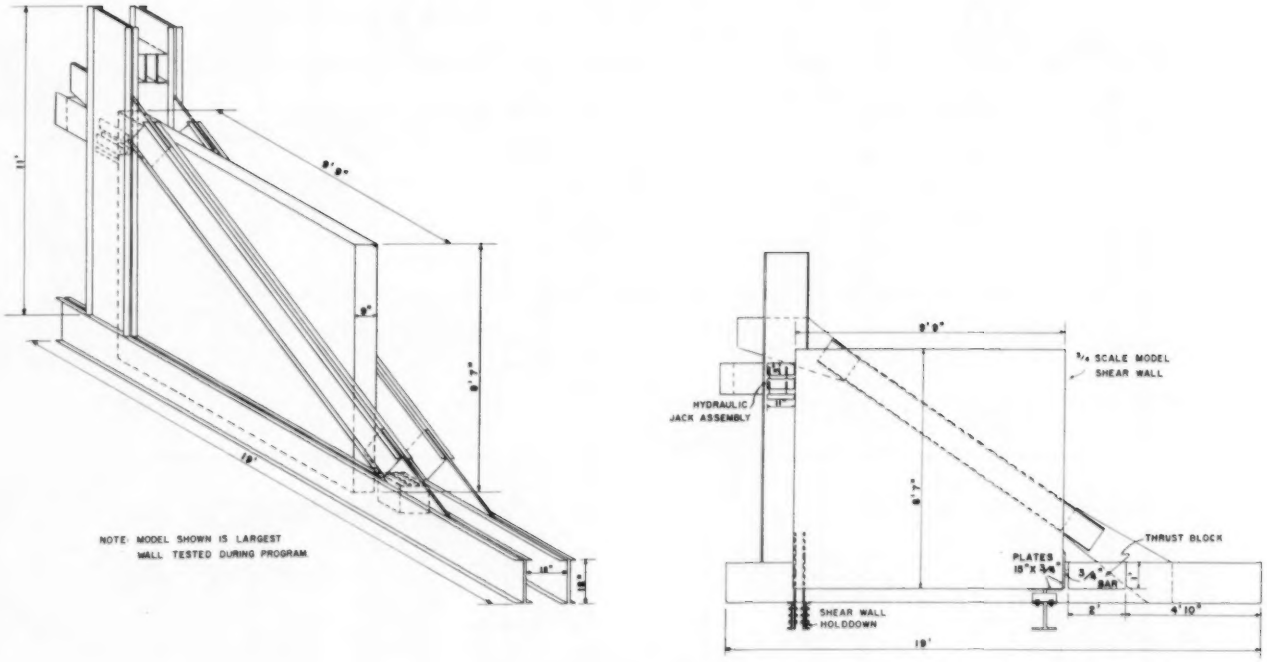

FIG. 7 - 300 KIP SHEAR JIG FOR TESTING TYPE C MODELS

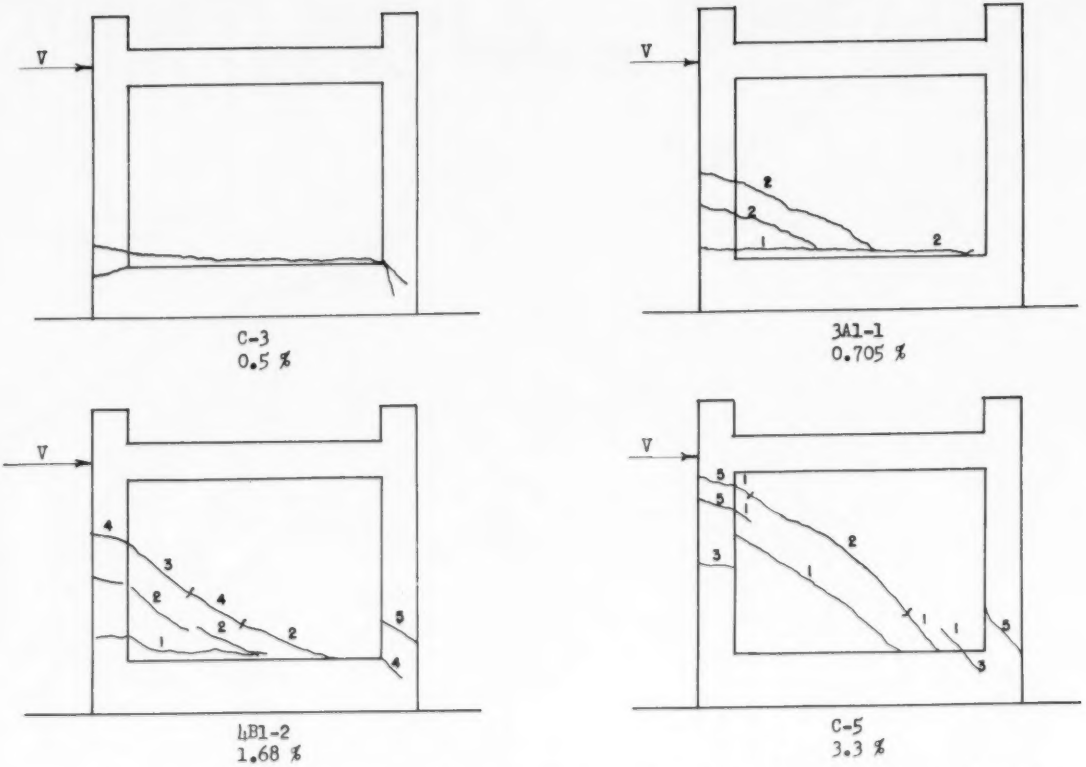

FIG. 8. CRACKING PATTERNS FOR WALLS WITH VARIED PERCENTAGES OF STEEL IN THE COLUMN. UNREINFORCED PANELS.

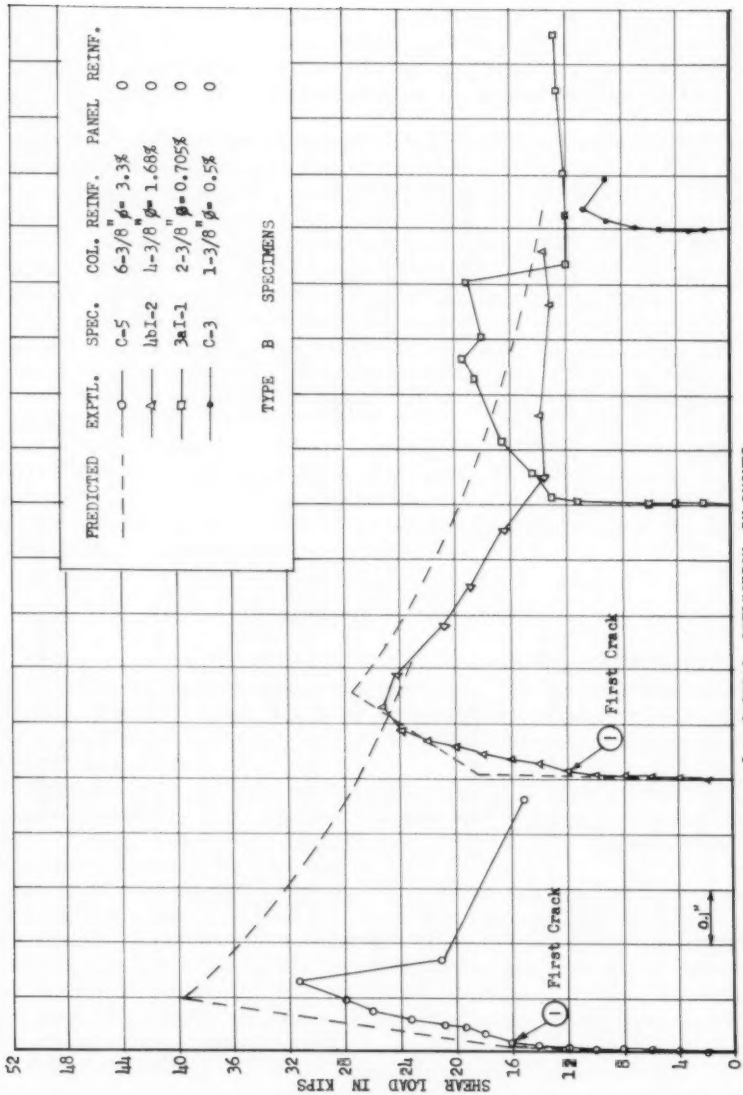

FIG. 9 . - EFFECT OF VARIED COLUMN STEEL ON LOAD - DEFLECTION CURVES WHEN AREA OF COLUMN WAS HELD CONSTANT. PLAIN CONCRETE PANELS.

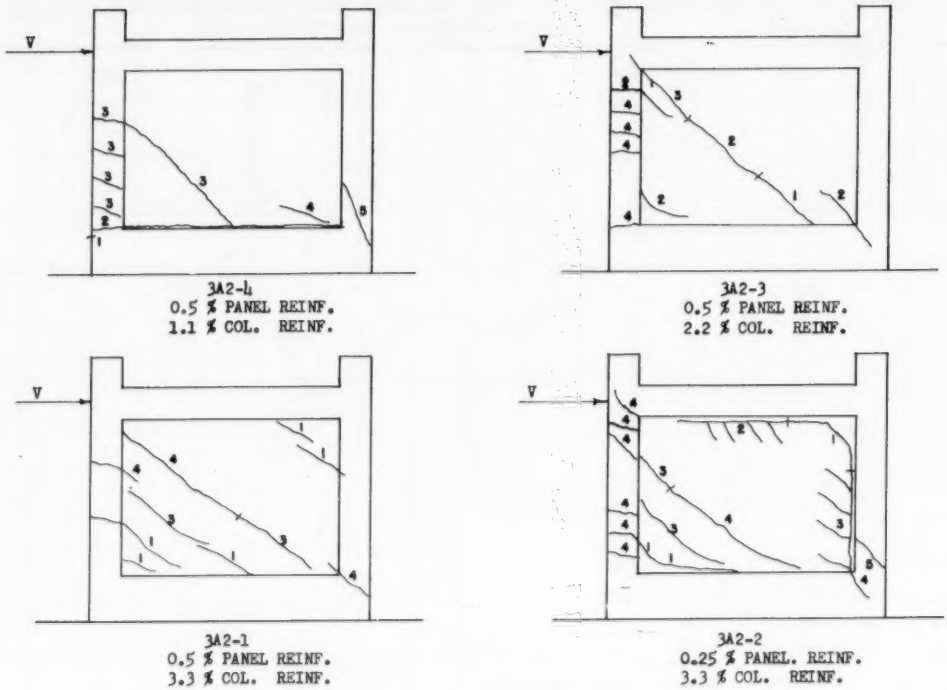

FIG. 10. CRACKING PATTERNS FOR WALLS WITH VARIED PERCENTAGES OF STEEL IN COLUMNS. REINFORCED PANELS.

concrete around the bars is crushed at the crack line and the bars bend.

If the panel is moderately reinforced, p. ≥ 0.0025, the failure mode is modified as a function of the amount of panel steel. The steel produces general diagonal cracking instead of a single major crack as with unreinforced panels. It is important to note that the first crack load and location are completely independent of the amount, type, and location of panel steel. The break in the load-deflection curve occurs at the advent of general cracking in the panel (Fig. 11). It is not generally at the load producing the first panel crack.

Panel reinforcing has a pronounced influence on the cracked wall behavior. This will be discussed in a later section. At ultimate load a major portion of the vertical panel steel is apparently at its yield point and a few of the horizontal bars are in the post yield condition approaching actual failure. Ultimate load then occurs with the compression column shearing off in the same manner as with unreinforced panels. The panel steel produces an important increase in ultimate strength and rigidity in the cracked region.

Other failure modes are possible. The failure could be associated with high panel cracking and a bending of the compression column. Some variations in panel reinforcing tend to produce this type of failure. No appreciable change in ultimate strength is associated with this failure mode unless carried to an extreme.

A tension column steel failure can occur after the panel has cracked if this steel is overstressed at any time. Composite failures involving tension column yielding, panel cracking, and compression column shearing were observed in a few isolated cases. The tension column influence was apparently small in the composite failures noted.

Influence of Panel Variations

The panel proportions, length, L, height, H, and thickness, t, and the panel reinforcing influence the shear wall behavior. The panel thickness is only of importance with uncracked panels. Cracking load and rigidity are influenced, the first directly, the latter as a product of its influence on the moment of inertia of the section.

The panel proportions, length-height ratio, L/H, have a direct and pronounced influence. This problem was studied using unreinforced and reinforced walls. The test results are given in Figs. 12 to 15, inclusive. Photographs are given in Figs. 16 and 17.

Study of the load-deflection curves discloses that as L/H increases, the load at first crack or at a major break in the load-deflection curve approaches the ultimate load. For the specimens tested, the two loads agree approximately at an L/H of three with unreinforced panels, and approximately at four for the reinforced walls. The crack pattern changes as the L/H ratio increases. The cracks become progressively higher in the wall, finally approaching a pure diagonal crack.

Panel reinforcing can be varied as to quantity and placement. In one series, the steel ratio, p, was varied from 0 to 0.015, both horizontally and vertically. Results are shown by the load-deflection curves of Fig. 18 and the photographs of Fig. 19. Note that all walls have essentially the same behavior before cracking. Panel reinforcing is only effective after cracking begins. As the panel reinforcing increases, the number of cracks before

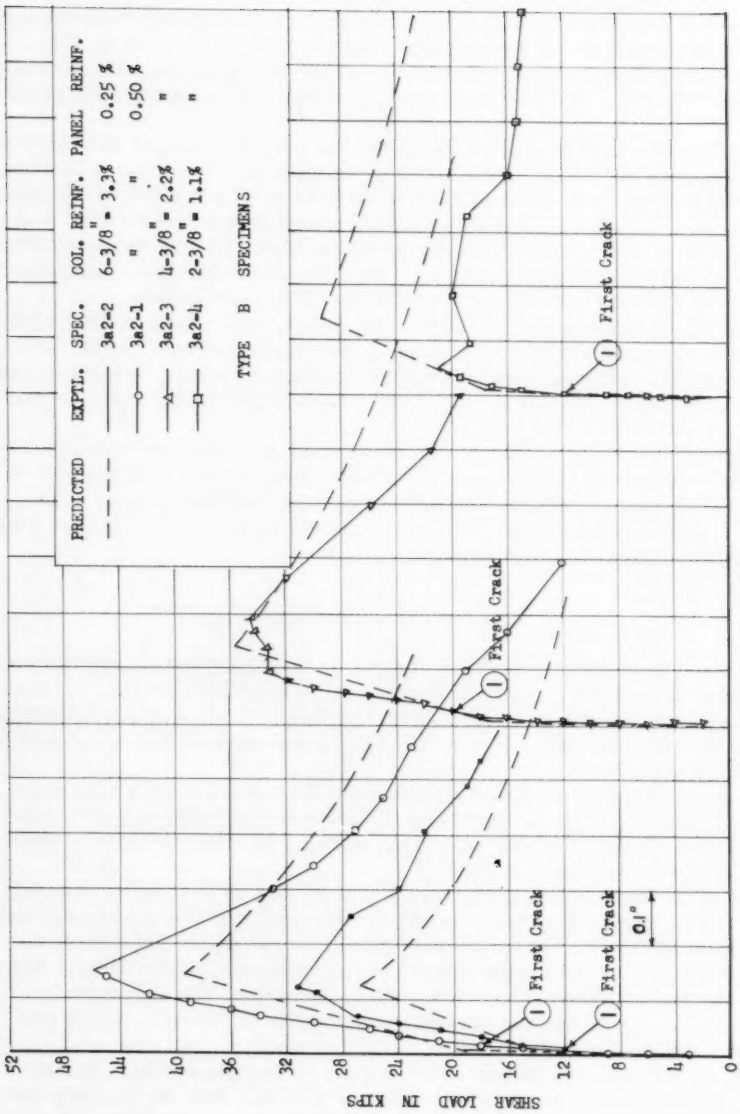

δ_h — LATERAL DEFLECTION IN INCHES

FIG. 11. - EFFECT OF VARIED AMOUNT OF COLUMN STEEL ON THE LOAD-DEFLECTION CURVE WHEN THE AREA OF THE COLUMN IS CONSTANT.

WALL PANEL PROPORTIONS

	SPEC-IMEN	A IN.	B IN.	L/H	f'_c PSI	RATIO V/δ_h BELOW CRACKING	SHEAR AT 1ST CRACK		SHEAR AT ULT.	
							V KIPS	$V\sqrt{3000/f'_c}$ KIPS	V KIPS	$V\sqrt{3000/f'_c}$ KIPS
PLAIN PANEL	4BI-1	16	20	0.9	2850	650	7	7.4	20.4	21.5
	4BI-2	28	20	1.45	3290	2080	12	11	25.3	23.2
	4BI-3	40	20	2	3260	3800	19.2	17.6	31.2	28.6
	4BI-4	62	20	3	3500	4200	39	33.5	48	41.2
REINFORCED PANEL	4BII-1	16	20	0.9	2920	590	9	9.3	20	20.4
	3A2-3	28	20	1.45	3120	2000	20	19.2	34.8	33.5
	4BII-3	40	20	2	2830	2000	15	15.9	45.3	47
	4BII-4	62	20	3	3830	2600	45	35.2	66	51.6

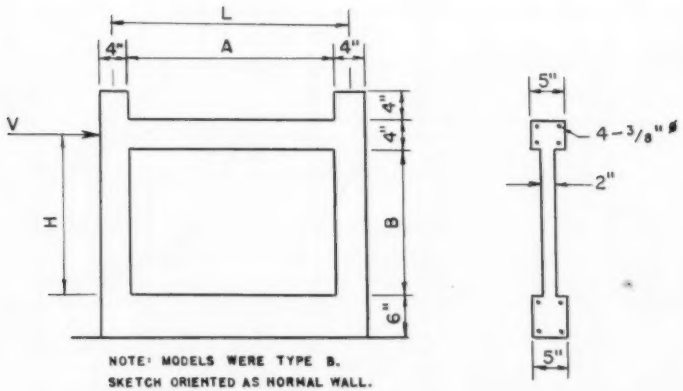

FIG. 12: DIMENSIONS OF MODELS USED IN DETERMINING THE EFFECT OF PANEL PROPORTIONS

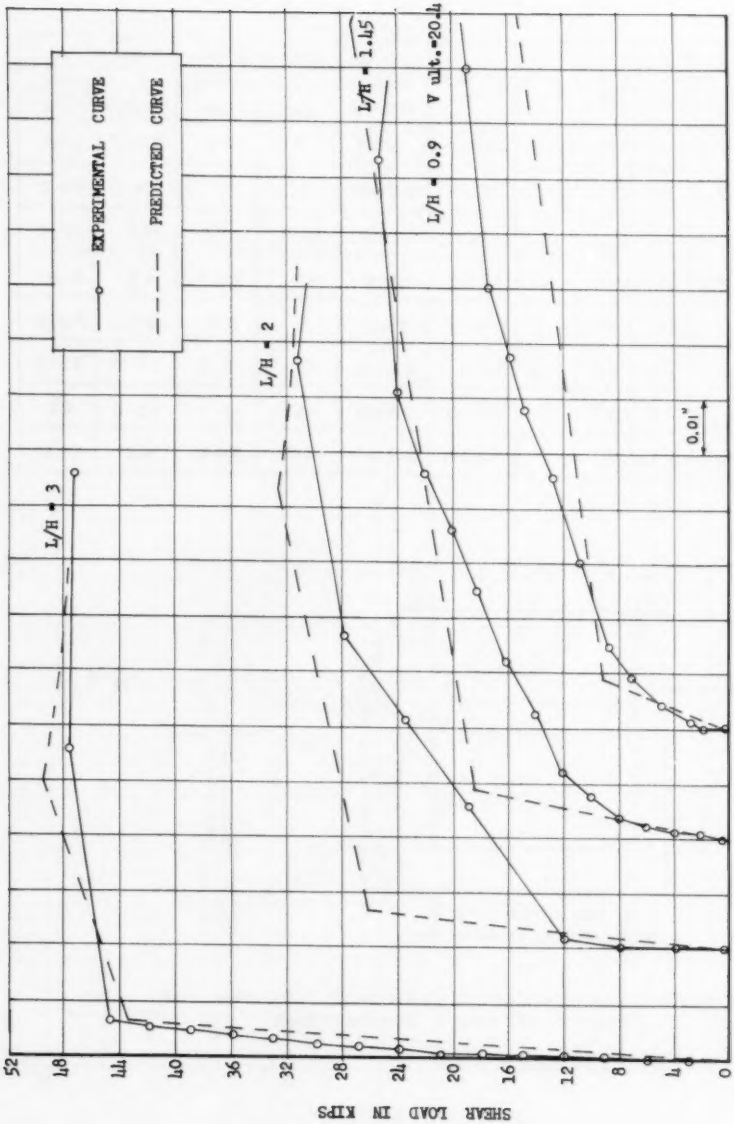

FIG. 13.- LOAD-DEFLECTION COMPARISION FOR WALLS WITH UNREINFORCED PANELS.

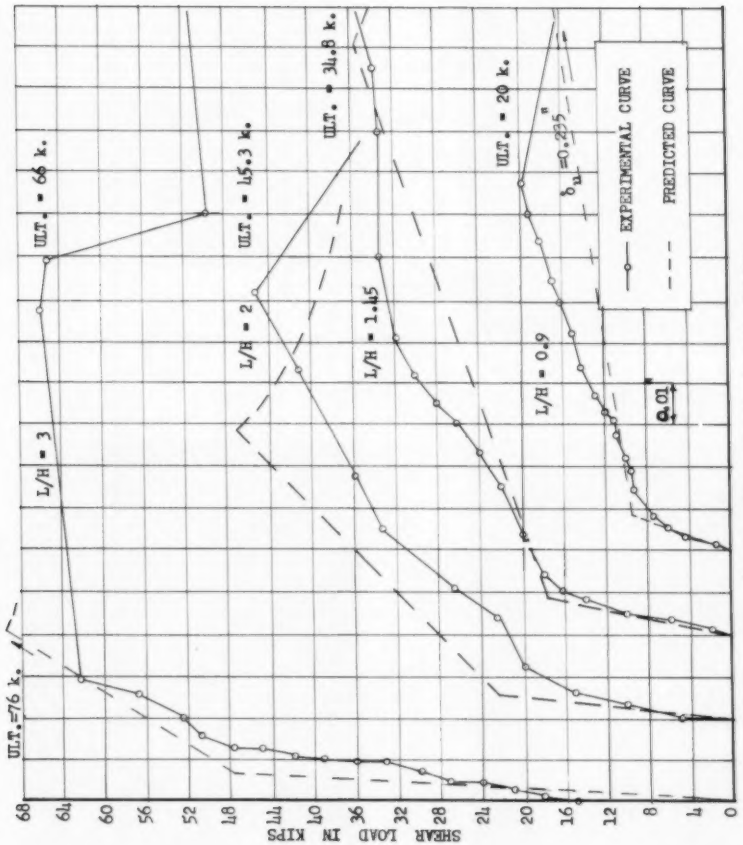

FIG. 14. - LOAD-DEFLECTION COMPARISION FOR WALLS WITH 0.5 % REINFORCEMENT

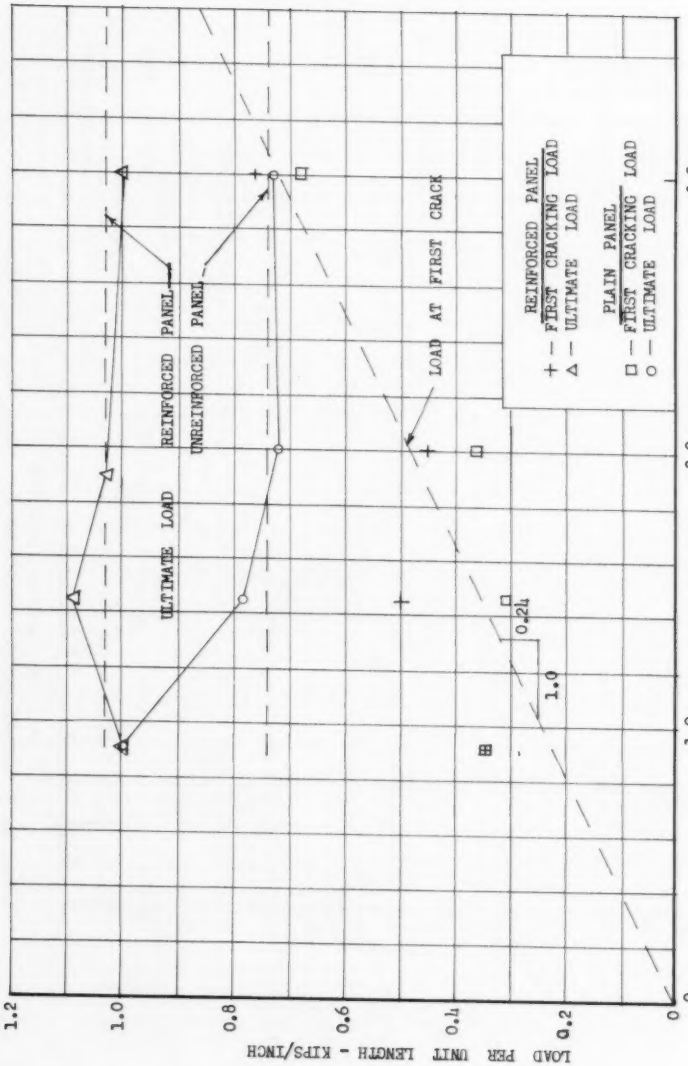

FIG. 15. - SHEAR LOAD PER UNIT LENGTH OF WALL AT FIRST CRACK AND ULTIMATE LOAD FOR SPECIMENS WITH VARYING PANEL PROPORTIONS.

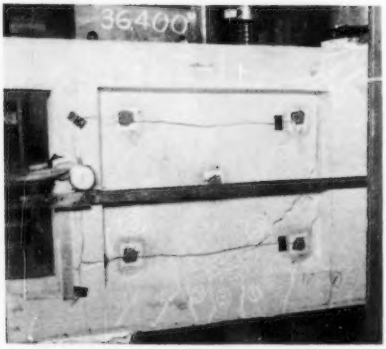

$\frac{L}{H} = 0.9$

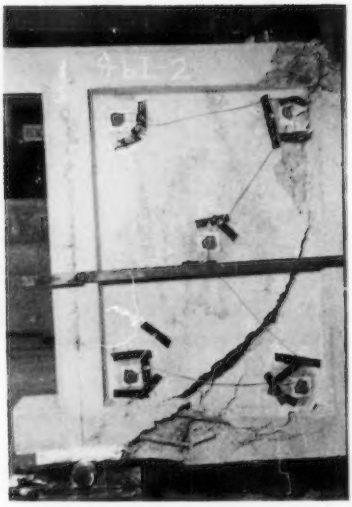

$\frac{L}{H} = 1.45$

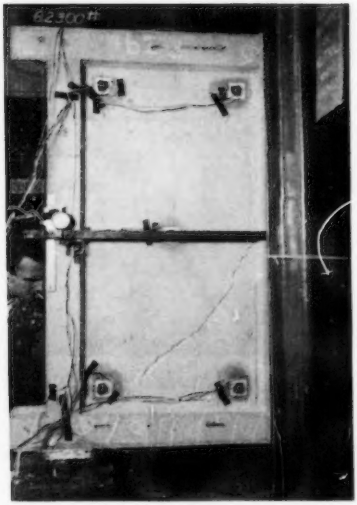

$\frac{L}{H} = 2$

$\frac{L}{H} = 3$

FIG. 16. SPECIMENS WITH PLAIN PANELS TESTED TO DETERMINE WALL LENGTH / HEIGHT RATIO EFFECT ON SHEAR WALL BEHAVIOUR . THE CRACKS ARE NUMBERED IN ORDER OF OCCURANCE.

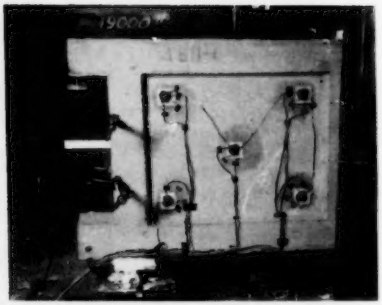

$\frac{L}{H}$ = 0.9

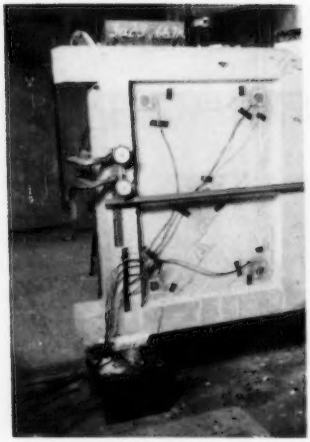

$\frac{L}{H}$ = 1.45

$\frac{L}{H}$ = 2

$\frac{L}{H}$ = 3

FIG. 17. SPECIMENS WITH 0.5 % REINFORCED PANELS TESTED FOR WALL LENGTH / HEIGHT RATIO EFFECT. THE CRACKS ARE NUMBERED IN ORDER OF OCCURANCE.

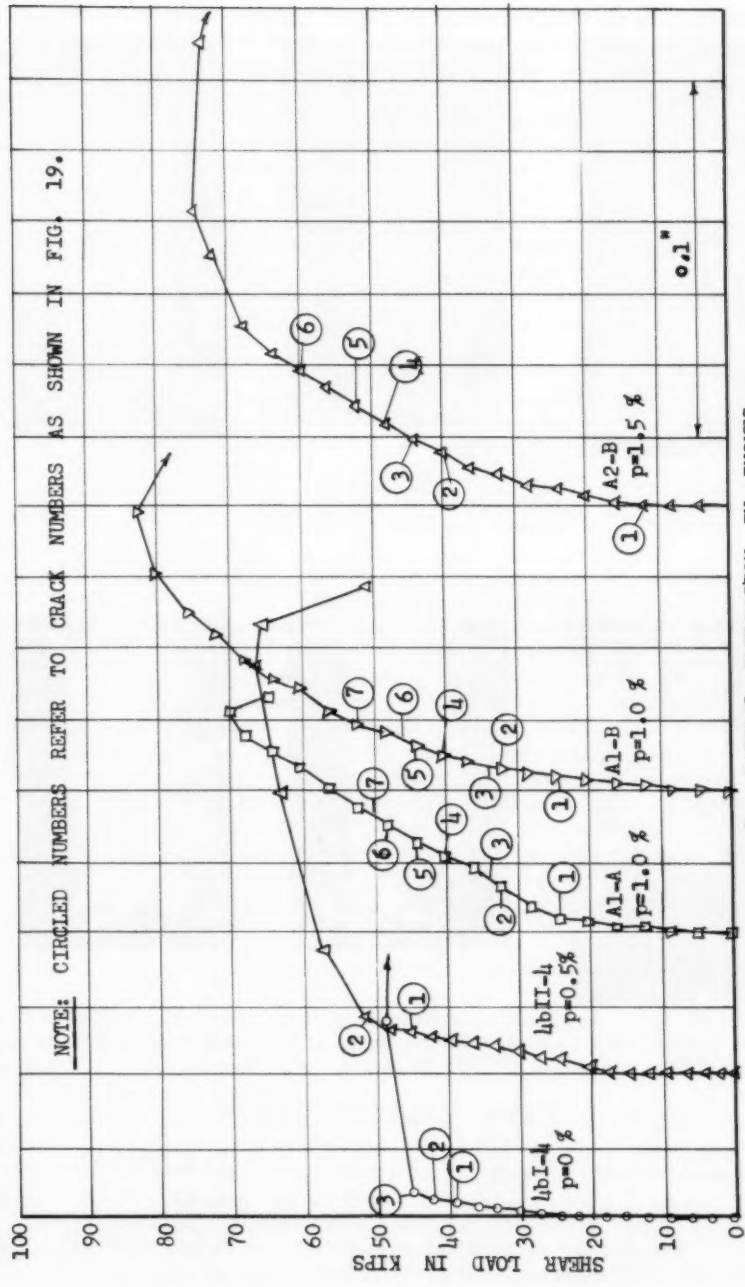

FIG. 18.- LOAD-DEFLECTION CURVES FOR WALLS WITH VARYING STEEL RATIOS, p, IN PER CENT.

4bI-4 Unreinforced.

4bI-4 Ultimate Shear Load, 47.9 kips.

4bII-4 Half Per Cent Reinforcing.

4bII-4 Ultimate Shear Load, 66 kips.

Al-A One Per Cent Reinforcing.

Al-A Shear Load 40 kips.

Fig 19 PHOTOGRAPHS OF REINFORCING STUDY WALLS

ultimate increases and the individual width of each crack decreases.

Variations in panel steel placement were studied with the purpose of obtaining the most efficient reinforcement system. Once again complex mathematical studies were completely ineffective. The first investigation was made with diagonal reinforcing as contrasted with the conventional type parallel to the sides of the panel. The diagonal reinforcing was varied from uniformly distributed to bands concentrated at the diagonals. Also, steel was concentrated at the diagonals and special corner reinforcing in regions of highest stress was added. Specimen details are given in Fig. 20 and load-deflection curves in Fig. 21. The total quantity of steel in the panel was kept as near constant as possible. In every case the diagonal reinforcing was less effective than rectangular reinforcing. Special corner steel was ineffective in improving wall characteristics. Heavy concentrations of steel on the panel diagonals produced large shrinkage cracks along the panel diagonals and decreased the wall rigidity.

The possibility of adding special steel to a conventional rectangular pattern was investigated next. The four specimens tested are shown in Fig. 22. Specimens VR-1 and VR-4 doubled normal steel in the region of highest stress. Specimens VR-2 and VR-5 were reinforced to control the crack pattern by doubling the steel in the central portion of the panel, thereby tending to force the cracks low in the panel. The progressive crack patterns were different in only a minor way and the final patterns and load-deflection curves were essentially identical.

Conventional rectangular bar patterns have the same bar spacing and size horizontally and vertically. Three specimens were tested to determine the relative effectiveness of horizontal and vertical reinforcing. The bar arrangements are shown in Fig. 23. The load-deflection curves are given in Fig. 24 and in the photographs of Figs. 25 to 28 inclusive. The tests show that the vertical steel is much more effective than the horizontal steel. In fact, vertical steel alone is fully as effective as vertical plus horizontal steel. Specimen VRR-7, Figs. 29 and 30, was tested as one possible practical application of this study. Horizontal steel was widely spaced in the upper 3/4 of the wall. Some horizontal steel is desirable to control the cracking of the concrete. The test results, Fig. 24, show this wall to have the same characteristics as one with conventional rectangular reinforcing. Note that if a parallel with beam shear reinforcing is drawn, vertical stirrups in a beam correspond to the horizontal and least efficient bars in the shear wall.

Influence of Column Variations

This effect was investigated by first varying the column cross section while keeping the reinforcing steel constant. Details of specimens are shown in Fig. 31, the resulting crack patterns in Fig. 32, and the shear load-deflection curves in Fig. 33.

The change in frame size affected the magnitude of the ultimate load, but all specimens failed in the same manner. Initial cracking occurred in the tension corner of the panel; ultimate load was reached when the compression column sheared through near its base.

The results appear inconsistent in that the wall with 5" x 2-1/2" columns had higher first cracking and ultimate loads than the one with the larger 5" x 12" columns. However, the first crack load is somewhat random in

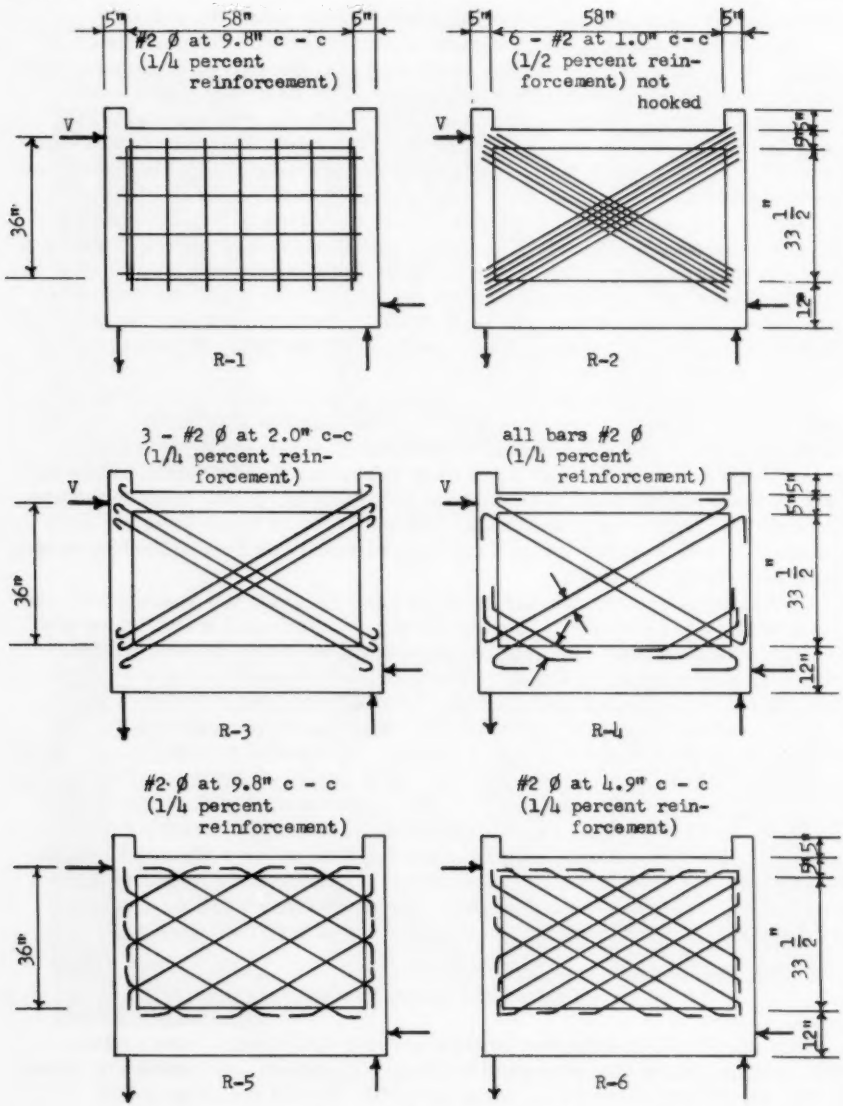

Notes: 1. Columns and beam are 5" x 7 1/2" with 4 - #4 Ø bars
2. Panel is 2" thick.

FIG. 20. DETAILS OF WALLS IN R - SERIES

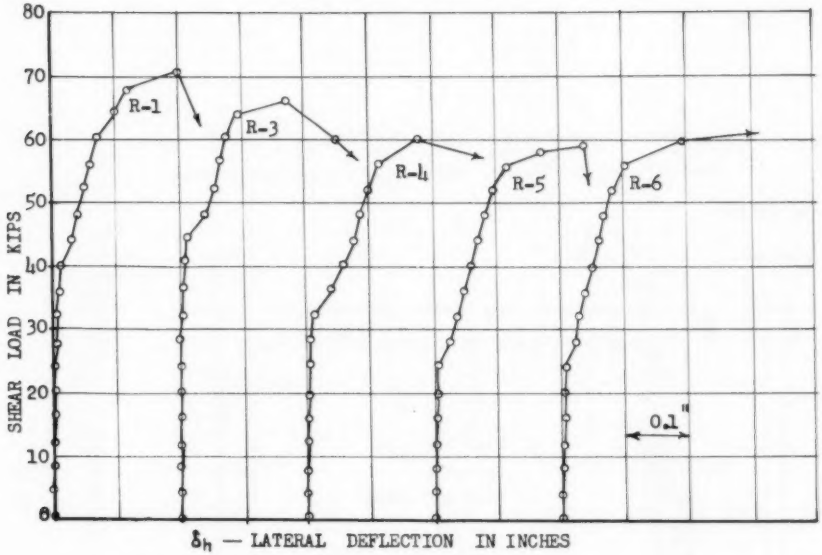

QUARTER PER CENT WALLS:

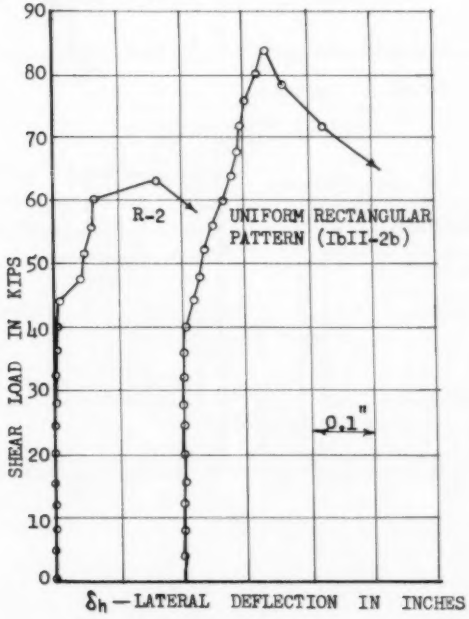

HALF PER CENT WALLS:

FIG. 21. - LOAD-DEFLECTION CURVES FOR DIAGONALLY REINFORCED WALLS & COMPARABLE RECTANGULARLY REINFORCED WALLS.

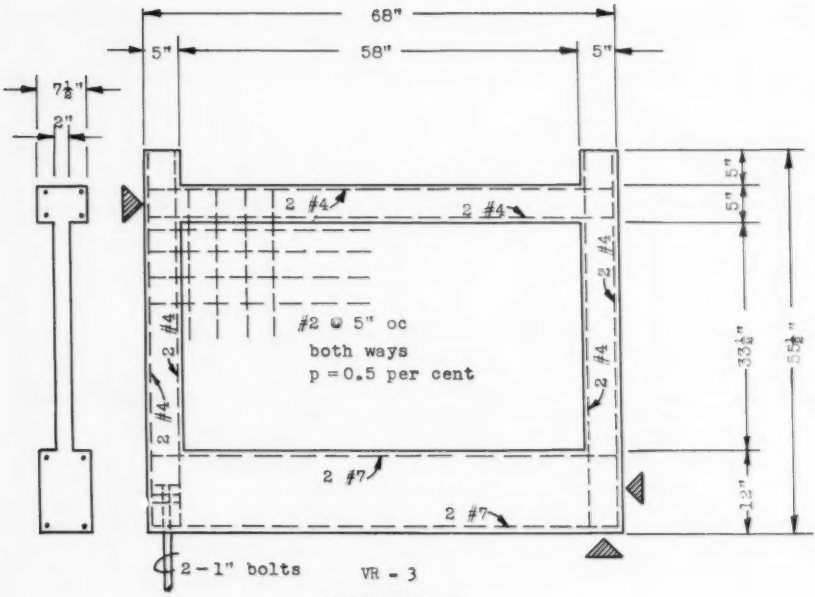

Typical Panel

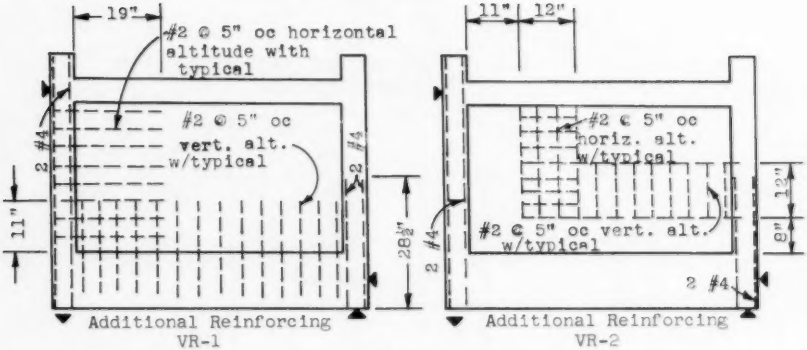

Additional Reinforcing
VR-1

Additional Reinforcing
VR-2

FIG. 22 .

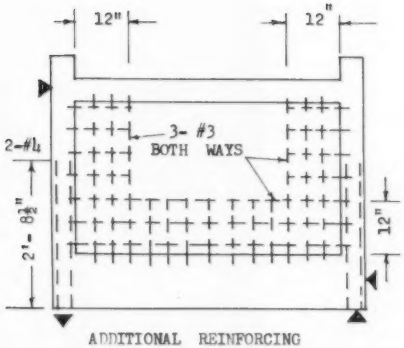

ADDITIONAL REINFORCING

VR - 4

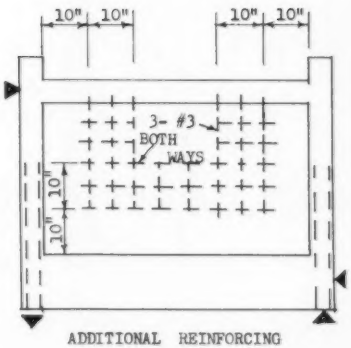

ADDITIONAL REINFORCING

VR - 5

FIGURE 22 (CONTINUED).

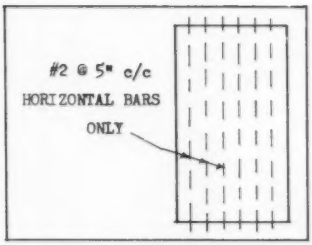

VRR - 2

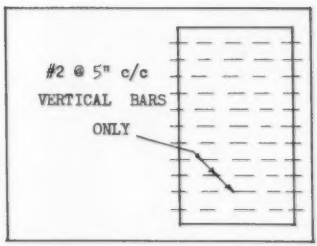

VRR - 3 & VRR - 6

REINFORCING DETAILS

FIGURE 23 .

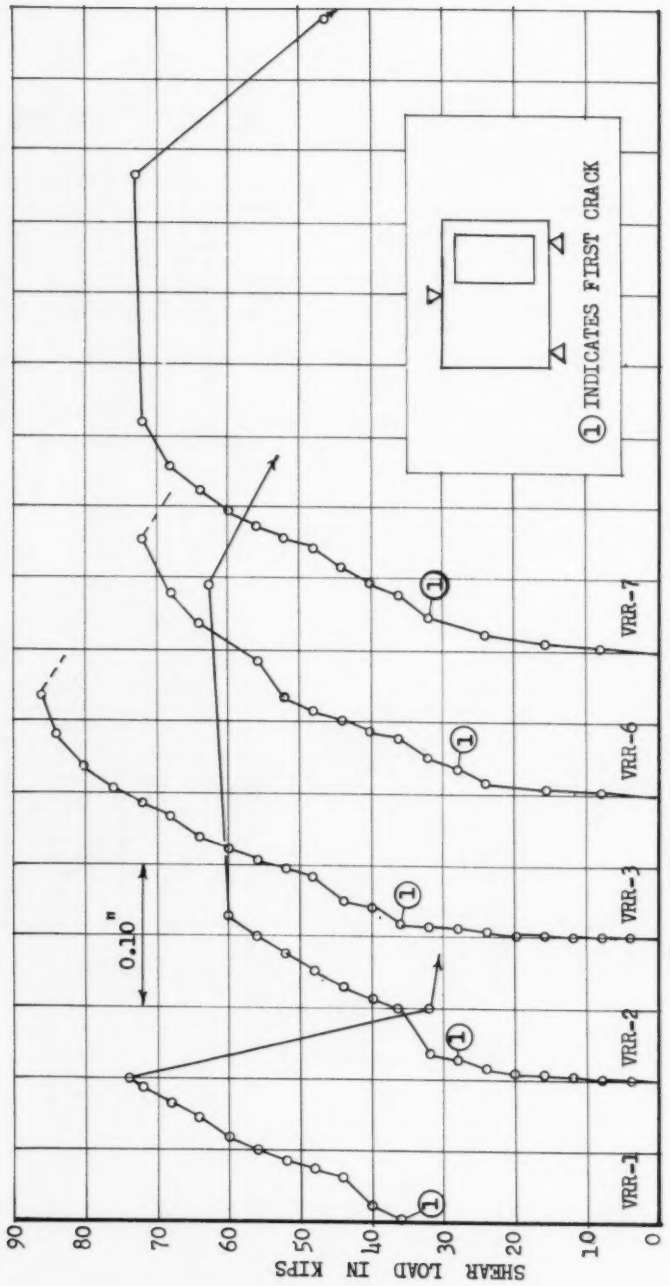

FIG. 24. - LOAD-DEFLECTION CURVES FOR VRR SERIES WALLS

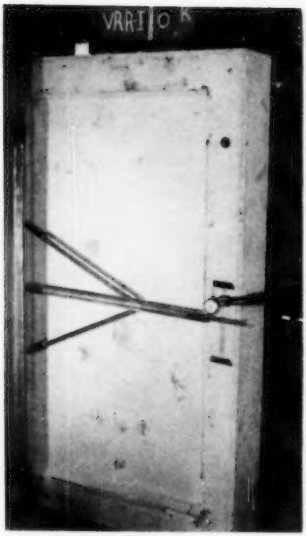

V = 0

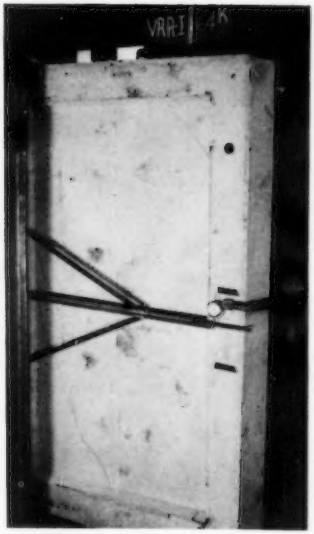

V = 32^{k}

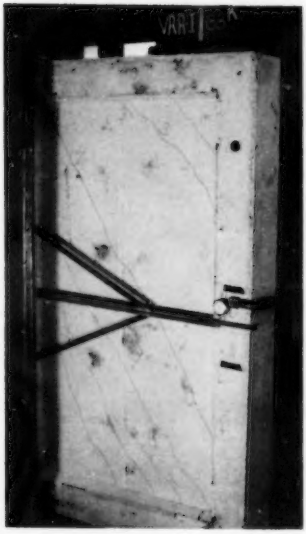

V = 44^{k}

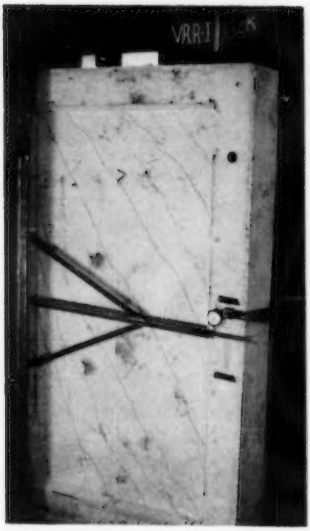

V = 72^{k}

FIG. 25 .--VRR-1

V = 0

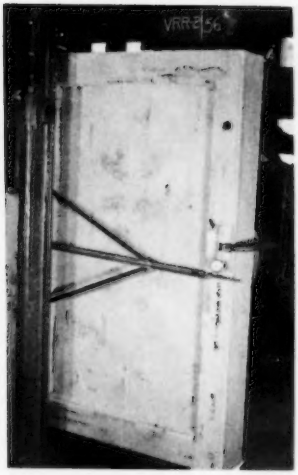

V = 28^K

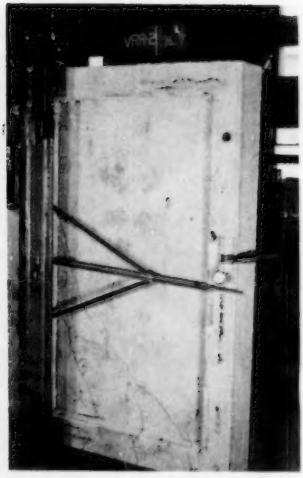

V = 48^K

V = 62.5
Ultimate

FIG. 26.--VRR2

V = 0

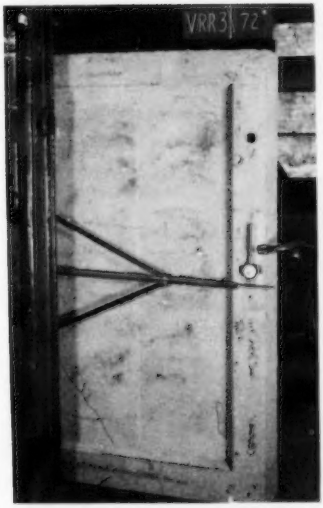

V = 36^{k}

V = 68^{k}

V = 86^{k}

FIG. 27.--VRR-3

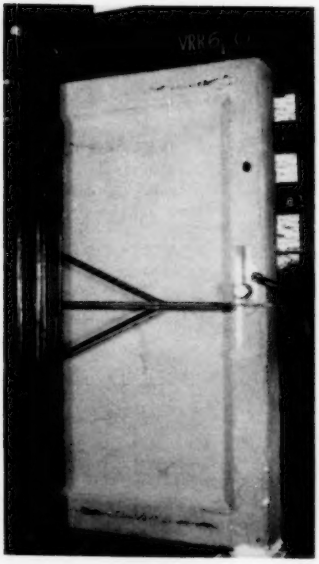

No Load

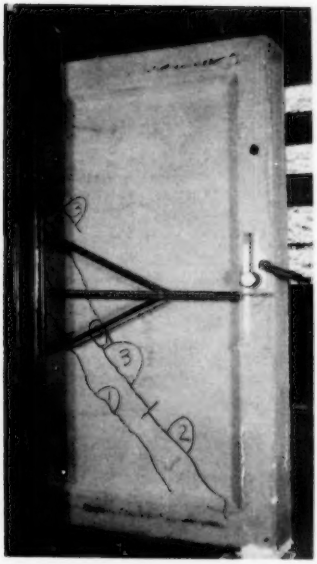

V = 72^{k}

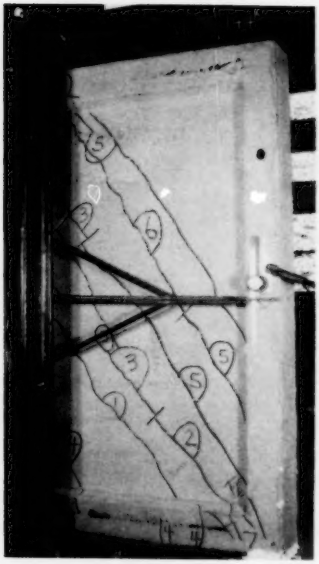

V = 144^{k}

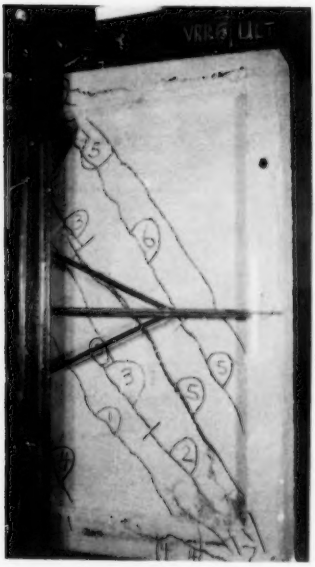

Ultimate - 144^{k}

Development of Crack Pattern

FIG. 28 .--VRR 6

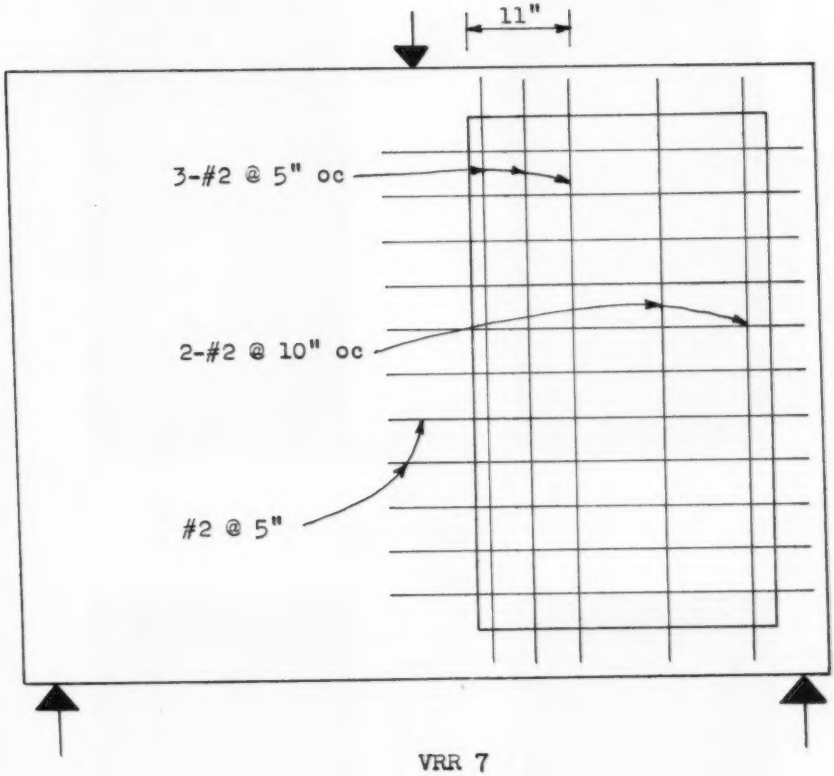

VRR 7

REINFORCING DETAILS

FIG. 29 .

No Load

V = 32^{k}

V = 48^{k}

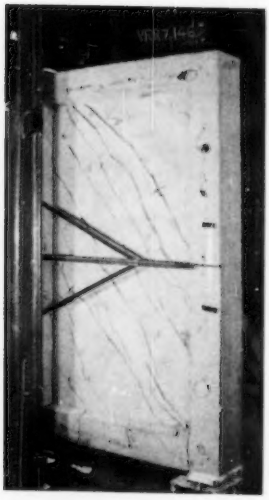

Ultimate
V = 73^{k}

Development of Crack Pattern

FIG. 30 .--VRR-7

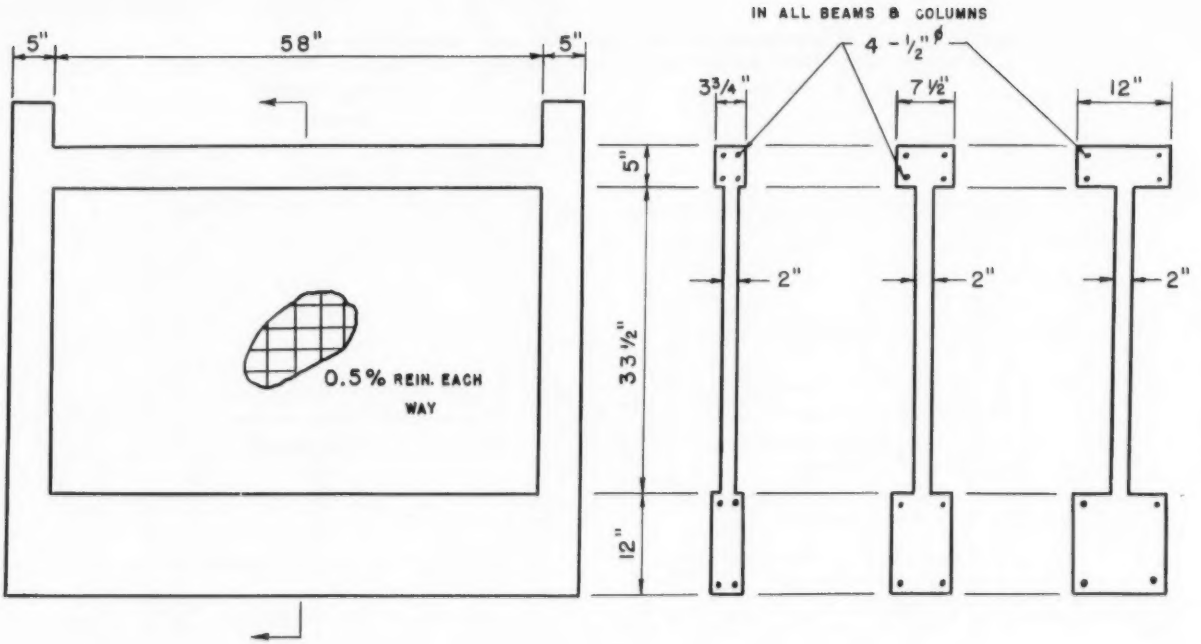

FIG. 31. – FRAME EFFECTS – FIRST SERIES USING TYPE C MODELS. COLUMN AREA VARIED WHILE THE AMOUNT OF STEEL WAS KEPT CONSTANT.

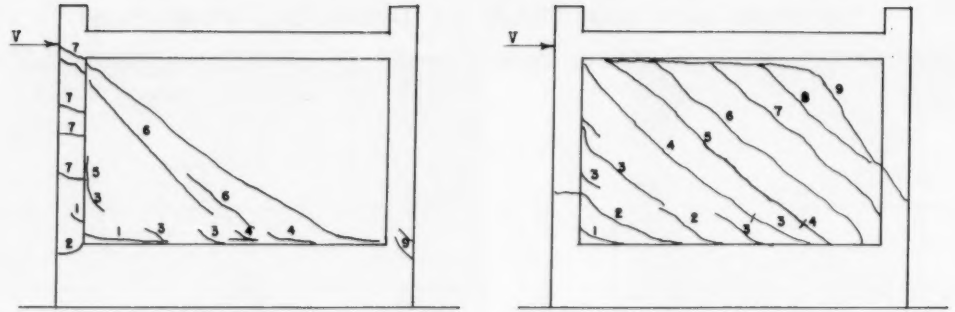

3BI-1
COLUMNS 5" x $3\frac{3}{4}$"

1BII-2A
COLUMNS 5" x $7\frac{1}{2}$"

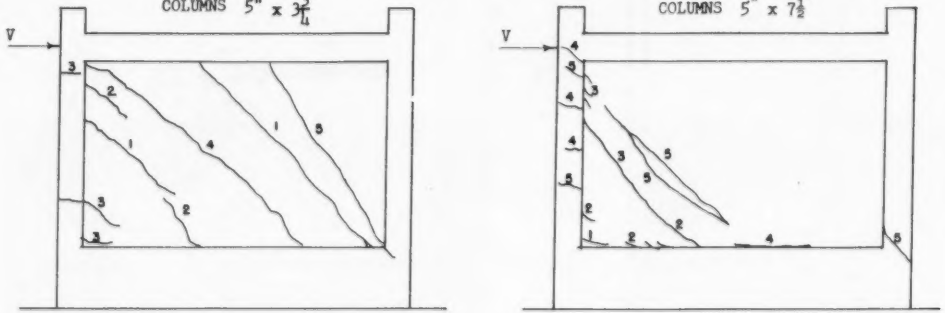

1BII-2B
COLUMNS 5" x $7\frac{1}{2}$"

3BI-3
COLUMNS 5" x 12"

FIG. 32. CRACK PATTERNS FOR SPECIMENS WITH VARIED COLUMN SIZE. THE AMOUNT OF COLUMN REINFORCEMENT HELD CONSTANT. ALL SPECIMENS HAD 0.5 % PANEL REINF.

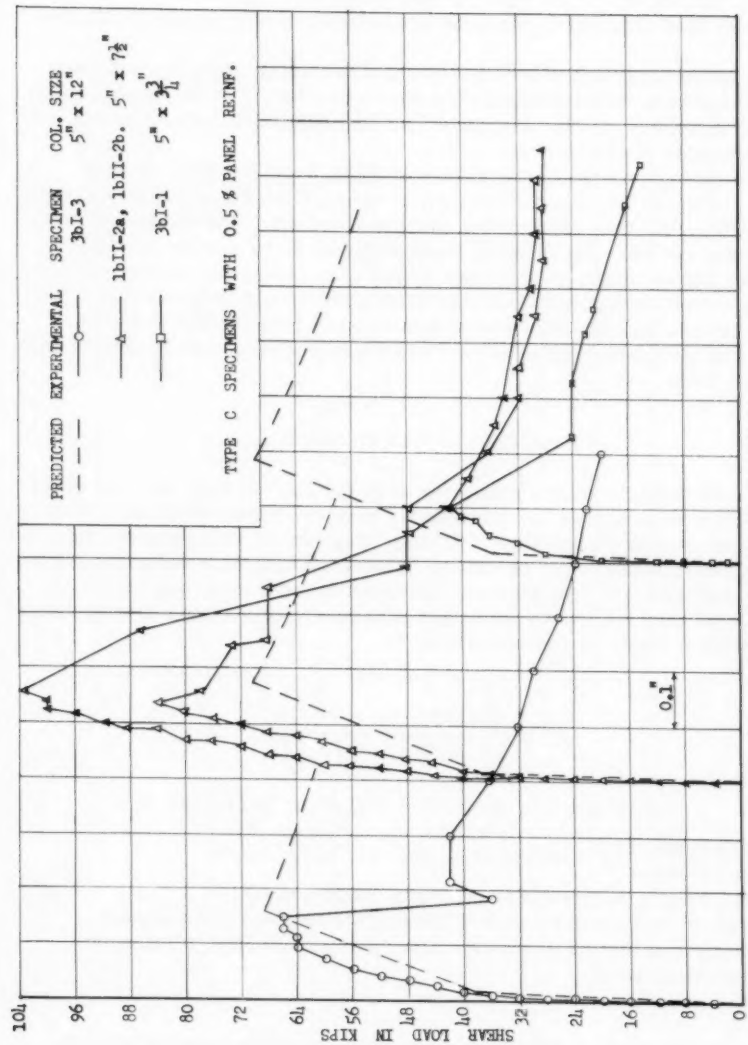

FIG. 33 - EFFECT OF VARIED COLUMN SIZE ON LOAD-DEFLECTION CURVES. COLUMN REINFORCEMENT HELD CONSTANT.

character because of shrinkage stresses in the panel. Also, the ultimate load may not increase with column size because of a tendency for the wall to punch through the wider member. This was shown to be true when columns were replaced with face walls. The shear panel punched through the compression face wall. Hence, it is quite possible that there is an optimum column width for ultimate load although these tests are not sufficiently comprehensive to prove it.

A second investigation varied the frame reinforcing while the concrete cross section remained constant. The specimens had 4" x 5" columns and 20" x 28" panels 2" thick. The panel had no reinforcing for one series and nominal amounts for the other.

The results are shown by the curves of Figs. 9 and 11, and are summarized in Fig. 34. Crack patterns are given in Figs. 8 and 10 and the photographs of Fig. 35. It is evident that additional column steel is quite effective in increasing not only the ultimate strength but also the energy absorption capacity of the specimen as indicated by the area under the complete load-deflection curve. It has been noted in other parts of the program that brick-walled bents can be quite effective in this respect if the frame is strong.

Figure 34 shows that added column steel has a nominal effect only on the first crack load.

Prediction of Wall Behavior

Shear wall deflections are proportional to the applied load until the panel cracks. This deflection is not necessarily elastic because of plastic flow and the presence of minor shrinkage cracking. This linear relationship cannot be predicted with any degree of certainty. Numerous studies were made involving exact mathematical procedures. The results were in no way better or more reliable than the most elementary procedures of strength of materials. The following formula is recommended:

$$\delta = V\left[\frac{H}{AG} + \frac{H^3}{3EI}\right]$$

δ = wall deflection
V = wall shear
H = wall height, foundation to center of loading beam
A = area of wall panel cross section neglecting steel and columns
I = moment of inertia of entire cross section including columns but neglecting steel
$G = \frac{E}{2.2}$
E = 2,000,000 psi to 2,600,000 for concrete strengths between 2000 psi and 4000 psi.

The linear portion of the load-deflection curve is a function of concrete strength beyond that reflected in the modulus of elasticity. With low strength concrete, 2000 psi, the linear range is shortened because of early cracking. With high strength concrete, 3500 to 4000 psi, the linear range is generally

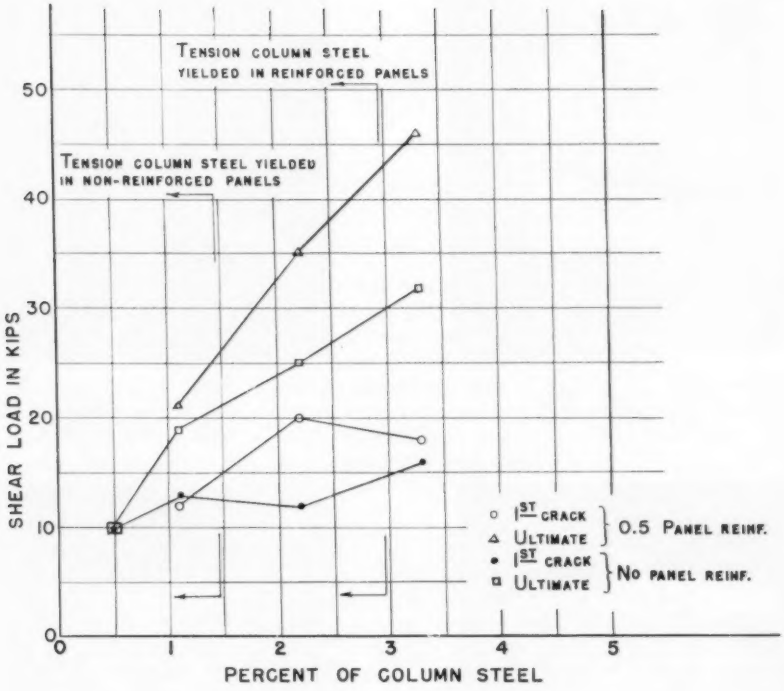

FIG. 34. FRAME EFFECT – SECOND SERIES USING TYPE B MODELS. COLUMN STEEL VARIED WHILE KEEPING THE AREA CONSTANT

3.3 % COL. REINF.
0.5 % PANEL REINF.

3.3 % COL. REINF.
0.25 % PANEL REINF.

2.2 % COL. REINF.
0.5 % PANEL REINF.

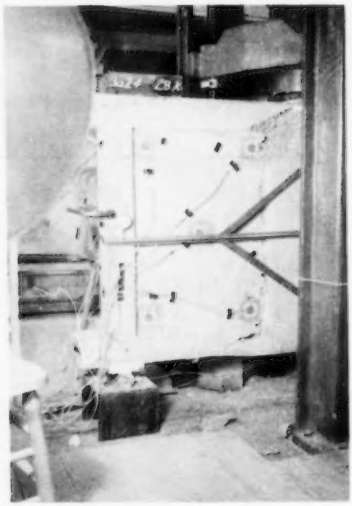

1.1 % COL. REINF.
0.5 % PANEL REINF.

FIG. 35. FINAL CRACK PATTERNS FOR THE FRAME EFFECT SERIES WITH VARIED COLUMN REINFORCEMENT. THE PATTERN INDICATES A PROGRESSION FROM PANEL SHEAR FAILURE TO TENSION COLUMN FAILURE AS THE COLUMN REINFORCEMENT IS REDUCED.

increased with the wall behaving in an increasingly brittle manner as the strength increases above 3000 psi.

Prediction of the first break in the load-deflection curve can be made the occasion of the most complex type of theoretical studies. None of the highly theoretical studies gave more reliable results than the most elementary approach. The reason is that stress alone does not control the crack pattern. Cracks are not only a product of stress but of the ability to form and propagate as well. Thus cracks are not observed necessarily in the most highly stressed regions but at locations where it is easier for cracks to form and propagate. The average shear stress is recommended as an index of the first break in the load-deflection curve. Thus

$V_c = 0.1\ f'_c\ A$

V_c = the load at first break in the load-deflection curve 0.1 f'_c is the approximate tensile strength of the concrete

A = the area of the panel section neglecting steel and columns

With particular specimens other approaches have proven more valid. The probable error of prediction is so large that only the simplest of formulas are justified. These approximations give the best results under conditions parallel to those most commonly used in building construction.

Ultimate load and deflection are highly statistical quantities. The results are influenced by the particular testing machine and test procedure. Numerous studies have been made of the parameters involved at ultimate load. The following equations are the best approximations available at this time.

$$V_u = \frac{0.1}{\frac{P}{C} + 0.1} C + 2.2 P$$

$$\delta_u = 24 \frac{H^2}{L^2} \delta_c$$

V_u = ultimate load, lb.

$C = A_s f'_c \left[15 + 1.9 \left(\frac{L}{H}\right)^2\right]$, compression column strength, lb.

$P = \sigma_y ptL$, panel strength, lb.

A_s = area of steel in compression column

f'_c = concrete compress on strength

L = wall length, center to center of columns

H = wall height, foundation to center of distributing beam

σ_y = yield point of panel steel

p = panel steel ratio

δ_u = deflection at ultimate load

δ_c = deflection at break in load-deflection curve, wall shear equals V_c

These empirical equations are subject to the following limitations:

1) Column steel—1 to 3.3 per cent
2) Column steel must be adequately encased in concrete
3) Concrete strength—2000 to 4000 psi
4) Length to height ratio—$\frac{L}{H}$ 0.9 to 3.0
5) Ratio $\frac{P}{C}$ —0 to 3.26
6) σ_y —42 to 52 ksi
7) Panel steel ratio, p—0 to 1.5 per cent

The post-ultimate curves shown in the figures were simply sketched in to provide a curve similar to that found experimentally. The post-ultimate curve is influenced both by the testing machine and rate of loading. Strengths increase with increase in rate of loading.

Other Investigations

The influence of possible bearing loads on wall behavior was studied in a minor way. It was found that if the total bearing load was equal to or less than the total shear force, its influence on the load-deflection curve was negligible. Very large bearing loads are necessary to change the load-deflection curves appreciably.

Five confirmatory tests were made on simple shear wall assemblies. They consisted of shear wall, face walls, and loading diaphragm. Wall details are given in Fig. 36. The shear jig was modified to test these specimens as shown in Fig. 37. Three one-story assemblies were tested along with two of two stories. The models were constructed as near to conventional practice as possible. They were constructed in several pours with successive pours doweled together. Shear keys were also used in M-5. Loads were applied to the diaphragm with the story loads being in the ratio two to one, first to second story.

The load-deflection curves are given in Fig. 38. Typical cracking is seen in Fig. 39. SR-4 rosettes were mounted on the wall panels to check stress distributions. The results were inconclusive.

The formulas recommended in this report are largely influenced by these tests. The utter futility of complex mathematical studies in such work was again amply demonstrated. Errors in prediction of the order of 20 per cent must be accepted with this type of work in reinforced concrete.

CONCLUSIONS

The following general conclusions have been reached as a result of this investigation:

1) The behavior of plain and reinforced concrete shear walls for single story buildings can be predicted within acceptable design limitations. The predicted load-deflection curve for such a wall can be approximated to a reasonable degree by one straight line from the origin for the uncracked range, by a second straight line for the cracked range up to the ultimate, and by a third line, somewhat indefinite, for the post ultimate range.

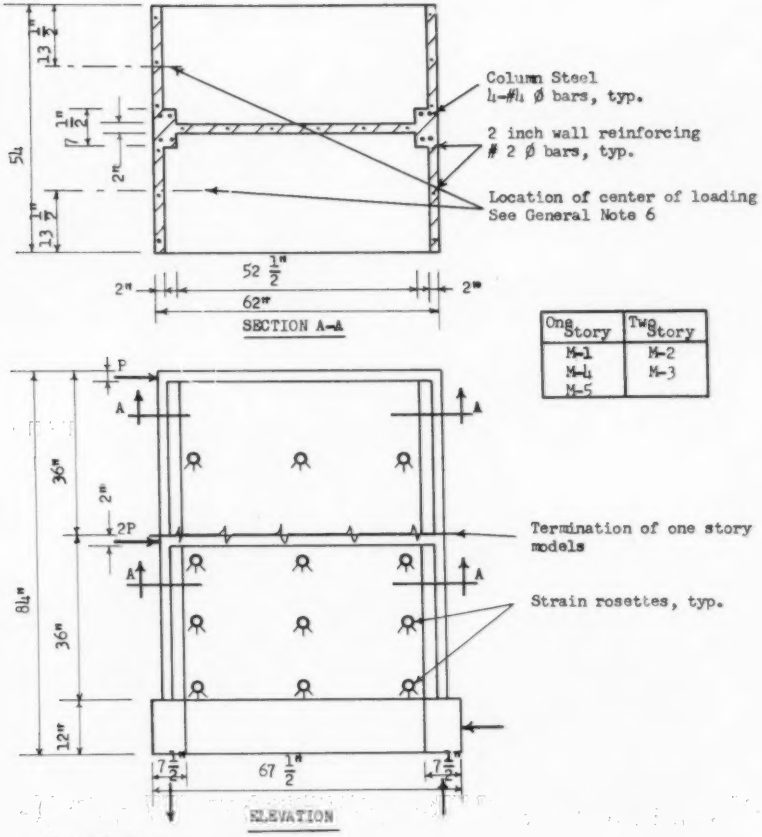

One Story	Two Story
M-1	M-2
M-4	M-3
M-5	

General Notes:

1. Construction joints are located between:
   a) Foundation and First Story
   b) First story wall and Slab
   c) Slab and Second Story wall
   d) Second story wall and slab.
2. Joints were grouted M-1 to M-4.
3. Wall M-5 employs Keys at the construction joints without grout. See Fig. 14
4. Reinforcing in all two inch walls consists of #2 Ø bars at 9.8" c - c.
5. All reinforcing joints are lapped 30 diameters.
6. Foundation reinforcing consists of 4 - #6 Ø bars.
7. Load is applied through 1/2" x 1-1/2" x 18" soft mastic boards located as shown.

FIG. 36. DETAILS OF M-SERIES WALLS, TYPE D

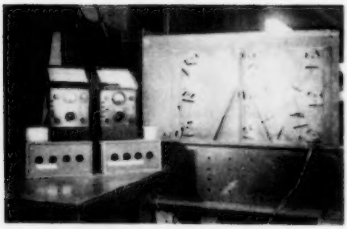

Test Set Up for Single Story M-1
Including SR-4 Strain Gage Apparatus

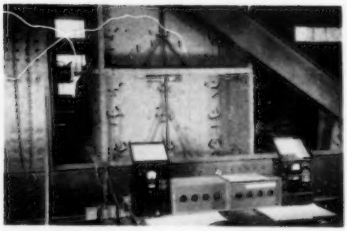

Test Set Up for Two Story M-2
Including SR-4 Strain Gage Apparatus

Shear Jig Adjusted for M-Series Walls

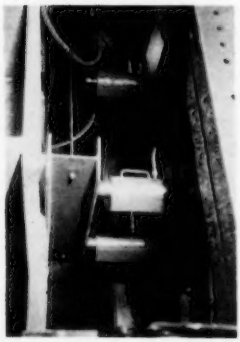

Hydraulic Jacks Applying Load to M-2

FIG. 37. EXPERIMENTAL SET UP FOR M-SERIES WALLS

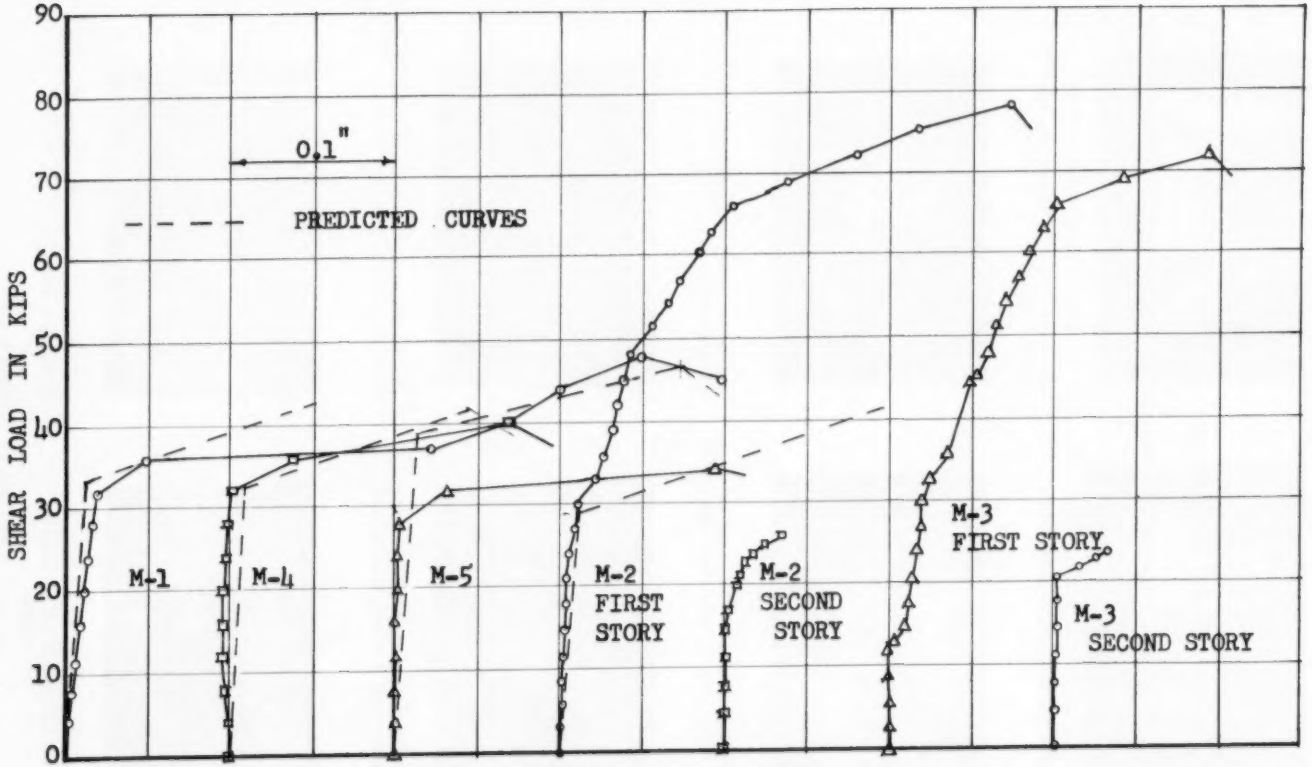

FIG. 38. LOAD DEFLECTION CURVES FOR M SERIES WALLS.

M-1 Single Story. Load Upper Right.

M-1 Post Ultimate Deflection. Load Upper Right.

M-2 Two Story. First Story Crack Pattern. Total Shear Load 78 kips. Load Upper Right.

M-2 Second Story Crack Pattern. Load Upper Right.

M-2 Front View of Compression Face Wall. Note Shear Wall Pushing Through Face Wall.

M-3 Two Story. Ultimate Shear Load, 73.5 kips total. Load Upper Right.

M-4 One Story. Shear Load 38 kips. Note Lack of Cracks Low in Tension Corner. Load Upper Right.

M-5 One Story. Post Ultimate Deflection. Load Upper Right.

Fig 39. PHOTOGRAPHS OF M-SERIES WALLS

2) Simple expressions from elementary strength of materials are adequate for the uncracked range. More involved methods of analysis are not justified because of the statistical nature of concrete, particularly when subjected to tensile stresses.

3) The prediction of the ultimate strength of a wall and the corresponding deflection appears possible only by means of empirical relationships. The expressions suggested in this paper have been revised a number of times during the investigations as more experimental evidence became available. While the authors believe that the approach will give results of reasonable value in most conventional cases, future investigations may offer further improvement.

Paper 1255 ST 3

Journal of the
STRUCTURAL DIVISION
Proceedings of the American Society of Civil Engineers

LATERAL LOAD DISTRIBUTION TEST ON I-BEAM BRIDGE

Ardis White[1] and William B. Purnell,[2] Associate Members, ASCE
(Proc. Paper 1255)

ABSTRACT

This paper presents procedures, results, and conclusions from a strain gage test performed on a highway bridge to determine (1) the degree of composite action obtained and (2) effectiveness of the diaphragms in lateral distribution of loads.

INTRODUCTION

Within the past three years the City of Houston has built a number of three span continuous haunched beam bridge units, and is in the process of building more. The test program discussed here was carried out on a typical member of this family of bridges.

The main purpose of this test program was to obtain specific information regarding (1) comparative effect of the diaphragms and slab on the lateral distribution of live loads, and (2) degree to which composite action of the beams and slab is developed. A secondary object of the test was to study methods of mounting and waterproofing SR-4 strain gages in a field test of this nature.

Excellent test programs conducted for purposes similar to those listed above have been carried out by other engineers, and reference to these test programs are given at the end of this paper.

Description of Test Structure

Bridge structure III of the City of Houston Memorial Drive project was selected for the test program described here. The main part of structure III

Note: Discussion open until October 1, 1957. Paper 1255 is part of the copyrighted Journal of the Structural Division of the American Society of Civil Engineers, Vol. 83, No. ST 3, May, 1957.

1. Associate Prof., Univ. of Houston, Houston, Tex.
2. Associate Prof., Univ. of Houston, Houston, Tex.

is a three span haunched continuous steel beam bridge, the spans being 72', 108', and 72'. A 33 WF 141 is used for the constant-I sections, and two 16 ST 70.5's are joined with a filler plate to form the haunched sections. (See Fig. 1.) The haunched sections are centered about the center pier bents and are each 54' in length.

Shear connectors are used in structure III only in the constant-I sections as shown in Fig. 2, these sections corresponding roughly to the positive moment regions of the continuous beams. Each shear connector consists of a #7 bar bent as shown in Fig. 2 and welded at 2' 4" centers to the center of the upper flange of the beam. The roadway slab concrete covers the shear connectors and composite action of the slab and beams is thus obtained.

Fig. 3 is a transverse cross section of the 3-lane north half of structure III. The north and south halves of this structure are actually twin bridges except that the median strip is fixed to the north half and bears on the slab of the south half. All beams of both halves rest on common pier bents, and are connected transversely by diaphragms except beam 5 and the corresponding beam of the south half of the structure. The typical diaphragm "A" shown in Fig. 3 is used at the midpoints of the 33 WF 141 sections and at the ends of the haunched sections. A detailed drawing of this typical diaphragm is given as Fig. 4. The three diaphragms marked "Dia. B" in Fig. 1 used at the center and quarter points of the haunched sections consist only of two 4 x 4 x 5/16 angles crossed between beams to form vertical diagonal bracing.

Instrumentation

All instrumentation of the test structure was done at two stations; Station A was at the center of the center span, and Station B was at the west center pier bent. The circles on Fig. 3 indicate the positions of the 1" A-1 SR-4 strain gages placed on the 33WF 141 beams at Station A. 6" A-9 strain gages were also placed on the bottom of the concrete slab alongside the top flanges of the I-beams. Fourteen A-1 strain gages were placed on the diaphragm members between beams 2 and 3 at Station A. Positions of these strain gages are shown in Fig. 4.

The total strain gage instrumentation at Station B consisted of fifteen A-1 gages mounted in the same relative locations indicated in Fig. 3.

Access underneath the bridge was obtained by use of a movable ladder hung over the guard rail and a catwalk system suspended from the beams. The ladder was chained and locked to the guard rail when not in use to prevent access to the test stations. The catwalk system connected all test beams at Station A and also ran from Station A to the Station B pier bent.

A 2" x 2" rod with a level tape attached to its lower end was hung from each of the five test beams at Station A, which was located directly above the center of Buffalo Bayou. Deflections of these beams were obtained by reading the tapes with five different levels set up beneath the bridge near Station B.

Dial gages reading to 1/10000th of an inch were used to detect any movement between the slab and the upper flanges of the beams during the test. The dial gage itself was fixed firmly to a bracket which had been attached to the bottom of the slab by a stud fired into the concrete. The plunger of the dial gage rested against a similar bracket held by a metal screw against the upper flanges of the beams. Dial gages were mounted at Stations A and B and at the two diaphragms between Stations A and B.

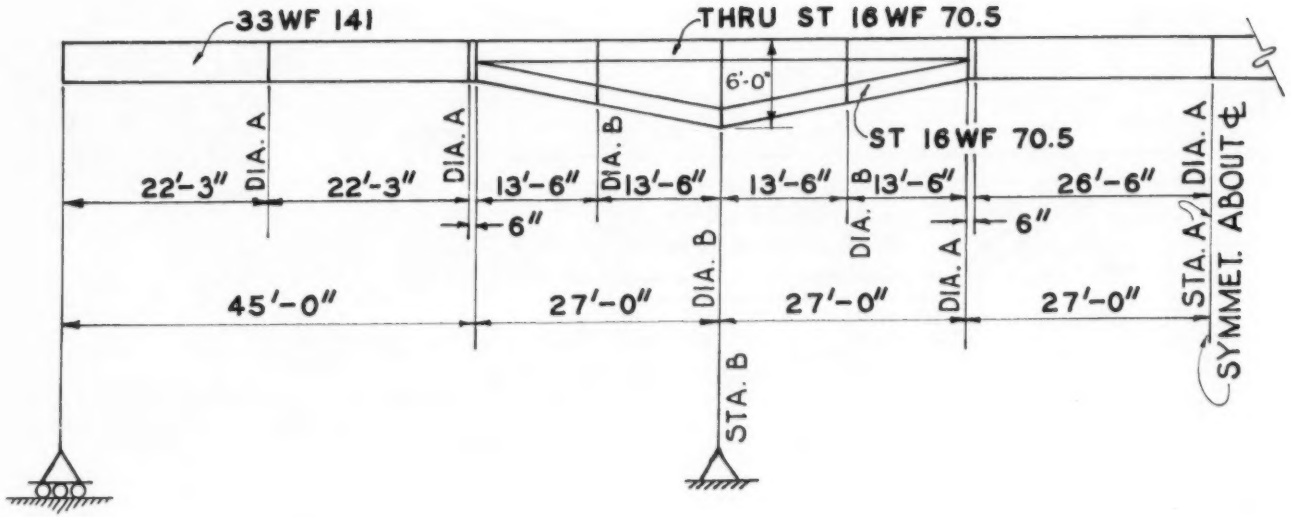

LONGITUDINAL SECTION
FIG. 1

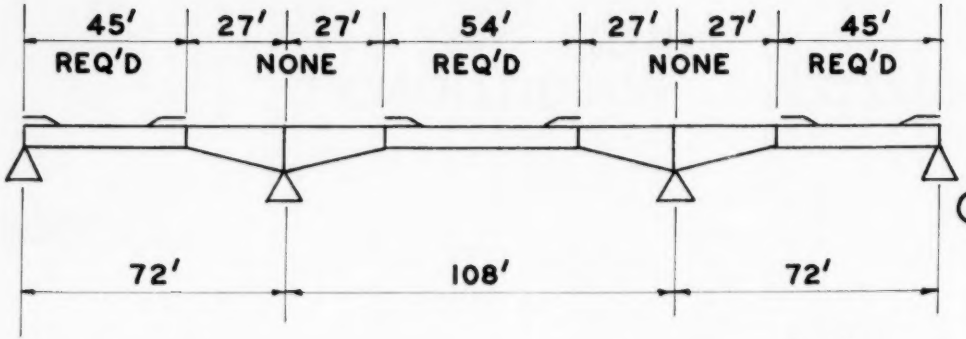

LOCATION OF SHEAR CONNECTORS

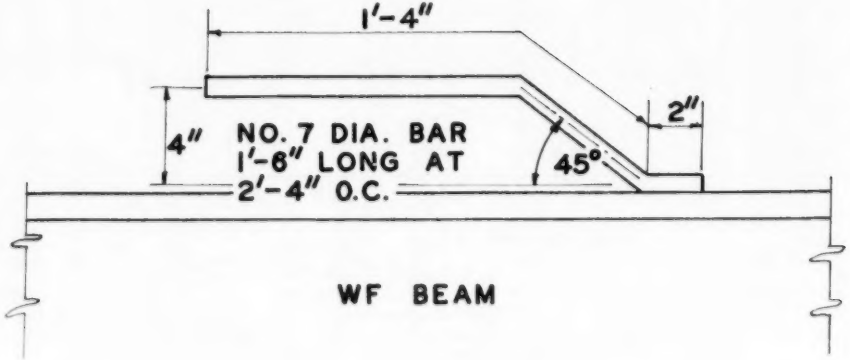

DETAIL OF SHEAR CONNECTOR

FIG. 2

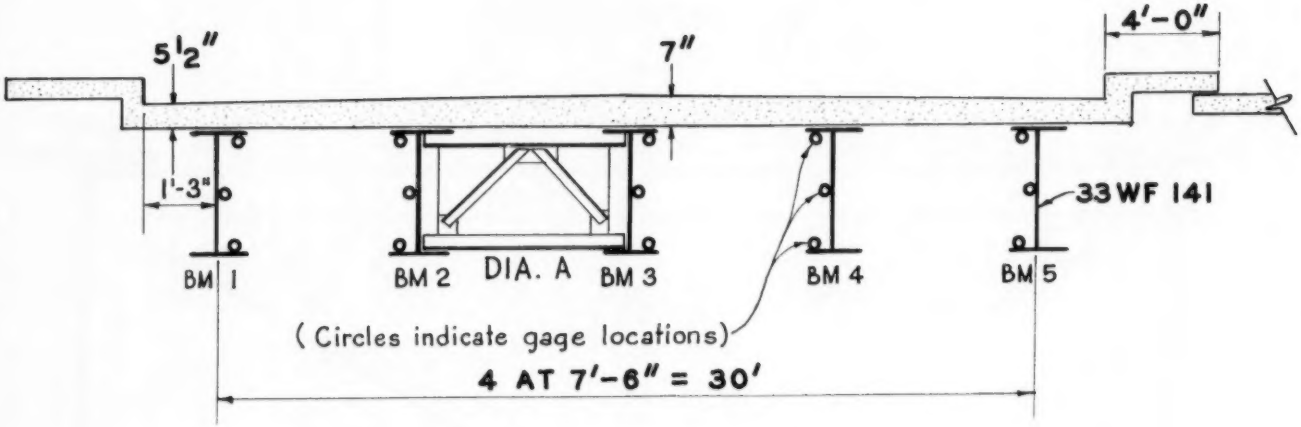

TRANSVERSE CROSS-SECTION
STATION A
FIG. 3

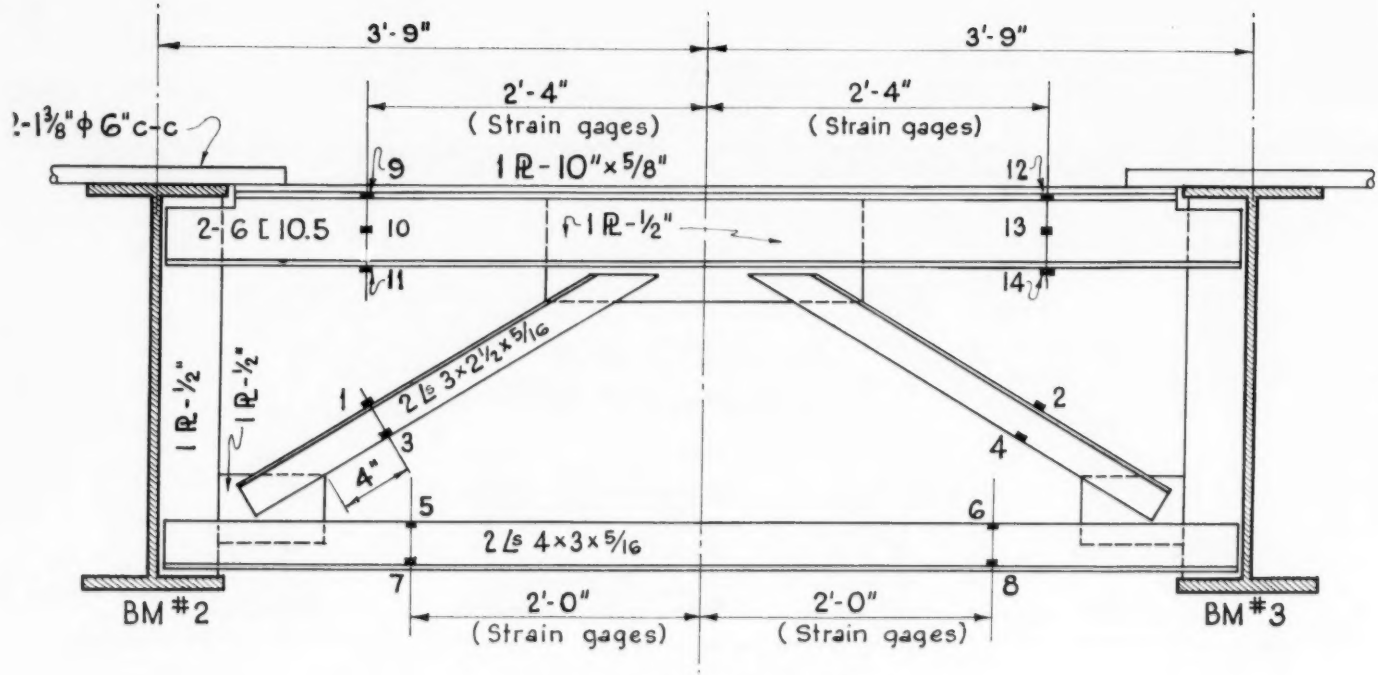

DIAPHRAGM "A"
FIG. 4

Preparation of steel surfaces to receive the SR-4 strain gages was done by sandblasting, with very little hand sandpaper work. The steel was warmed with a small propane hand torch prior to mounting the gages, and the gages were then cemented to the prepared surfaces with Duco cement. The gages were either pressed in place with the fingers or held by sponge rubber pads backed with wooden strips until the cement began to harden. Gages were curved to a ground resistance of 1000 megohms using 250 watt heat lamps powered by a portable power plant stationed on top of the bridge. The Cerese wax used for water-proofing was then melted and poured inside balsa wood frames cemented around the gages on the bottom flanges. Similar frames were used with the gages on the webs and upper flanges, and the wax was softened with heat and placed over the gages inside the frames with a spatula. As soon as the wax was applied, the heat was removed and the gages allowed to cool. Lead wires from all strain gages at Station A were collected at one point for convenience in reading the gages. This was also done at Station B. All lead wires were solid copper 18 gage covered with Polyethlene.

The concrete areas to receive the A-9 gages were ground smooth with a power sander, cleaned with acetone, and primed with a coat of diluted Duco cement. After the primer coat hardened, additional cement was applied to the gage and to the concrete. Gages were pressed in place with the fingers until the cement began to harden and were air dried only; no heat was used in curing them.

Loading of Structure

Test loads consisted of two 38,000 pound draglines, one mounted on rubber tires, the other mounted on steel tracks. These two machines were always placed back to back at Station A, which was at the center of the center span. Fig. 5 shows the longitudinal distribution of the total 76,000 pound load imposed by the two draglines.

Three lateral load positions were used in the test, the draglines being placed in each of the three lanes of the north half of structure III.

Test Procedure

A Baldwin type L strain indicator was used to read strains from the SR-4 gages. Compensator gages were mounted on steel plates and concrete cylinders. The process of taking data was relatively simple; zero readings of strain, deflection, and dial gages being taken with the loads off the structure, and then the corresponding readings being taken with the loads on the structure. All readings were checked by at least one duplicate loading, and zero readings were always taken immediately before and after a given loading. A complete set of data for one cycle of loading (i.e., unloaded, loaded, unloaded) required about 30 minutes.

PRESENTATION AND DISCUSSION OF RESULTS

Composite Action

Fig. 6 gives a plot of all positive bending moment strains obtained from gages on the beams and concrete slab at station A. No effort is made here

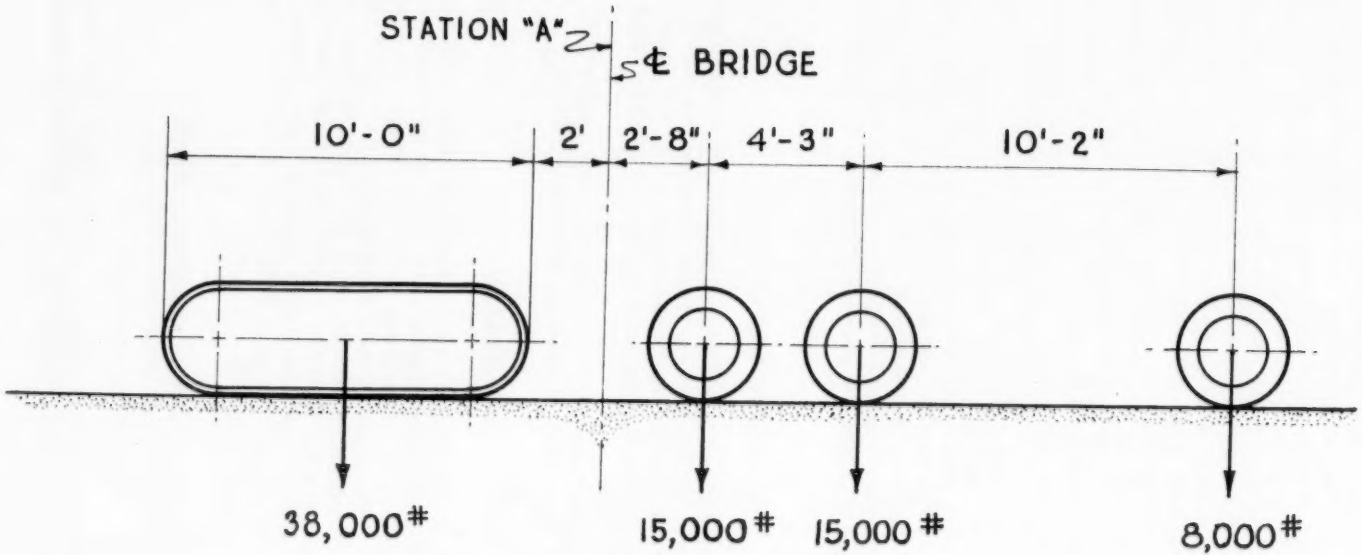

LOADS ON BRIDGE

FIG. 5

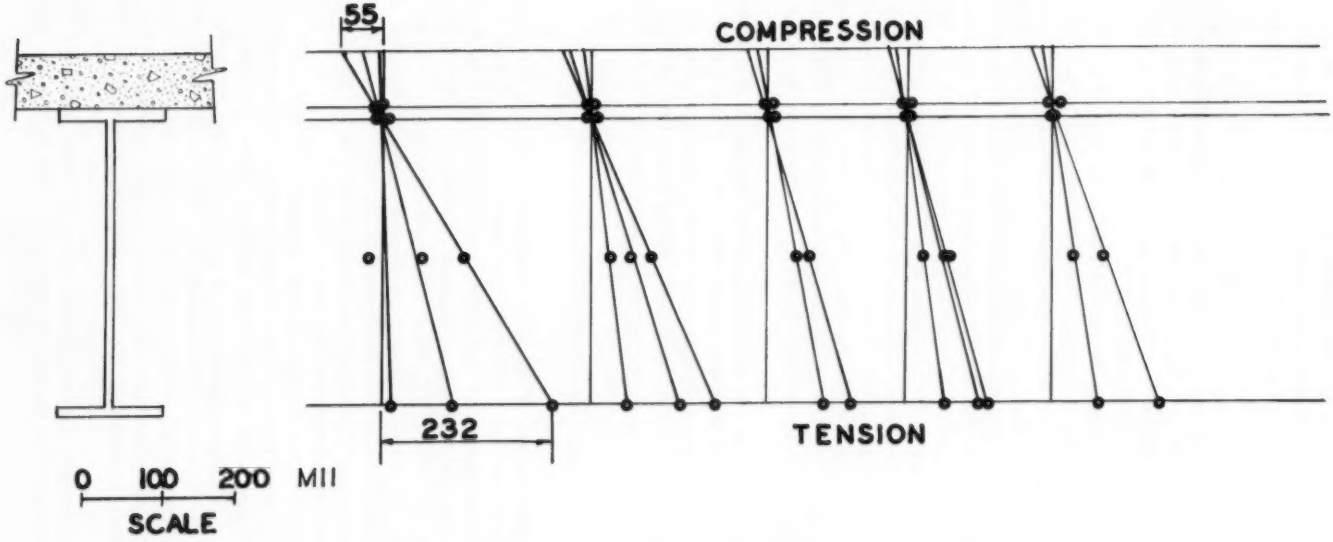

STRAINS AT STATION A
FIG. 6

to distinguish between different lateral positions of the loads, as the purpose of this figure is to show the experimental position of the neutral axis of the composite beams formed by the beams and slab. If there were no composite action at all, the neutral axis would appear at the center of the I-beams. The average position of the neutral axis from Fig. 6 is just below the bottom of the top flange, which is an inch or two above the theoretical neutral axis computed using an E_c of 3.5×10^6 psi. It is thus evident that full and complete composite action is being obtained at Station A, and the actual composite I is thus about two times the I of the 33 WF 141.

The maximum concrete strain obtained at Station A was 55 microinches per inch, which would indicate a compressive stress of 193 psi. The maximum steel stress corresponding to the maximum strain of 232 microinches per inch is 6840 psi, for $E = 29.5 \times 10^6$ psi.

Fig. 7 gives a plot of the negative moment strains obtained from the gages on the haunched beams at Station B. The apparent position of the neutral axis on two of these beams is about 19.5 inches below the bottom of the top flange, which is about 10 inches below the position of the theoretical neutral axis assuming full composite action at this station. It is thus seen that the composite action which occurs at Station B is not complete, and furthermore, by comparison of strain curves for all beams in Fig. 7, that this composite action is somewhat erratic. No shear connectors were used in this region of negative moment, and the concrete was possibly cracked due to shrinkage before the test began.

The maximum slip between the slab and the top flanges of the beams was only 3/10,00th of an inch, and this maximum value was obtained only once. Most of the dial readings were less than this value, indicating that for all practical purposes, no slip between slab and beams occurred, even at the points of negative moment.

Load Distribution to Beams

Fig. 8 gives the distribution of the total moment to the five different beams at station A for each of the three different load positions. It is clear that the distribution to the different beams is almost exactly linear for load position 1, the outside beam taking about 40.2% of the total moment and the beam near the median strip taking practically none. The distribution for load position 2 is not quite symmetrical due to influence of the cantilevered median strip, this influence being evident also for load position three.

Fig. 8 also gives the distribution of moments at station B, this being similar to that at station A, but considerably more erratic.

Summation of the ordinates for the curves marked 1, 2 and 3 for station A in Fig. 8 would permit the drawing of a new curve which would represent the percentage of total moment carried by each beam if loads 1, 2 and 3 were applied simultaneously. Such summation gives a value of 62% for beam 1, 69% for beam 2, and 63% for beam 3. This shows that the practice of permitting the outside beam of a bridge structure to be lighter than the inside beams is not in agreement with the actual lateral distribution of moments. The outside beam should be at least as heavy as the inside beams, perhaps even heavier in some cases.

Fig. 9 presents deflection curves plotted from the level readings taken on the rods suspended beneath the beams at station A. The maximum deflection

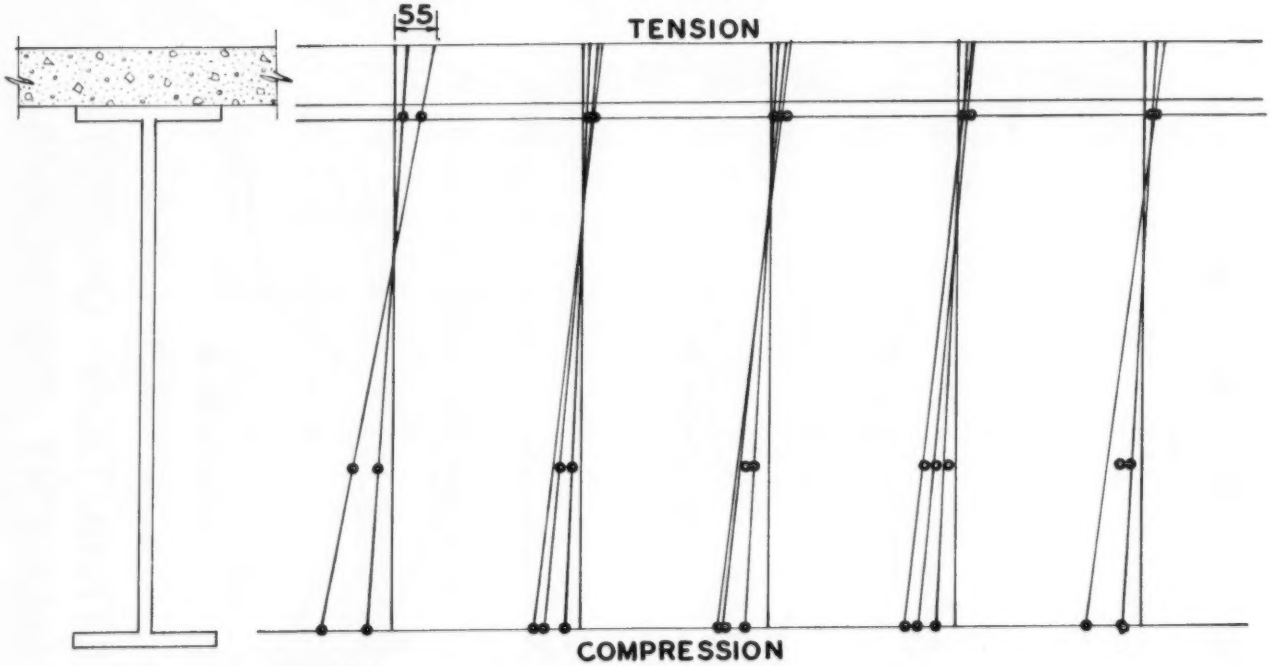

STRAINS AT STATION B

FIG. 7

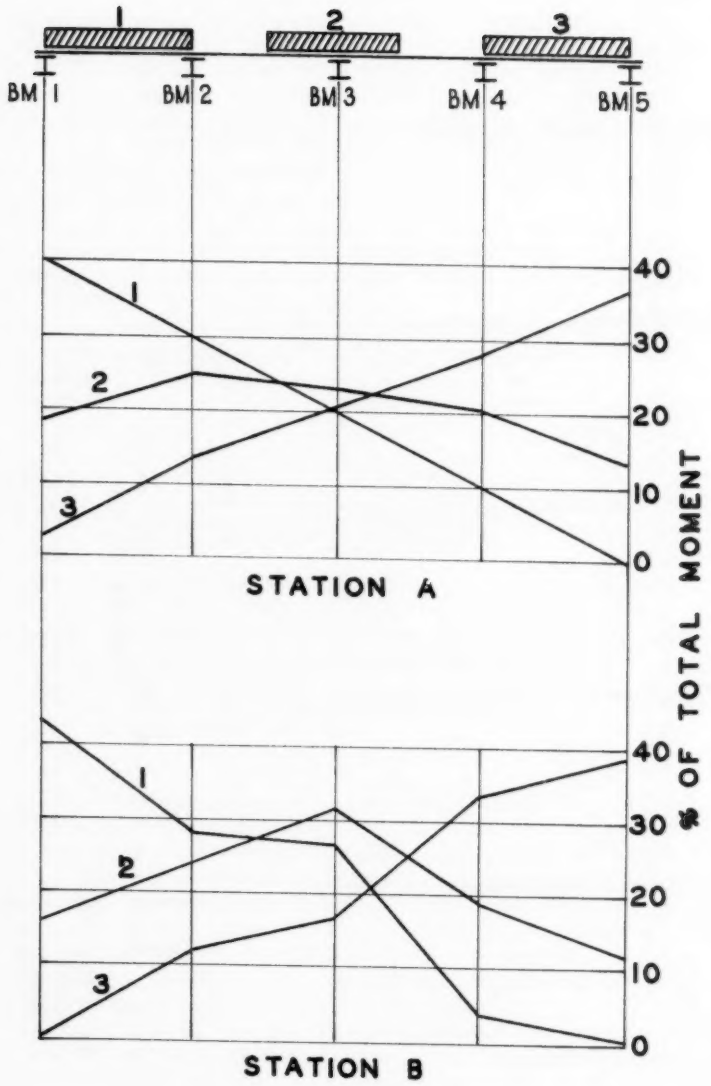

DISTRIBUTION OF TOTAL MOMENT TO BEAMS

FIG. 8

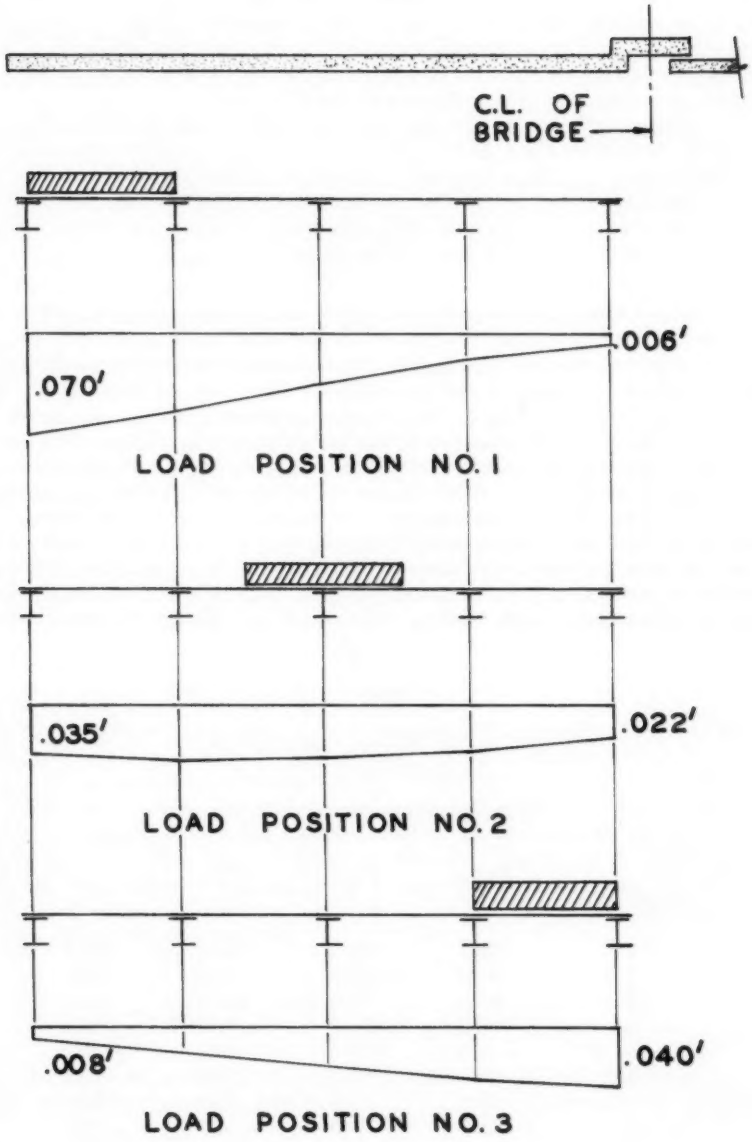

BEAM DEFLECTIONS

FIG. 9

of 0.070' was obtained under the outside beam when the load was in position 1; i.e., in the outside lane near the curb. The corresponding deflection of the beam near the median strip was only 0.006'. For load position 2 the deflection pattern is almost uniform, giving evidence, as did the curves of Fig. 8, of the very effective lateral distribution of the live loads.

The marked influence of the cantilevered median strip is obtained by comparing the deflection curve for load position 3 in Fig. 9 to the deflection curve for load position 1. The difference between the 0.070' maximum deflection for load position 1, and the 0.040' maximum deflection for load position 3 is a direct indication of the considerable amount of load being transferred to the south half of structure III by the median strip.

Effect of Slab and Diaphragm on Lateral Distribution of Loads

Table I gives stresses indicated by each of the strain gages mounted on the diaphragm between beams 2 and 3 at station A (See Fig. 4.) with the test loads centered above beams 1 and 2. This loading position gives the maximum shear load which may be imposed on the instrumented diaphragm with the test loads used, and the results from three separate identical loadings are given to show the variation in the stress at each point for different applications of the load. (No such tabulation of stresses is given for the gages mounted on the beams, as successive applications of load did not cause stress variations of more than about three or four percent for beam gage positions.) It should be noted that some of the stresses in Table I are very small, corresponding to a strain gage reading equal or nearly equal to the least reliable

Table I

STRESSES IN DIAPHRAGM "A"
LOAD IN POSITION 1

(See Fig. 4 for gage positions)

Gage No.	Trial 1	Trial 2	Trial 3	Ave.
1	1330	1180	1330	1280
2	-1475	-1620	-1330	1470
3	3100	3245	3245	2190
4	-3690	-3540	-3540	3590
5	- 885	-1330	- 440	- 880
6	1030	295	1330	880
7	295	0	885	390
8	- 295	- 740	- 150	- 395
9	0	150	150	100
10	295	150	440	295
11	440	295	590	440
12	- 150	- 150	- 150	- 150
13	- 295	- 440	- 150	- 295
14	- 440	- 885	- 590	- 640

reading of the strain gage indicator.

An examination of Table I reveals that average stresses in the diagonal and top diaphragm members (See Fig. 4 for gage locations.) near beam No. 3 are higher than for the corresponding diaphragm gage positions near beam 2. However, stresses at both ends of the lower diaphragm member are the same. This is believed to be due to additional load brought into the center of the diaphragm by the roadway slab, as such additional load would affect stresses in the top and diagonal members, but would not affect stresses in the bottom diaphragm member. The maximum load transferred laterally by the diaphragm may be obtained by summing the vertical shear carried by the top, diagonal, and bottom diaphragm members near beam No. 3.

Assuming a point of inflection at the midpoint of the bottom member of the instrumented diaphragm, the shear in this member may be obtained as follows, using the stress from gage No. 6, which was mounted about 0.50" from the edge of the angle: (See Fig. 10a.)

$$M = 2(12)V = 24\,V \text{ in-lbs.}$$

Also:

$$M = \left(\frac{SI}{c}\right)2 = 2(880)\frac{3.4}{2.24}$$

$$= 2671 \text{ in-lbs.}$$

$$V = \frac{M}{24} = \frac{2671}{24} = 111 \text{ lbs.}$$

Therefore, the shear in the bottom diaphragm member is only about 111 lbs.

It may be noted from Table I that gages 9, 10 and 11 indicated tension, while 12, 13 and 14 indicated compression. It seems reasonable to assume a point of inflection in the center of the top diaphragm member. This member is clearly a composite member and its I may be found as shown below.

The distance (x) (See Fig. 11) from the bottom of the 6" 10.5# channels to the neutral axis of the composite beam formed by these channels, the 10" x 5/8" plate, and the roadway slab, may be found as follows, using stresses for gages 12 and 14 from Table I.

$$\frac{x}{640} = \frac{x - 6.00}{150} \qquad x = 7.84"$$

The transformed width (b) of slab acting with the channels and plate may be found as follows, using an n of 8.43. ($E_c = 3.5 \times 10^6$ psi.)

$$\frac{b(5.785)^2}{2(8.43)} = \frac{b(1.215)^2}{2(8.43)} + 2(3.07)4.84 + 10(.625)(1.527)$$

$$b = 20.70"$$

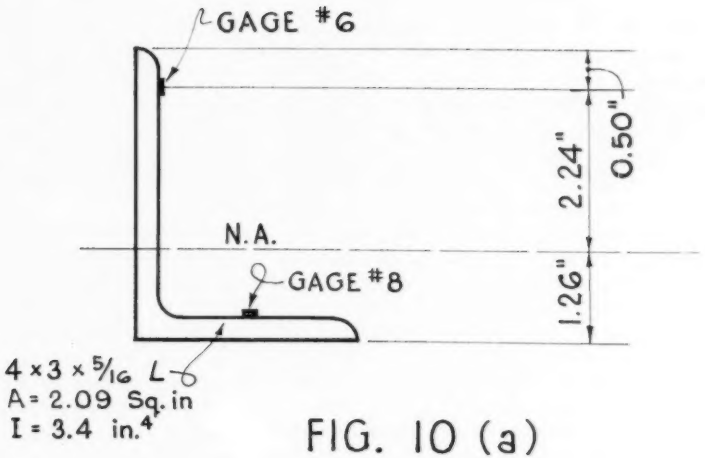

FIG. 10 (a)

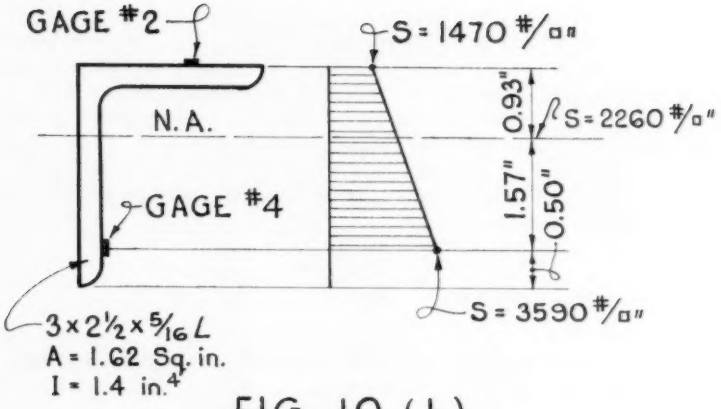

FIG. 10 (b)

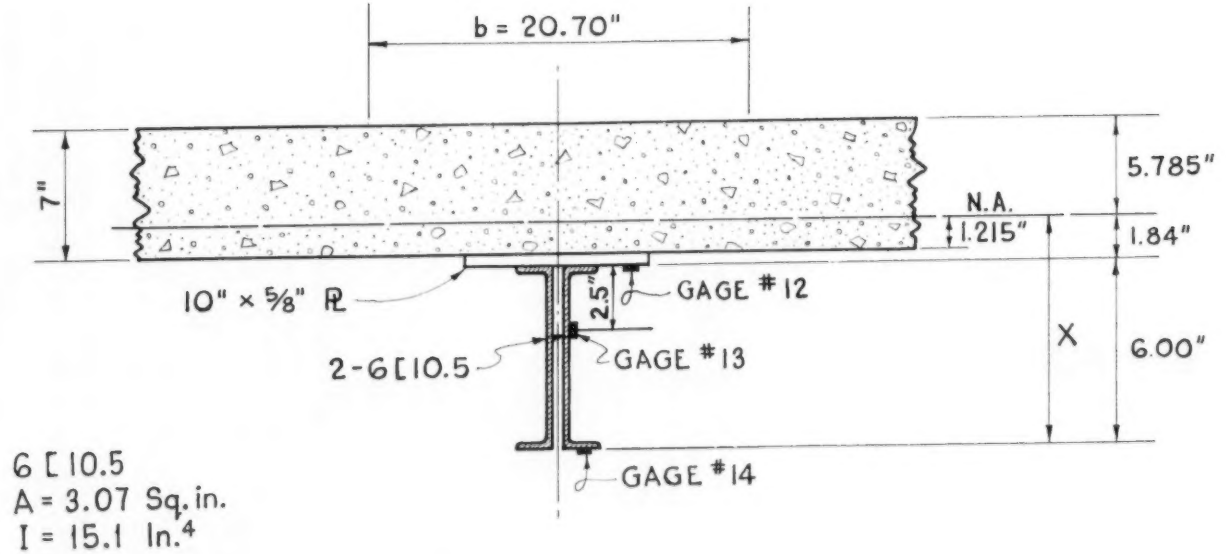
b = 20.70"
7"
5.785"
N.A.
1.215"
1.84"
10" × 5/8" PL
2.5"
GAGE #12
2-6[10.5
GAGE #13
X
6.00"
GAGE #14
6 [10.5
A = 3.07 Sq. in.
I = 15.1 In.4

FIG. 11

The I of this composite diaphragm member then equals

$$2(15.1) + (2)3.07(4.84)^2 + 10(.625)(1.527)^2 + \frac{(20.70)(5.785)^3}{3(8.43)} + \frac{20.70(1.215)^3}{3(8.43)}$$

$$I = 346.5 \text{ in.}^4$$

$$M = \frac{SI}{c} = \frac{640(347)}{784} = 28,330 \text{ in.-lbs.}$$

Also: $M = 2.33\ V$ ft.-lbs.

$= 28\ V$ in.-lbs.

$$V = \frac{28,330}{28} = 1012 \text{ lbs.}$$

Thus, the shear in the top diaphragm member is 1012 lbs.

The vertical shear carried by the diagonal diaphragm member consists of two parts; (1) that due to the axial force in the member, and (2) that related to the moment in the member.

The stress at the neutral axis of the angle (See Fig. 10b) is due only to the axial load in the member, and this stress equals

$$1470 + \frac{(3590 - 1470)\ 0.93}{(0.93 + 1.57)} = 2260 \text{ lbs./in.}^2$$

The axial load (P) in the diagonal diaphragm member equals the stress at the N. A. of the member multiplied by the area of the two angles making up this member.

$$P = 2(1.62)(2260) = 7320 \text{ lbs.}$$

The slope of this member is 6.75" to 12", and the vertical component of the axial load in the member is thus

$$\frac{6.75}{13.75}(7320) = 3590 \text{ lbs.}$$

Assuming a horizontal distance of 9" from the position of gages 2 and 4 to a point of inflection in the diagonal diaphragm member, $M = 9V$ in-lbs. Also $M = SI/c$, and

$$M = \frac{(3590 - 2260)\ 1.4}{1.57} = 1190 \text{ in-lbs.}$$

$$V = \frac{1190}{9} = 130 \text{ lbs.}$$

The total maximum vertical shear carried by the diaphragm between beams 2 and 3 is 111 + 1012 + 3590 + 130 = 4843 lbs.

Fig. 8 shows that beams 1 and 2 carry a total of about 70% of the total moment in all beams with the load in position 1. The total test load was 76,000 lbs, of which only 30% or 22,800 lbs. is carried by beams 3, 4, and 5. The diaphragm transfers laterally 4843 lbs. of the 22,800 lbs, which is about 20% of the total load transferred laterally by the diaphragm and slab. This means that the roadway slab itself is four times as effective as the diaphragm in lateral distribution of live loads.

Strain Gage Stability

The waterproofing techniques used in the test described here provided ground resistances in excess of 100 megohms one month after the gages were waterproofed, and about 70 megohms one year later. The gages were quite stable during the test, and even at six months after the test, when the ground resistance varied between 90 and 100 megohms, the zero readings of more than half of the A-1 gages varied from the original zero readings by only 5 to 15 microinches per inch. Another one fourth of the A-1 gages showed zero drifts of only about 25 or 30 microinches per inch.

The zero drift of the unprotected A-9 strain gages mounted on the bottom side of the slab was very slight during the test, but became excessive within a few weeks after the test. Six months after the test, zero drift of some of these A-9 gages had increased to several hundred microinches per inch.

CONCLUSIONS

A brief summary of the conclusions from this test may be listed as follows:

1) Full and complete composite action was obtained in the region of positive moment in the continuous beams. None of the data indicated any reason for doubting the reliability of this composite action, and it should certainly be considered in the design of beam and slab bridges in which adequate shear connectors may be used in positive moment regions.

2) Partial composite action of the slab and beams was obtained in the region of negative moment, even though no shear connectors were used in these regions. However, this partial composite action was erratic and variable, and it is not believed that composite action should be considered in design in negative moment regions, even if shear connectors are used there.

3) Effective lateral distribution of the test loads was obtained, with about 80% of the lateral transfer of load being through the roadway slab and only about 20% being carried by the diaphragm. Stresses obtained in the diaphragm members were rather low, with a maximum value of about 3600 psi. This indicates the possibility of reducing the size of the members which make up a diaphragm of the type tested.

4) The procedures used in this test for mounting and waterproofing the A-1 Sr-4 strain gages were quite adequate to provide satisfactory performance of the gages for a period of more than a year, and it is believed that the

gages would have performed properly for a considerably greater period.

5) Results of this test indicate that the outside beam of a structure of the type tested should be at least as heavy as the inside beams, perhaps even heavier if the roadway slab projects very far past the outside beam.

ACKNOWLEDGMENTS

The writers are indebted to the Public Works Department of the City of Houston for sponsorship of the test work described in this paper. Special acknowledgment is given to Mr. J. G. McKenzie, City Bridge Engineer at the time of the tests, for his interest and encouragement during the test work.

Appreciation is also expressed to Mr. R. J. Houghton for assistance in preparation of the paper, and to Mr. J. L. Coffman for preparation of drawings.

BIBLIOGRAPHY

1. "Distribution of Load Stresses in Highway Bridges," Highway Research Board Research Report 14-B (National Academy of Sciences National Research Council Publication 253) 1952.
2. "Investigation of Stresses in the San Leandro Creek Bridge," Research Report Nos. 13 and 13a. The Institute of Transportation and Traffic Engineering, University of California, by T. Y. Lin, R. Horonjeff, R. W. Clough, and C. F. Scheffey.
3. "Highway Bridge Floors—A Symposium," Transactions ASCE, Vol. 114, 1949. F. E. Richart, N. M. Newmark, and C. P. Siess.
4. "Load Distribution over Continuous Deck Type Bridge Floor Systems," W. S. Hindman, L. E. Vandegrift. Ohio State University Engineering Experiment Station Bulletin No. 122, 1945.
5. "Distribution of Wheel Loads on a Timber Bridge Floor," G. P. Boomsliter, C. H. Cather, D. T. Worrell. West Virginia University Engineering Experiment Station Research Bulletin 24, 1951.
6. "Dynamic Stresses in Continuous Plate Girder Bridges," R. C. Edgerton, Gordon W. Beecroft. Paper 973, Journal of the Structural Division, Proceedings of the American Society of Civil Engineers, Vol. 82, No. ST 3, May 1956.

Journal of the
STRUCTURAL DIVISION
Proceedings of the American Society of Civil Engineers

CONTENTS

DISCUSSION
(Proc. Paper 1259)

(over)

Note: Paper 1259 is part of the copyrighted Journal of the Structural Division of the American Society of Civil Engineers, Vol. 83, No. ST 3, May, 1957.

* There will be no closure.

Page

Discussion of
"ELASTI-PLASTIC DESIGN OF SINGLE-SPAN BEAMS AND FRAMES"

by Herbert A. Sawyer, Jr.
(Proc. Paper 851)

CORRECTIONS TO CLOSURE PUBLISHED IN PROC. PAPER 1156.—

p. 1156-3, lines 6 and 7, "convenient" should be "conventional": "evaluated by a conventional plastic analysis"

p. 1156-4, insert in line 15 from bottom the underlined words: "needed to determine: (a) strengths of frames with ratios of plastic to elasti-plastic strengths over 1.40, and (b) the effect. . ."

p. 1156-5, Fig. 18, "ϕ_e" at extreme upper right should be "ϕ_u."

Minor Additions

p. 1156-4, lines 10 and 11 from top, insert parentheses: "right footing of the second frame (although it occurred at the right knee of the first), and two factors."

p. 1156-4, line 3 from botton, add words, "both statics and": "is that it accounts for both statics and the curvature capacities of all portions of the".

Discussion of
"DYNAMIC STRESSES IN CONTINUOUS PLATE GIRDER BRIDGES"

by Roy C. Edgerton and Gordon W. Beecroft
(Proc. Paper 973)

CORRECTIONS.—On page 23, the second sentence of the first full paragraph was reproduced incorrectly. This sentence should be changed to read:

> Since vibration is a function of the internal energy alternately stored and released by the beam, a uniform moment of inertia required to do the same internal work as that done by the actual variable depth girders was calculated for each span.

ROY C. EDGERTON[1] and GORDON W. BEECROFT,[2] ASSOCIATE MEMBERS, ASCE.—The writers wish to express their appreciation for Mr. Wen's comments on dynamic bridge studies in general and for his discussion of this paper.

It is agreed that a uniform terminology that would adequately describe various physical conditions of road or deck surfaces would be desirable; however, any terminology will require further explanatory material to define the degree of "profile variation" or "roughness." For example, one could have a sizable "profile variation" without adverse effects on the riding quality or significant dynamic effects on the bridge deck if the variation increased slowly through an appreciable length and then decreased slowly through a similar length. Historically, "roughness" as applied to highways or bridges is used to indicate any surface that is not smooth. It includes surface texture, profile variations, cracks, holes and joints. Due to this common usage, it seems undesirable to limit its meaning in discussions pertaining to dynamic bridge studies. As commonly used, "roughness" would be an over-all term paralleling Mr. Wen's suggested "unevenness," with the exception that the highway grade is not considered. To use and limit the meaning of a word in the vernacular would lead to confusion. The surface texture might be described as "broomed finish," "open grid," "nonskid," or by other appropriate description.

As stated at various times in the paper, the surface profile of the North Dillard Bridge was not as smooth as that of the Troutdale Bridge. Also, the test results show that the amplitude of vibration of the North Dillard Bridge is appreciably larger than that of the Troutdale Bridge. Since the superstructures of these two bridges were fabricated and erected from the same plans and the same test vehicle was used in the tests of both bridges, the obvious conclusion was that the roughness of the North Dillard Bridge contributed significantly to the vibration. The calculations pertaining to amplitudes of vibration were performed to determine whether or not the excessive vibration of the North Dillard Bridge could reasonably be attributed to deck roughness. In the opinions of the authors, the calculations served to show the likelihood that the degree of roughness of the North Dillard Bridge deck was sufficient to cause the difference in measured amplitudes of vibration between

1. Research Engr., State Highway Dept., Salem, Ore.
2. Asst. Research Engr., State Highway Dept., Salem, Ore.

the two bridges. The values were included in the paper for this purpose. It was explicitly stated that no correlation between measured and computed amplitudes of vibration was accomplished, but calculations based on an assumed deck contour indicate that the excessive vibration of the North Dillard Bridge can be attributed to deck roughness.

In connection with the assumed contour of the bridge deck and the calculations pertaining thereto, reference is again made to pp. 238-240 in Timoshenko's "Vibration Problems in Engineering," 2nd edition. The profile of the 160-foot center span was assumed to be represented by the first equation, p. 238 in this text, using a wave height of 1/4 inch and wave length of 25 feet. Equation (h) p. 240 was used to calculate the given value for the increased force on the bridge deck. A vehicle speed of 37 miles per hour was used since a maximum measured deflection occurred in both girders at about this speed. The unsprung weight of the vehicle was assumed to be 6,000 pounds. The average of the measured frequencies of vibration for Vehicle B was 2.39 cycles per second, giving an average period of 0.418 seconds, which was used in the calculations. This period of 0.418 seconds and a value of 65,000 pounds for the sprung weight of the vehicle were used in calculating the spring constant of 38,000 pounds per inch. At the speed of 37 miles per hour and the wave length of 25 feet mentioned above, the period of the vehicle's traverse along the wavy contour of the deck is 0.461 seconds. With these values for the periods, equation (h) reaches a maximum at intervals of about 0.44 seconds. Since it was assumed the sinusoidal curve was applicable to the center span, a maximum was picked at $t = 1.42$ seconds at which time the vehicle would have traveled 77 feet from the pier or within three feet of mid-span. By substituting $t = 1.42$ seconds and the other values discussed above in equation (h), the value of 36,600 pounds was obtained for the additional pressure on the deck. As explained in the paper, the additional force would probably be appreciably less than this calculated value due to the different axles being out of phase, the yielding of the bridge deck and the fact that the actual roughness is variable both in the length and amplitude of the waves. However, the calculations did serve to indicate the likelihood that the roughness of the North Dillard Bridge deck is the principal reason for the marked difference in vibration between two bridges constructed from the same plans.

In his discussion, Mr. Wen suggests that comparisons should be made between the experimental static and dynamic stresses and between the theoretical static and dynamic stresses and that cross comparisons of these quantities needlessly complicate the picture for those engaged in dynamic studies. Attention should be brought to the fact that to the bridge engineer, whose responsibility it is to design and maintain structures that will adequately serve the needs of the traveling public at a minimum cost, the comparisons between measured and calculated static stresses and between measured and calculated dynamic stresses are more meaningful. A principal purpose of bridge studies of this type is to prove or disprove the adequacy of existing specifications and to acquire data from which specifications providing greater safety or greater economy may some day be drawn. It seems, therefore, that these are the logical comparisons; however, all information has been presented so that those having other interests can make any comparisons they wish.

Discussion of
"DEVELOPMENT AND DESIGN OF THE WALT WHITMAN BRIDGE"

by Milton Brumer and C. W. Hanson
(Proc. Paper 1019)

MILTON BRUMER,[1] and C. W. HANSON,[2] MEMBERS ASCE.—The writers are deeply appreciative of the discussions contributed by Messrs. Cevdet Z. Erzen, George S. Vincent, Louis Balog and Gerald K. Gillan.

Mr. Erzen treats with the factors which safeguard the structure against torsional oscillation. He points out, as the authors have long realized, that among the important safeguards are the suspended weight, the width of structure and the use of a second lateral system, which in essence establishes a torsion box. Where combinations of weight, width and stiffness of the suspended structure are ample it may not be essential to use a second lateral system. However, the authors wish to emphasize that the use of a double lateral system increases the resistance of the bridge to torsional oscillation very materially and is well worth the relatively low cost involved.

Mr. Vincent advocates the use of section model tests in conjunction with the design of suspension bridges. The designers have no particular brief against such procedure, yet they do have reservations as to the validity of such section tests when applied to the structure as a whole. The dampening action of the suspended system, as well as the uncertain action of the variable and non-uniform character of the wind, cannot be evaluated properly by such tests and in fact may result in misleading interpretations. Section model tests are of particular value in furnishing indications of the behavior of one type of deck design with respect to another, but not as reliable proof of the degree of stability of the design. It is interesting to note that Mr. Balog is also of the opinion that "the similitude between the section model in the wind tunnel and the prototype in natural wind is questionable from important considerations." The authors are of the opinion that tests on models of the entire system at reasonable scale would lead to more reliable results. In view of the similarity of the general design with that of the Delaware Memorial Bridge, which has demonstrated adequate resistance against wind action, the designers of the Walt Whitman Bridge determined to employ the "stiffness index" approach, using trussed floorbeams, open stiffening trusses and the double lateral system to assure ample vertical and torsional rigidity, without resorting to model tests.

Mr. Balog questions the wisdom of using the "stiffness index" as a criterion for sufficient rigidity against wind action. In support of this position he gives statistics on three suspension bridges of relatively short span length. According to published records the motions of these bridges are not of significant magnitude even under severe wind and should have no effect on the safety and durability of the structures. However, some of these motions were easily detected by the human senses. In order to avoid even such small

1. Associate Partner, Ammann & Whitney, Cons. Engrs., New York, N. Y.
2. Partner, Modjeski & Masters, Cons. Engrs., Harrisburg, Pa.

motions, the authors agree that it is advisable to provide a more ample margin of stiffness in short-span bridges, particularly where severe local wind conditions are indicated.

Mr. Balog advocates the use of a formula, which requires a minimum $I=0.005\ell^2$. The authors are obliged to point out that Mr. Balog's guide is also not without its limitations in application. It neglects an important element contributing to stability in any suspension bridge, namely that of dead weight. His approach cannot be applied to a practically unstiffened bridge, such as the George Washington Bridge in which the I is zero. It does not recognize the stiffness contributed by the cables. Mr. Balog advocates, as do the authors, the use of a closed or boxed section to increase the torsional rigidity of the suspended structure.

Mr. Gillan objects to the use of the term "coefficient of friction" to the factor of 0.60 determined by tests made on cable bands of the original Philadelphia-Camden Bridge. In this respect he is correct. It is more appropriate to refer to that coefficient as the ratio between the ultimate slipping load and the clamping force delivered by means of the tightened cable band bolts. Suspension bridge designers have long recognized this and have always employed the coefficient correctly in the design even though they may have used the phrase "coefficient of friction" rather loosely.

Present knowledge of the aerodynamic behavior of suspension bridges is limited, and there is no theoretical solution available which satisfactorily embodies all of the aspects of the problem. As a consequence differences of opinion between designers are inevitable. The writers are confident that a suspension bridge design, having adequate vertical and torsional rigidity, will be secured with a discerning employment of the following principles:

1. Use of open stiffening trusses and trussed type floorbeams instead of deep solid web girders.
2. Use of top and bottom lateral systems to secure a closed section for the suspended deck.
3. Venting of the floor to the extent practicable.
4. Use of as large a distance between cables as reasonably feasible.
5. Use of as low a sag-span ratio for the cables as reasonable, compromising between minimum cost and maximum desired degree of flexibility of the system.
6. Providing the additional vertical and torsional rigidity desired by the selection of the proper moment of inertia for the stiffening trusses. For long span suspension bridges the writers know of no better approach to this than by the use of the empirical "stiffness index" values mentioned in the paper.

   To allow an ample margin of stability and resistance against even small, but noticeable motions, such as have been observed in some relatively short suspension spans, it is advisable and economically insignificant to provide a stiffness index appreciably greater than the range recommended for long-span bridges, especially when severe local wind conditions are indicated.
7. Checking the adequacy of the component parts of the stiffening trusses thus selected against the various static load and temperature variation requirements. The intensity of static wind load to be used for design purposes should be fixed with such factors in mind as local exposure conditions, height of structure and regional wind intensity experiences.

CORRECTIONS TO DISCUSSION BY LOUIS BALOG WHICH APPEARED IN PROC. PAPER 1156—

Page 1156-13, 8th line from bottom, replace "is most of its length" by "in most of its length."

Page 1156-14, Table 2, 2nd line, change 15,500 to 15,500* (asterisk added)

change 483 to 493

Page 1156-15, insert after "respectively. (4)," in paragraph 2, the following paragraph:

Section model tests resulting in low critical wind velocities can be regarded as a guide in revising a design. If the critical wind velocities are high, the section model results become less dependable. Very minor details greatly change the results. Furthermore, the deformations of the actual bridge and the section model increasingly deviate with increasing wind velocity. (12) The high critical wind velocities obtained on the section model lose practical significance because the static pressure of such winds make the actual structure useless before any dynamic effects could occur. The authors' criticism of accepting section model data as reliable proof of the degree of stability of a bridge, like stable in infinite mph wind, is justified. (6)

Page 1156-15, paragraph 3, change $I_t = 8.0078\ 1^2$ to $I_t = 0.0078\ 1^2$

insert in the 9th line of this paragraph between the words "advantageous" and "arrangement" the words "composite box-girder," to read "advantageous composite box-girder arrangement"

Page 1156-17, in Ref. 8, insert, at the end of the first line, "Stabilität der"

after Ref. 11, add:

12. "Aerodynamische Stabilität von Hängebrücken unter Windbelastung," by A Hirai (Japan), edited by A. Hoyden, Der Bauingenieur, Vol. 31, 1956, pp. 402-408.

Discussion of
"MOMENTS IN FLAT SLABS"

by M. W. Huggins and W. L. Lin
(Proc. Paper 1020)

M. W. HUGGINS,[1] M. ASCE, and W. L. LIN.[2]—The authors wish to thank Professor Chinn for his careful and critical review of their paper. Professor Chinn's discussion of the effect of Poisson's ratio is particularly valuable as it points up the likelihood that the actual positive moments in a concrete slab would be smaller than those found in the test slab, while the negative moments would be larger.

It is apparent however, that the actual positive moments should be taken as considerably larger than those obtained by the A.C.I. recommended method of analysis.

The 1951 A.C.I. Code states "The numerical sum of the maximum positive and the average maximum negative bending moments for which provision is made in the design in the direction of either side of a rectangular panel shall be assumed as not less than $1/10\ Wav\ .L\ (a-\frac{4Aav}{3L})2"$. Thus, as written, it makes no provision for downward adjustment of moments.

The somewhat similar section 1002(a) of the 1956 Code is intended for "flat slabs within the limitations of section 1004." The model tested does not satisfy those limitations.

Professor Chinn's proposal that the bents should be bounded laterally by lines of zero shear appears to be a very good one.

1. Asst. Prof. of Civ. Eng., Univ. of Toronto, Toronto, Ont., Canada.
2. Asst. Bridge Design Engr., Dept. of Highways, Ont., Canada.

Discussion of
"SIMPLIFICATION OF DESIGN BY ULTIMATE STRENGTH PROCEDURES"

by Phil M. Ferguson
(Proc. Paper 1022)

PHIL M. FERGUSON,[1] M. ASCE.—The interest expressed in practical ultimate strength design is quite encouraging. Each discusser of this paper has attempted to extend the practical field of ultimate strength design or to make such design still simpler. Also to be noted is a recent paper by Whitney and Cohen(6) which has added design curves for circular columns and square columns with circular cores, both of which were unavailable earlier.

Professor Au has presented formulas for the balanced load P_b for circular columns and square columns with circular cores. These are helpful and have not, insofar as the author knows, been presented elsewhere. He is to be commended for his study of the differences between the formula value of P_b and the intersection of the tension and compression failure lines as given by formula. This matter deserves some further consideration as ultimate strength design is codified.

The curves and nomographs prepared by Mr. Schick are examples of how beam design charts may be adapted to the thinking of the individual designer. It is regretted that Mr. Schick did not extend his discussion to include specific examples of the use of his curves and thereby demonstrate their advantages. The original chart from the Report as reprinted in Fig. 2 suffered from the scarcity of subdivisions on the ordinates for percentage of steel. Whitney and Cohen(6) in their Chart 1 have done an excellent job of correcting this condition.

Mr. Sobotka's study of the economical arrangement of unsymmetrical steel in columns is somewhat more advanced than the simplified approach adopted for the original paper. As engineers use ultimate strength design it is certain that many such studies will follow and point out economical procedures. The inherent simplicity of ultimate strength design makes such studies more feasible.

The comparison between various stress blocks presented by Mr. Spanovich indicates that differences are negligible from the practical design viewpoint. It is probable that research on eccentrically loaded columns can be better correlated on the basis of a trapezoidal or parabolic stress block. However, practical design is simplified by use of the rectangular stress block and the resulting accuracy appears to be much more than adequate.

It is possible that the author misunderstands Mr. Spanovich's statement about the possible effect of design criteria for shear, bond, and diagonal tension upon the simplicity of design by ultimate strength methods. Design methods for shear need overhauling and possibly extensive revision. The impact of these changes would appear to be identical upon working stress methods and upon ultimate strength design.

Whether design is by working stress methods or by ultimate strength,

1. Prof. of Civ. Eng., Univ. of Texas, Austin, Tex.

certain members are now more critical in shear than in moment. If ultimate strength design leads ultimately to smaller members, it appears that shear has more chance to control such members. But ultimate strength design for steel in members of given size is not made more complex. After section size is established from shear, the steel is still simply established from moment.

The semi-graphical solution of the column with load eccentric about both axes, as suggested by Mr. Ulicny, will appeal to many engineers as simpler than the iteration process of Professor Craemer. Whitney and Cohen[6] present a similar procedure. The author has not used either method sufficiently to choose between them. It may be that the choice depends upon an engineer's general attitude towards graphical solutions.

The author wishes to thank the discussers for their interest and their constructive comments. The change to ultimate strength design will probably not be sudden and complete in the immediate future. But since better balanced designs will result, with eventually some economies, all efforts towards a better understanding of the inherent simplicity of ultimate strength design should be encouraged.

BIBLIOGRAPHY

6. "Guide for Ultimate Strength Design of Reinforced Concrete," by Charles S. Whitney and Edward Cohen, Journal, A.C.I., Vol. 28, November, 1956, p. 455.

Discussion of
"INTERNAL TIES IN SLOPE DEFLECTION AND MOMENT DISTRIBUTION"

by Morris Ojalvo
(Proc. Paper 1096)

ARTURO J. BIGNOLI.[1]—The author proposes the use of internal imaginary ties to prevent joint translation in the analysis of structures, using "slope deflection" or "moment distribution" methods. The writer shares the author's opinion that the use of these ties simplifies the analysis of complicated structures (with non-orthogonal members) as seen in the first example of this work.

In structures having orthogonal members, however, the writer believes that there is some extra complication in using these ties instead of other known restraints for joint translation, as can be seen from an analysis of a Vierendeel truss with parallel chords and vertical stanchions. The idea, however, is a valuable one.

It does not appear that joint translations are independent of joint rotations and therefore it is not possible to establish an independent system of equations for the translations. This then invalidates Mr. Ojalvo's opinion on page 3 (lines 22 to 24). To be able to write equations for joint translations only, as the author does on pages 5 and 9, it is necessary to reduce the unknowns to these translations only, and this means solving, previously, the other unknowns (joint rotations for loads and for arbitrary values of joint translations). In other words, Mr. Ojalvo uses a principal structure in which joints can rotate but not translate. In the first example for instance, he must solve—at least three times (see table 2)—the structure with non-translating joints (10 equations with 10 unknowns each time) and then another system of 2 equations with 2 unknowns. If the complete system of equations should be solved, instead of all this work, it would have been enough to solve a system of 14 equations with 14 unknowns reduced by symmetry, to 6 equations with 6 unknowns, which is much less work and time. By complete system of equations is meant the system in which all influences among rotations and translations of joints are taken into account simultaneously (see the well-known works of K. Beyer and R. Guldan).

1. Prof., Theory of Structures, Univ. La Plata, Argentina.

Discussion of
"INFLUENCE LINES FOR CIRCULAR RING REDUNDANTS"

by Henry M. Lummis
(Proc. Paper 1097)

HAROLD G. LORSCH,[a] A.M. ASCE.—Elementary stress analysis, in the sense in which it is generally applied by civil engineers to problems of strength of materials and statically indeterminate structures, is based upon (1) the laws of static equilibrium, (2) a constant modulus of elasticity, and (3) certain additional assumptions regarding the deformations of the cross section. Static equilibrium is always valid for motionless bodies; the modulus of elasticity for most civil engineering materials is fairly constant within the range of allowable stresses. The limitations on the additional assumptions, however, are often completely forgotten.

In order to arrive at the usual flexure formula $S = \frac{Mc}{I}$ it is necessary to postulate that plane cross sections before bending remain plane after bending. It can be shown by Theory of Elasticity (ref. 1) that this so-called Bernoulli-Navier postulate holds true for beams whose ratio of depth to span length is small, provided the section is taken at distances from all loads not less than the beam depth. If these requirements are not fulfilled, all the commonly used formulae for stress and deflection are not valid, nor are the usual methods of statically indeterminate analysis valid all of which are based on the simple "Strength-of-Materials" equations for stress and deflection. The present paper ought to be reviewed in the light of these fundamental facts.

The author initially determines influence tables and diagrams for the three redundants acting at the elastic center of the ring due to horizontal loads, vertical loads, and moments acting at any point of the ring. He then uses them to evaluate the moments, shears, and thrusts at any point of the ring due to these load effects: Table 1 and Figs. 1 through 4. The basic equations used in this part of the paper are correct; the ones for vertical loads can be found in many standard texts on statically indeterminate structures (refs. 2, 3). The graphs, however, are more easily read than any this writer has seen.

It is when the author attempts the "solution for Redundants Due to Tangential Shears caused by Vertical Shear and Torsion" that his approach becomes incorrect. For he sets out by looking at the ring as a cross section in order to obtain his shear stress distribution due to vertical shear and due to torsion, but then he uses this stress distribution in order to analyze the ring as a structure by itself. This procedure is in conflict with the limitations on the Bernoulli-Navier postulate that plane sections remain plane.

The assumed shear stress distribution due to vertical shear $S_S = \frac{W \sin a}{\pi R}$ (first equation on page 12) and the assumed shear stress distribution due to

a. Asst. Prof. of Civ. Eng., The City College, New York, N. Y.

torsion $S_s = \frac{M}{2\pi R^2}$ (first equation below Fig. 7 on page 15) are valid for a pipe, whose span length is long compared to its diameter, at points about 2R removed from such externally applied vertical shears or torsional moments. (Fig. 13). The author, however, uses these shear stress distributions for the analysis of a pipe either very short (Fig. 14a) or very long and uniformly loaded (Fig. 14b). In neither case are they applicable. Hence all of the author's work on pages 12 through 19, including Figs. 5-10 and Table 2, is based on unjustified assumptions and therefore incorrect.

The fallacy of the paper is further illustrated by a closer examination of the figures on page 19 of the paper. Fig. 9 purports to show moment, shear, and thrust at any point of the ring section due to vertical shear; but the basis for the curves shown is the elementary shear stress distribution $S_s = \frac{W \sin a}{\pi R}$ which neglects all stresses "in" the cross section, i.e. those very moments, shears, and thrusts. The same objection applies to Fig. 10 which purports to show these same quantities due to torsion; yet the basic torsion formula $S_s = \frac{M}{2\pi R^2}$ which was used to obtain the curves of Fig. 10 neglects all other stresses in the cross section, including the moments and thrusts depicted. One can see at a glance that Fig. 10 is incorrect by realizing that the initially assumed shear stress distribution due to torsion is circularly symmetrical; the curves of Fig. 10 are not. This indicates the basic error of the author's approach in which the effect of boundary conditions, i.e. the method of support of the pipe, was not taken into account.

A valid procedure would have been to compute a shear stress distribution on the basis of arbitrarily assumed moments, shears and thrusts; then carry out the author's analysis and show that the moments, shears, and thrusts thus obtained are identical to the ones assumed. This would justify the initial assumptions. The author's Figs. 9 and 10 however clearly show the incompatibility of the initial assumptions with the final results.

In summing up it can be said that the results up to page 11 of the paper and that part of the corresponding illustrative example on page 20 and parts of page 21 are correct, but that pp. 12-19, 21 bottom, and 22 are incorrect and should not be used.

REFERENCES

1. "Theory of Elasticity" by Timoshenko and Goodier, McGraw-Hill Book Co., 2d edition, 1951, p. 326.

2. "Statically Indeterminate Structures" by L. C. Maugh, John Wiley & Sons, 1946, p. 242.

3. "Theory of Modern Steel Structures" by L. E. Grinter, MacMillan Co., 1949, vo. II, p. 248.

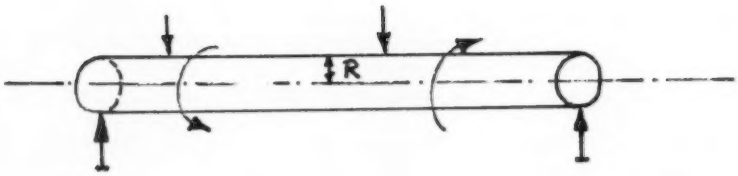

Fig. 13

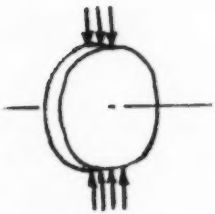

Fig. 14a

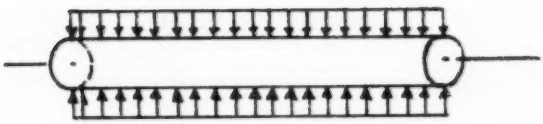

Fig. 14 b

Discussion of
"ANALYSIS OF RIBBED DOMES WITH POLYGONAL RINGS"

by Tsze-Sheng Shih
(Proc. Paper 1101)

A. F. FOERSTER,[1]—On page 1101-18, the author recommends, in accordance with S. Timoshenko, "Theory of Plates and Shells," use of a sine law for the wind load distribution on a hemispherical dome:

$$W = W_0 \sin \phi \sin \theta .$$

In the writer's opinion such a distribution is too unrealistic to serve as a basis for the wind load analysis of a dome. The sine law results in a horizontal wind load which is much higher than the actual drag; it fails, however, to yield any lift although actually the lift of a hemispherical dome at supercritical Reynolds numbers is many times greater than its drag.

A realistic wind load distribution may be obtained from various literary sources, for instance:

Aerodynamic Drag. By S. Hoerner. Published by the author 1951.

Engineering Aerodynamics. By W. S. Diehl. The Ronald Press Company, New York. 1936.

R & M* No. 1766. Experiments on a Sphere at Critical Reynolds Number. By A. Fage.

R & M* No. 1678. Laminar Boundary Layer on the Surface of a Sphere in a Uniform Stream. By S. Tomotika.

NACA Report No. 185. The Resistance of Spheres in Wind Tunnels and in Air. By Bason and Redi. 1924.

NACA Report No. 253. Flow and Drag Formulas for Simple Quadrics. By Zahm. 1927.

(* Aeronautical Research Committee Reports and Memoranda.)

For the purpose of structural analysis of the dome, the wind load distribution may be approximated by a finite trigonometric series, which automatically separates the wind loads into symmetrical and anti-symmetrical parts.

1. Structural Design Analysis, Goodyear Aircraft Corp., Akron, Ohio.

Discussion of
"SIMPLIFIED ANALYSIS OF RIGID FRAMES"

by Robert M. Barnoff
(Proc. Paper 1106)

I-CHEN CHANG,[1] A.M. ASCE.—For a quarter of a century, numerous writers both in the United States and abroad have attempted to bring some new techniques to the method of moment distribution.[2] Nevertheless Professor Hardy Cross' achievement was so great that no supplement seems able to keep pace with the elegant simplicity of his original paper.

It has been noticed by many writers that a more complicated form of the moment-distribution method either expressed by formulas or illustrated by diagrammatical successive correction may be found helpful under certain conditions:

1. In routine design calculation as plotted curves and tabulated coefficients are always at hand.
2. In a brief investigation when only several key figures of a structural system are desired.
3. In a tedious balancing process of slow convergence.
4. When one or several degrees of side-sway are present in the structural system.

Mr. Barnoff has given a very interesting illustration. A more general approach is by introducing the physical concept and structural terminology of Hardy Cross into the slope and deflection equations of G. A. Maney. The resulting equations will lead us to a direct solution for all kinds of simple structures and an approximate solution for complicated ones.

Derivation of the Rigid-Joint Equations

A. For Structures without Joint Displacement

The Slope-deflection equations for any joint A shown as Fig. 1 may be written as:

$$M_{Ai} = 2\,E\,K_{Ai}\,(2\,\theta_A + \theta_i) + M_{FAi} \quad (i = 1,\ 2,\ \ldots\ldots\ n) \qquad (1)$$

Since

$$\sum_{i=1}^{n} M_{Ai} = 0 \quad (i = 1,\ 2,\ \ldots .n) \qquad (2)$$

1. Structural Engr., John F. Meissner Engrs., Chicago, Ill.
2. Published in May, 1930, proceedings and Vol. 96, 1932, Transactions, ASCE.

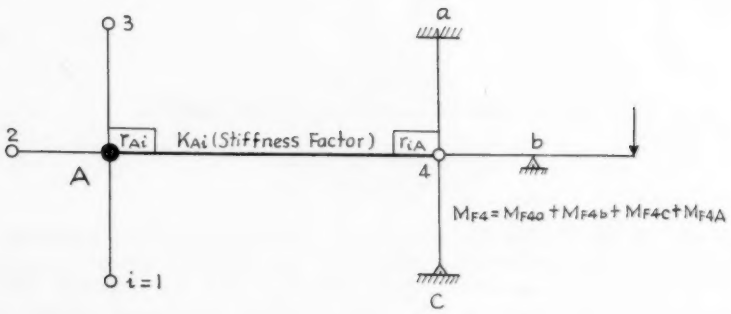

Fig. 1. Typical Exterior joints i and interior joint A of simple structures.

From eqs. (1) and (2) we obtain

$$4\,E\,K_A\theta_A = -2\,E\sum_{i=1}^{n} K_{Ai}\theta_i - M_{FA} \tag{3}$$

Where

$$M_{FA} = \sum_{i=1}^{n} M_{FAi} \tag{a}$$

$$K_A = \sum_{i=1}^{n} K_{Ai} \tag{b}$$

Similarly for joint i, if we know or can estimate its joint fixed-end moment M_{Fi}, we may write

$$4\,E\,K_i\theta_i = -\,(2\,E\,K_{iA}\theta_A + M_{Fi}) \tag{4}$$

Substituting (4) into (3) we have

$$EK_A\theta_A = -\frac{1}{D_A}\left[M_{FA} - (1/2)\sum_{i=1}^{n} K_{Ai}\left(\frac{M_{Fi}}{K_i}\right)\right]$$

Where $D_A = 4 - \sum_{i=1}^{n} r_{Ai} \cdot r_{iA}$

And $r_{Ai} = \frac{K_{Ai}}{K_A}$, $r_{iA} = \frac{K_{iA}}{K_i}$, are known as distribution factors

For symmetrical beams $K_{Ai} = K_{iA}$, so $\frac{K_{Ai}}{K_i} = \frac{K_{iA}}{K_i} = r_{iA}$

Let $M'_{FA} = M_{FA} - (1/2)\sum_{i=1}^{n} r_{iA} \cdot M_{Fi}$

We obtain

$$E\,K_A\theta_A = -\frac{1}{D_A}\,M'_{FA} \tag{5.1}$$

Again by Eq. (4) we have

$$E K_i \theta_i = -(1/4)\left(M_{Fi} - \frac{2 r_{Ai}}{D_A} M'_{FA}\right) \tag{5.2}$$

We observe from Eq. (d) that M'_{FA} is the total moment potential at joint A, since the term M'_{FA} is the sum of fixed-end moments at joint A and the term $(1/2) \sum_{i=1}^{n} r_{iA} M_{Fi}$ is the sum of all moments carried to joint A from its adjacent joints 1, 2, ... n.

By substituting Eqs. (5.1) and (5.2) into Eq. (1) and after verifying we obtain

$$M_{Ai} = M'_{FAi} - R_{Ai} \cdot M'_{FA} \tag{6}$$

Where

$$M'_{FAi} = M_{FAi} - \frac{1}{2} r_{iA} M_{Fi} \tag{e}$$

$$R_{Ai} = \frac{r_{Ai}(4 - r_{iA})}{D_A} \tag{f}$$

Similarly $M_{iA} = 2 E K_{Ai} (2 \theta_i + \theta_A) + M_{FiA}$

$$= M'_{FiA} - R_{iA} \cdot M'_{Fi} \tag{7}$$

Where $M'_{FiA} = M_{FiA} - r_{iA} M_{Fi}$ (g)

$$R_{iA} = \frac{2 r_{Ai}(1 - r_{iA})}{D_A} \tag{h}$$

Since $R_{Ai} = \sum_{i=1}^{n} \frac{r_{Ai}(4 - r_{iA})}{D_A} = \frac{4(\sum_{i=1}^{n} r_{Ai}) - \sum_{i=1}^{n} r_{Ai} r_{iA}}{4 - \sum_{i=1}^{n} r_{Ai} r_{iA}}$

and $\sum_{i=1}^{n} r_{Ai} = 1$

So $\sum_{i=1}^{n} R_{Ai} = 1$

Also $\sum_{i=1}^{n} M_{Ai} = \sum_{i=1}^{n} M'_{FAi} - M'_{FA} \sum_{i=1}^{n} R_{Ai} = 0$

B. For Structures with Joint Displacement

When the magnitude of side-sway is known, the term $6 E K_{Ai} \frac{\delta}{h_{Ai}}$ is calculated and added to the fixed-end moment M_{FAi}; otherwise it is considered as unknown and solved by the static equilibrium condition of shears.

Examples

Example 1. Two column rigid frame

Consider the frame shown in Fig. 2-1

Where

$$r_{BC} = r_{CB} = r = \frac{4K_2}{3K_1 + 4K_2}$$

$$R_{BC} = R_{CB} = \frac{r(4-r)}{4-r^2}$$

$$M_{FBC} = M_1 - M_2, \quad M_{FCB} = M_3 - M_4$$

$$M_{FB} = M_1 - M_2 + 3EK_1 \frac{\delta}{h}$$

$$M_{FC} = M_3 - M_4 + 3EK_1 \frac{\delta}{h}$$

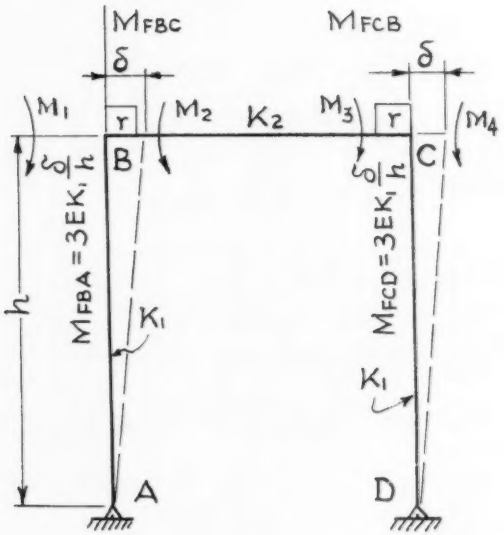

Fig. 2-1

And δ is the assumed side-sway

By Eq. (6) i.e.

$$M_{BA} = -M_{BC} = -(M_{FBC} - \tfrac{1}{2} r_{BC} M_{FC}) + R_{BC}(M_{FB} - \tfrac{1}{2} r_{CB} M_{FC})$$

We have

$$M_{BA} = (1-R)\left[(-M_1 + M_2) - \frac{r}{2}(M_3 - M_4)\right] - M^{\delta} \qquad (A)$$

$$M_{CD} = (1-R)\left[(-M_3 + M_4) - \frac{r}{2}(M_1 - M_2)\right] - M^{\delta} \qquad (B)$$

$$M_{BA} = -M_{CD} = \frac{A-B}{2} = (1/4)(1-R)(2+r)(-M_1 + M_2 + M_3 - M_4)$$

$$= \left(\frac{1-r}{2-r}\right)(-M_1 + M_2 + M_3 - M_4) = Q_1 (-M_1 + M_2 + M_3 - M_4)$$

Where $M^{\delta}=(R+\frac{1}{2}r-\frac{1}{2}rR)(3EK_1\frac{\delta}{h})$

$$Q_1=\frac{3K_1}{6K_1+4K_2}=\frac{1-r}{2-r}$$

For lateral displacement of column shown as Fig. 2-2

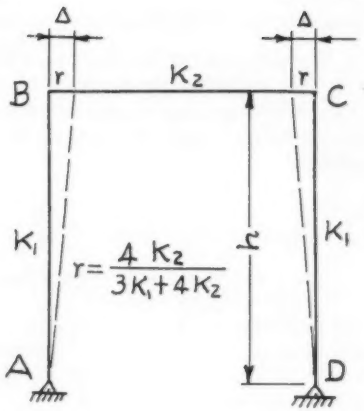

Fig. 2-2

$$M_{FBC}=M_{FCB}=0$$

$$M_{FB}=3EK_1\frac{\Delta}{h},\quad M_{FC}=-3EK_1\frac{\Delta}{h}$$

$$M_{BA}=-(\frac{1}{2}r-R-\frac{1}{2}rR)\ (3EK_1\frac{\Delta}{h})=Q_1\cdot(4K_2\frac{\Delta}{h})$$

Example 2. Three column rigid frame

For a numerical example we shall take a two-bay bent shown in Fig. 3-1. It will illustrate that Eqs. (5.1) (5.2) are convenient for calculating angle changes.[3] Assume $E\frac{\Delta}{h}$ = 100 Kips/ft.^{2}

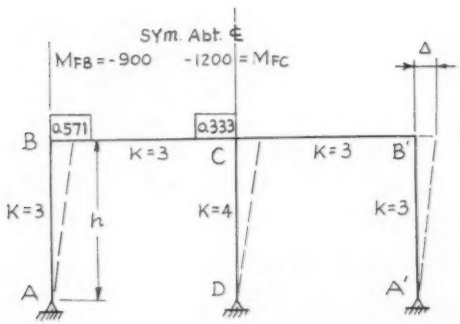

Fig. 3-1

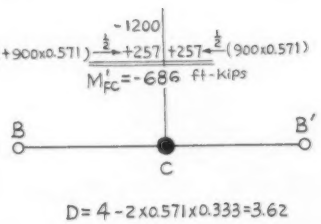

Fig. 3-2

As shown in Fig. 3-2

Or by Eq. (d) $M'_{FC}=-1200+2\times0.571\times(1/2)\times900=-686$ ft-Kips

By Eq. (5.1) $E\theta_C=\frac{1}{9x3.62}\times686=21.1$ Kips/ft^2

(5.2) $E\theta_B=\frac{1}{4x5.25}\ (-900+\frac{2x0.333x686}{3.62})=36.9$ Kips/ft^2

3. "Theory of Modern Steel Structures" by L. E. Grinter, The Macmillan Co., New York, N. Y., 1949, Vol. II. p. 164.

Example 3. A structure of academic interest

For illustration we shall take the rigid frame shown in Fig. 4-1, while Fig. 4-2 indicates its equivalent part around joint C. Joint C after reduced from minor members still has the same joint-stiffness and total moment potential M'_{FC}. Here we assume that our main interest is M_{CB} & M_{CD} at joint C.

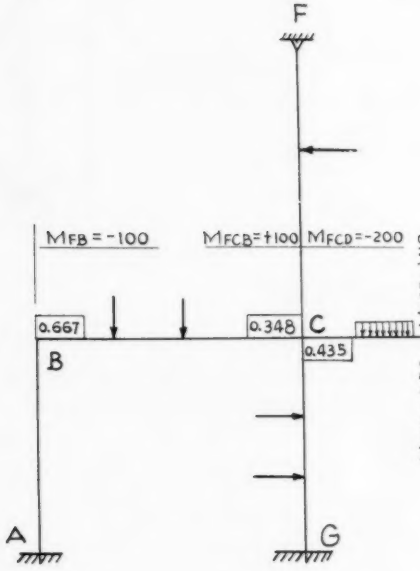

Fig. 4-1

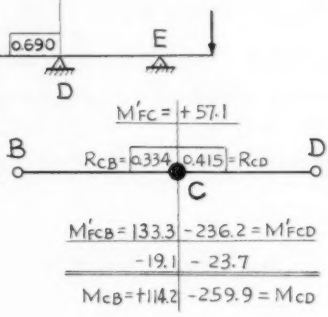

Fig. 4-2

In Fig. 4-2 $M'_{FCB} = 100 + (1/2) \times 0.667 \times 100 = 133.3,$

$M'_{FCD} = -200 - (1/2) \times 0.69 \times 105 = -236.2$

$M'_{FC} = 133.3 + 110 - 236.2 + 50 = 57.1,$

$D = 4 - (0.667 \times 0.348 + 0.690 \times 0.435) = 3.47$

$R_{CB} = 0.348(4 - 0.667) \div 3.47 = 0.334,$

$R_{CD} = 0.435(4 - 0.69) \div 3.47 = 0.415$

$M_{CB} = 133.3 - 57.1 \times 0.334 = 114.2,$

$M_{CD} = -236.2 - 0.415 \times 57.1 = -259.9$

Check: A check can be added and it is similar to that we have in the ordinary method of moment of distribution by applying the condition

$$\sum_{i=1}^{4} R_{Ci} = 1 \text{ or } \sum_{i=1}^{4} M_{Ci} = 0. \quad \text{Notice here } R_{CF} = \frac{4}{D_A} \cdot r_{CF'}$$

$$\text{and } R_{CG} = \frac{4}{D_A} \cdot r_{CG'}$$

The equation $R_{Ai} = \frac{4}{D_A} \cdot r_{Ai}$ for joint i which is either fixed or hinged is obtained from a more general case. This general treatment is useful not only for frames with variable moment of inertia,[4] but also for buckling strength[5] and frequency analysis.[6] In order to avoid making this discussion too lengthy, the writer will not take this occasion to present the general case.

Acknowledgment—The writer gratefully acknowledges the benefit he has derived from discussing his attempt with T. Y. Lin M. ASCE, of the University of California, E. I. Feisenheiser M. ASCE of Illinois Institute of Technology, E. F. Masur of the University of Michigan. Special thanks are due L. E. Grinter M. ASCE, Dean of the Graduate School, University of Florida, for his teachings and guidance in originating this discussion.

4. "Statically Indeterminate Structures" by L. C. Maugh, John Wiley and Sons, Inc., New York, N. Y., 1946, p. 132.
5. "Buckling Strength of Metal Structures" by Friedrich Bleich, McGraw Hill Book Co., Inc., New York, N. Y., 1952, p. 210.
6. For a full explanation of this point, see the writer's discussion on "Behavior of Structures Subjected to a Forced Vibration" by Charles T. C. Looney, Proceedings Separate No. 589, January, 1955.

Discussion of
"EFFECT OF BEARING RATIO ON STATIC STRENGTH
OF STRUCTURAL JOINTS"

by Jonathan Jones
(Proc. Paper 1108)

CORRECTIONS.—The indented paragraph immediately preceding the heading "Summary of Second or 1950 Static Series" should be changed to read:

> The overall efficiency, meaning by this the ratio of breaking load to the product of the gross plate area by the coupon ultimate strength, was not reduced as the bearing ratios increased from 1.54 to 3.05 (3/4" rivets) or from 1.57 to 2.90 (1" rivets). See Fig. 15, Reference No. 8.

PROCEEDINGS PAPERS

The technical papers published in the past year are identified by number below. Technical-division sponsorship is indicated by an abbreviation at the end of each Paper Number, the symbols referring to: Air Transport (AT), City Planning (CP), Construction (CO), Engineering Mechanics (EM), Highway (HW), Hydraulics (HY), Irrigation and Drainage (IR), Pipeline (PL), Power (PO), Sanitary Engineering (SA), Soil Mechanics and Foundations (SM), Structural (ST), Surveying and Mapping (SU), and Waterways and Harbors (WW), divisions. Papers sponsored by the Board of Direction are identified by the symbols (BD). For titles and order coupons, refer to the appropriate issue of "Civil Engineering." Beginning with Volume 82 (January 1956) papers were published in Journals of the various Technical Divisions. To locate papers in the Journals, the symbols after the paper numbers are followed by a numeral designating the issue of a particular Journal in which the paper appeared. For example, Paper 1113 is identified as 1113 (HY6) which indicates that the paper is contained in the sixth issue of the Journal of the Hydraulics Division during 1956.

VOLUME 82 (1956)

MAY: 961(IR2), 962(IR2), 963(CP2), 964(CP2), 965(WW3), 966(WW3), 967(WW3), 968(WW3), 969 (WW3), 970(ST3), 971(ST3), 972(ST3)[c], 973(ST3), 974(ST3), 975(WW3), 976(WW3), 977(IR2), 978(AT2), 979(AT2), 980(AT2), 981(IR2), 982(IR2)[c], 983(HW2), 984(HW2), 985(HW2)[c], 986(ST3), 987(AT2), 988(CP2), 989(AT2).

JUNE: 990(PO3), 991(PO3), 992(PO3), 993(PO3), 994(PO3), 995(PO3), 996(PO3), 997(PO3), 998 (SA3), 999(SA3), 1000(SA3), 1001(SA3), 1002(SA3), 1003(SA3)[c], 1004(HY3), 1005(HY3), 1006 (HY3), 1007(HY3), 1008 (HY3), 1009 (HY3), 1010 (HY3)[c], 1011 (PO3)[c], 1012 (SA3), 1013 (SA3), 1014(SA3), 1015(HY3), 1016(SA3), 1017(PO3), 1018(PO3).

JULY: 1019(ST4), 1020(ST4), 1021(ST4), 1022(ST4), 1023 (ST4), 1024(ST4)[c], 1025(SM3), 1026 (SM3). 1027(SM3), 1028(SM3)[c], 1029(EM3), 1030(EM3), 1031(EM3), 1032(EM3), 1033(EM3)[c].

AUGUST: 1034(HY4), 1035(HY4), 1036(HY4), 1037(HY4), 1038(HY4), 1039(HY4), 1040(HY4), 1041(HY4)[c], 1042(PO4), 1043(PO4), 1044(PO4), 1045(PO4), 1046(PO4)[c], 1047(SA4), 1048 (SA4)[c], 1049(SA4), 1050(SA4), 1051(SA4), 1052(HY4), 1053(SA4).

SEPTEMBER: 1054(ST5), 1055(ST5), 1056(ST5), 1057(ST5), 1058(ST5), 1059(WW4), 1060(WW4), 1061(WW4), 1062(WW4), 1063(WW4), 1064(SU2), 1065(SU2), 1066(SU2)[c], 1067(ST5)[c], 1068 (WW4)[c], 1069(WW4).

OCTOBER: 1070(EM4), 1071(EM4), 1072(EM4), 1073(EM4), 1074(HW3), 1075(HW3), 1076(HW3), 1077(HY5), 1078(SA5), 1079(SM4), 1080(SM4), 1081(SM4), 1082(HY5), 1083(SA5), 1084(SA5), 1085(SA5), 1086(PO5), 1087(SA5), 1088(SA5), 1089(SA5), 1090(HW3), 1091(EM4)[c], 1092 (HY5)[c], 1093(HW3)[c], 1094(PO5)[c], 1095(SM4)[c].

NOVEMBER: 1096(ST6), 1097(ST6), 1098(ST6), 1099(ST6), 1100(ST6), 1101(ST6), 1102(IR3), 1103 (IR3), 1104(IR3), 1105(IR3), 1106(ST6), 1107(ST6), 1108(ST6), 1109(AT3), 1110(AT3)[c], 1111(IR3)[c]; 1112(ST6)[c].

DECEMBER: 1113(HY6), 1114(HY6), 1115(SA6), 1116(SA6), 1117(SU3), 1118(SU3), 1119(WW5), 1120(WW5), 1121(WW5), 1122(WW5), 1123(WW5), 1124(WW5)[c], 1125(BD1)[c], 1126(SA6), 1127 (SA6), 1128(WW5), 1129(SA6)[c], 1130(PO6)[c], 1131(HY6)[c], 1132(PO6), 1133(PO6), 1134(PO6), 1135(BD1).

VOLUME 83 (1957)

JANUARY: 1136(CP1), 1137(CP1), 1138(EM1), 1139(EM1), 1140(EM1), 1141(EM1), 1142(SM1), 1143(SM1), 1144(SM1), 1145(SM1), 1146(ST1), 1147(ST1), 1148(ST1), 1149(ST1), 1150(ST1), 1151(ST1), 1152(CP1)[c], 1153(HW1), 1154(EM1)[c], 1155(SM1)[c], 1156(ST1)[c], 1157(EM1), 1158 (EM1), 1159(SM1), 1160(SM1), 1161(SM1).

FEBRUARY: 1162(HY1), 1163(HY1), 1164(HY1), 1165(HY1), 1166(HY1), 1167(HY1), 1168(SA1), 1169(SA1), 1170(SA1), 1171(SA1), 1172(SA1), 1173(SA1), 1174(SA1), 1175(SA1), 1176(SA1), 1177(HY1)[c], 1178(SA1), 1179(SA1), 1180(SA1), 1181(SA1), 1182(PO1), 1183(PO1), 1184(PO1), 1185(PO1)[c].

MARCH: 1186(ST2), 1187(ST2), 1188(ST2), 1189(ST2), 1190(ST2), 1191(ST2), 1192(ST2)[c], 1193 (PL1), 1194(PL1), 1195(PL1).

APRIL: 1196(EM2), 1197(HY2), 1198(HY2), 1199(HY2), 1200(HY2), 1201(HY2), 1202(HY2), 1203 (SA2), 1204(SM2), 1205(SM2), 1206(SM2), 1207(SM2), 1208(WW1), 1209(WW1), 1210(WW1), 1211(WW1), 1212(EM2), 1213(EM2), 1214(EM2), 1215(PO2), 1216(PO2), 1217(PO2), 1218 (SA2), 1219(SA2), 1220(SA2), 1221(SA2), 1222(SA2), 1223(SA2), 1224(SA2), 1225(PO)[c], 1226 (WW1)[c], 1227(SA2)[c], 1228(SM2)[c], 1229(EM2)[c], 1230(HY2)[c].

MAY: 1231(ST3), 1232(ST3), 1233(ST3), 1234(ST3), 1235(IR1), 1236(IR1), 1237(WW2), 1238(WW2), 1239(WW2), 1240(WW2), 1241(WW2), 1242(WW2), 1243(WW2), 1244(HW1), 1245(HW1), 1246 (HW1), 1247(HW1), 1248(WW2), 1249(HW1), 1250(HW1), 1251(WW2), 1252(WW2), 1253(IR1), 1254(ST3), 1255(ST3), 1256(HW1), 1257(IR1)[c], 1258(HW1)[c], 1259(ST3)[c].

---

c. Discussion of several papers, grouped by Divisions.

AMERICAN SOCIETY OF CIVIL ENGINEERS

OFFICERS FOR 1957

PRESIDENT

MASON GRAVES LOCKWOOD

VICE-PRESIDENTS

Term expires October, 1957:
FRANK A. MARSTON
GLENN W. HOLCOMB

Term expires October, 1958:
FRANCIS S. FRIEL
NORMAN R. MOORE

DIRECTORS

Term expires October, 1957:
JEWELL M. GARRELTS
FREDERICK H. PAULSON
GEORGE S. RICHARDSON
DON M. CORBETT
GRAHAM P. WILLOUGHBY
LAWRENCE A. ELSENER

Term expires October, 1958:
JOHN P. RILEY
CAREY H. BROWN
MASON C. PRICHARD
ROBERT H. SHERLOCK
R. ROBINSON ROWE
LOUIS E. RYDELL
CLARENCE L. ECKEL

Term expires October, 1959:
CLINTON D. HANOVER, Jr.
E. LELAND DURKEE
HOWARD F. PECKWORTH
FINLEY B. LAVERTY
WILLIAM J. HEDLEY
RANDLE B. ALEXANDER

PAST-PRESIDENTS

Members of the Board

WILLIAM R. GLIDDEN

ENOCH R. NEEDLES

EXECUTIVE SECRETARY
WILLIAM H. WISELY

TREASURER
CHARLES E. TROUT

ASSISTANT SECRETARY
E. L. CHANDLER

ASSISTANT TREASURER
CARLTON S. PROCTOR

PROCEEDINGS OF THE SOCIETY

HAROLD T. LARSEN
Manager of Technical Publications

PAUL A. PARISI
Editor of Technical Publications

DANIEL GOTTHELF
Asst. Editor of Technical Publications

COMMITTEE ON PUBLICATIONS

JEWELL M. GARRELTS, *Chairman*

HOWARD F. PECKWORTH, *Vice-Chairman*

E. LELAND DURKEE
MASON C. PRICHARD
R. ROBINSON ROWE
LOUIS E. RYDELL